This thesis was financially supported by a PhD scholarship from Fundação para a Ciência e a Tecnologia (Ref.: SFRH/BD/110723/2015), under the scope of the strategic funding of UID/BIO/04469/2013 unit and COMPETE 2020 (POCI-01-0145-FEDER-006684) and BioTecNorte operation (NORTE-01-0145-FEDER-000004) funded by European Regional Development Fund under the scope of Norte2020, Programa Operacional Regional do Norte.

Development of whey protein network systems under application of moderate electric fields – Effects on protein structure and interactions

Rui Miguel Martins Rodrigues

UMinho | 2019

Universidade do Minho
Escola de Engenharia

Rui Miguel Martins Rodrigues

Development of whey protein network systems under application of moderate electric fields – Effects on protein structure and interactions

September 2019

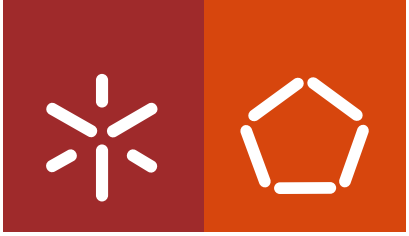

Universidade do Minho
Escola de Engenharia

Rui Miguel Martins Rodrigues

Development of whey protein network systems under application of moderate electric fields – Effects on protein structure and interactions

PhD Thesis
Chemical and Biological Engineering

Work carried out under the supervision of:
Ricardo Nuno Correia Pereira, PhD
António Augusto Martins de Oliveira Soares Vicente, PhD

September 2019

COPYRIGHT AND WORKING CONDITIONS BY THIRD PARTIES

ACKNOWLEDGEMENTS/AGRADECIMENTOS

Ao longo deste percurso, muitos foram aqueles que contribuíram para a minha chegada até aqui. Em primeiro lugar quero agradecer a aqueles que me deram a oportunidade de iniciar o meu trajeto na ciência, que acreditaram em mim, que me apoiaram e orientaram ao longo deste caminho. Ao Professor António Vicente e ao Ricardo Pereira, o meu obrigado por todos os ensinamentos, pelo seu apoio no plano profissional e pessoal, porque mais do que exemplos a seguir, os tenho como exemplos de amizade. Agradeço também ao Professor Steffen Petersen, que muito contribuiu com o seu conhecimento experiência e dedicação para o meu percurso.

A todos os colegas e amigos do LIP, ao longo dos anos, por proporcionarem um ambiente de trabalho extraordinário, companheirismo e ajuda sempre que necessário. Em particular queria agradecer a: Óscar Ramos, Lívia Simões, Ana Bourbon, Miguel Cerqueira, Bruno Fernandes, Ana Pinheiro, Joana Martins, Eduardo Pires, Luiz Fazolin, Pedro Geada, Michele Michelin, Pedro Silva, Daniel Madalena, Artur Martins, Raquel Gonçalves, Filipe Maciel, Zita Avelar, Jean-Michel Fernandes, Luís Loureiro, João Araújo. Em especial, obrigado àqueles com quem tive o prazer de colaborar em alguns trabalhos e que tiveram uma contribuição decisiva no meu percurso. À Maria José Costa, a "BFF" que me acompanha desde o dia 1, obrigado pelo companheirismo, amizade e generosas doses de loucura.

Uma palavra de apreço ao Centro de Engenharia Biológica, a instituição que me acolheu, e todos os professores, colegas e corpo técnico. Em particular agradeço ao Sr. Santos, à Madalena Vieira, Paula Pereira, Vitória Maciel, Aline Barros e Diana Vilas Boas por terem sido insuperáveis no apoio técnico prestado.

Agradeço à Odete, ao Fabri e à Flávia, que tornaram Aalborg numa segunda casa e fizeram da minha estadia uma experiência fantástica.

Um obrigado a todos os amigos, que à margem da ciência, sempre estiveram presentes com apoio, bons momentos e amizade.

Um obrigado muito especial à Raquel pelo amor, companheirismo, por todo o apoio e incentivos. Obrigado por estares sempre presente!

Finalmente agradeço à minha Família, especialmente aos meus pais, a quem devo tudo o que sou, pelo amor, incentivo e apoio que sempre me deram!

STATEMENT OF INTEGITY

I hereby declare having conducted this academic work with integrity. I confirm that I have not used plagiarism or any form of undue use of information or falsification of results along the process leading to its elaboration.

I further declare that I have fully acknowledged the Code of Ethical Conduct of the University of Minho.

Development of whey protein systems under the influence of moderate electric fields – Effect on protein structure and interactions

Abstract

This thesis describes the study of the MEF effects on protein structure and interactions, aiming at the development of whey protein network systems. For the first time MEF effects were verified in protein structure and conformation, revealing to be synergetic with thermal action and dependent of the pH of the protein solutions. MEF effects in protein structure demonstrated a linear dependence on the voltage gradients applied and were more evident at low electrical frequencies. The structural changes resultant from the electric treatment also lead to changes in protein's interactions with hydrophobic compounds, namely ANS affinity increase and retinol binding conservation.

The effects of MEF in protein aggregation and gelation were accessed in WPI cold-set gels. The presence of the MEF inherent to OH contributed to the formation of smaller aggregates with lower content of reactive thiol groups and lower viscosity. The cold-set gels produced presented distinctive properties such as finer stranded structures with lower disulphide crosslinking but higher hydrophobic interactions and hydrogen bonds. These changes resulted in weaker and more elastic gel structures, with higher water retention and swelling capacity. These changes in aggregation and gel properties were potentiated by the use of higher EF strength and lower frequency treatments. As a proof of concept, the potentiality of OH and MEF application in innovative protein applications were evaluated in the production of protein-based scaffolds for tissue engineering. OH demonstrated to be an adequate technique to promote protein functionalization and to tune the scaffold´s functional properties. The variation of the EF strength during the denaturation and aggregation process resulted in scaffolds with distinctive functional properties and improved cellular proliferation. These scaffolds can be used as a support for cellular growth for tissue regeneration or as support to growing cultured meat.

The effects of MEF during OH influenced the denaturation process, resulting in distinctive protein structural features and interactions. These changes at molecular level were reflected in protein aggregation, network formation and final functional properties. Therefore, an accurate selection of the MEF process variables allows controlling the functionality of protein systems, opening innovative perspectives on the use of OH and MEF not only in food and bioprocessing applications, but also in the pharmaceutical and biomedical areas.

Key words: Electric fields; Gelation; Protein functionality; Protein structure; Whey proteins.

Desenvolvimento de sistemas á base de proteínas de soro sobe a influencia de campos elétricos moderados – Efeitos na estrutura e interação das proteínas

Resumo

Esta tese descreve o estudo dos efeitos dos campos elétricos moderados (MEF) na estrutura e interação de proteínas, visando o desenvolvimento de sistemas de proteínas de soro de leite. Pela primeira vez os efeitos dos MEF foram comprovados na estrutura de proteínas, revelando ser sinérgicos com a ação térmica e dependentes do pH. Os efeitos dos MEF na estrutura das proteínas apresentaram uma dependência linear da voltagem aplicada e foram mais acentuados com o uso de baixas frequências elétricas. As alterações resultantes dos tratamentos elétricos também alteraram as interações das proteínas com os compostos hidrofóbicos, nomeadamente no aumento da afinidade com ANS e a conservação da ligação ao retinol.

Os efeitos do MEF foram avaliados na agregação e gelificação a frio de WPI. A presença dos MEF contribuiu para a formação de agregados menores, com menor teor de grupos tiol reativos e menor viscosidade. Os géis produzidos apresentaram propriedades distintas, tais como estruturas mais homogéneas, com menos pontes dissulfureto, mas mais interações hidrofóbicas e pontes de hidrogénio. Estas alterações resultaram em estruturas mais fracas e elásticas, com maior capacidade de retenção de água e inchamento. Essas mudanças nas propriedades do gel foram potenciadas pelo incremento da voltagem e pelo uso de baixas frequências. Como prova de conceito, o uso de MEF em aplicações inovadoras foi avaliado na produção de substratos de bases proteica, para a engenharia de tecidos. O aquecimento óhmico (OH) demonstrou ser uma técnica adequada para promover a funcionalização proteica e ajustar as propriedades funcionais dos substratos. A variação da voltagem durante o processo de desnaturação e agregação resultou em substratos com propriedades funcionais distintas e no aumento da proliferação celular. Estes substratos podem ser utilizados como suporte de crescimento celular para regeneração de tecidos ou como suporte para o crescimento de carne cultivada.

Os efeitos de MEF durante OH, influenciaram o processo de desnaturação, resultando em características estruturais e interações proteicas diferenciadas. Estas alterações a nível molecular refletiram-se na agregação, na formação da rede estrutural e nas propriedades funcionais das estruturas formadas. Portanto, uma seleção precisa das variáveis de processo de MEF permite controlar a funcionalidade de proteínas, abrindo perspetivas inovadoras no seu uso não apenas em aplicações alimentares e de bioprocessos, mas também nas áreas de farmacêutica e biomédica.

Palavras-chave: Campos elétricos; Estrutura de proteínas; Funcionalidade proteica; Gelificação; Proteínas de soro.

TABLE OF CONTENTS

LIST OF FIGURES

LIST OF TABLES

LIST OF GENERAL NOMENCLATURE

Abbreviations

2-Me - 2-Mercaptoethanol

DTNB - 5.5′-dithiobis-(2-nitrobenzoic acid)

ANS - 8-anilino-1-naphthalenesulfonic acid

AC - Alternating current

AF- Auto fluorescence

β-lg - Beta-lactoglobulin

BSA – Bovine serum albumin

CD - Circular dichroism

CLSM - Confocal laser scanning microscopy

Cov - Conventional

Cys - Cysteine

DSC - Differential scanning calorimetry

DC - Direct current

DFA - Desirability function analysis

DLS - Dynamic light scattering

DTT - Dithiotreitol

EF- Electric field

EM - Electromagnetic

HAS - Human serum albumin

MEF - Moderate electric field

MTT - 3-(4,5-dimethylthiazol-2-yl)-2,5-diphenyltetrazoliumbromide

OH - Ohmic heating

PB - Phosphate buffer

PCA - Principal component analysis

PS - Phosphate buffer saline

PdI - Poly-dispersity index

PCA - Principal component analysis

PEF - Pulsed Electric Fields

PTFE - Polytetrafluoroethylene

SEM - Scanning electronic microscopy

SDS - Sodium dodecyl sulphate

SPI - Soy protein isolate

SLS - Static light scattering

SH - Sulfydryl

Trp - Tryptophan

Tyr - Tyrosine

UV - Ultraviolet

Vis - Visible

WHC - Water-holding capacity

WPI - Whey protein isolate

Z-ave - Hydrodynamic size diameter

Symbols:

A - Area

F - Fluorescence

I - Electric current

g - Gravitational acceleration

h - Height

q - Internal energy generation rate

R - Resistance

T - Temperature

W - Weight

V - Voltage

A_0 - Pre-exponential factor

T_m - Melting temperature

ε_H - Hencky strain

σ_H - Hencky stress

k_q - Quenching rate constant

σ - Shear stress

θ - Ellipticity

G^* - Complex modulus

K_{SV} - Stern–Volmer quenching constant

τ - Decay constant

τ_0 - Florescence lifetime

$\dot{\gamma}$ - Shear rate

LIST OF PUBLICATIONS

This thesis is based on the work presented in the following publications:

Rui M. Rodrigues, António A. Vicente, Steffen B. Petersen, Ricardo N. Pereira. Electric field effects on β-lactoglobulin thermal unfolding as a function of pH – Impact on protein functionality. Innovative Food Science & Emerging Technologies, Volume 52, 2019, Pages 1-7,ISSN 1466-8564

Rui M. Rodrigues, Zita Avelar, António A. Vicente, Steffen B. Petersen and Ricardo N. Pereira. Influence of moderate electric fields in β-lactoglobulin thermal unfolding and interactions. Food Chemistry, In Press, available online: 28 August 2019. doi.10.1016/j.foodchem.2019.125442

Rui M. Rodrigues, Zlatina Genisheva, Cristina M.R. Rocha, José A. Teixeira, António A. Vicente, Ricardo N. Pereira. Ohmic heating for preservation, transformation and extraction. Book-chapter - Green Food Processing Techniques, Publisher: Elsevier, October 2019

Rui M. Rodrigues, Bárbara Claro, Margarida Bastos, Ricardo N. Pereira, António A. Vicente and Steffen B. Petersen. Multi-step thermally induced transitions of β-lactoglobulin - an *in situ* spectroscopy approach. Accepted in the International Dairy Journal, Elsevier. In press.

Rui M. Rodrigues, Luiz H. Fasolin, Zita Avelar, António A. Vicente and Ricardo N. Pereira. Effects of Moderate Electric Fields in cold-set gelation of whey proteins – from molecular interactions to functional properties. Submitted to Food Hydrocolloids, Elsevier

CHAPTER 1.

GENERAL INTRODUCTION

1.1 RESEARCH BACKGROUND AND MOTIVATION

Conventionally milk whey serum is discarded as a waste in dairy industry, resulting in a considerable environmental issue and economical cost. Over the last few decades, several efforts have been made on the valorisation of whey and its constituents. Particularly whey proteins have found extensive technological applications as gelling agents, stabilizers of emulsions and foams, ingredients for films and coatings, among others (Guo, 2019; Nicolai, Britten, & Schmitt, 2011; Ramos et al., 2015). Moreover, whey proteins are triggering a great interest in biotechnology and particularly in nano- and micro-technology. They can be used in the development of functional complexes, entirely biodegradable structures or delivery systems with no need of chemical crosslinking agents in their preparation, thus gathering some of the major requirements for a wide use not only in many food and bioprocessing applications, but also in the pharmaceutical area (Nicolai et al., 2011; Ramos et al., 2017).

Protein´s function and activity are closely linked to their structure, conformation and interactions, which means that even a small change of these factors can result in functionality changes. Understanding and controlling environmental factors that can affect protein functionalization is still a major topic in bioscience and technology. Besides the traditional studies on protein structure and functionality based on temperature, pH variations and presence of denaturants (Bryant & McClements, 1998), the use of novel processes is opening new perspectives on protein functionalization and technological applications. Emerging technologies such as ultrasounds (Jambrak, Mason, Lelas, Herceg, & Herceg, 2008; Zhang, Claver, Zhu, & Zhou, 2011), high pressure (Baier, Purschke, Schmitt, Rawel, & Knorr, 2015; Prehoda, Mooberry, & Markley, 1998), electric fields (EF) and electromagnetic fields (R N Pereira et al., 2016; Rodrigues et al., 2015a; Xiang, Ngadi, Ochoa-Martinez, & Simpson, 2011), have proven to be interesting processing alternatives and hold a lot of potential yet to explore. In particular, EF effects on protein-based systems have been recently reported and confirmed (R.N. Pereira et al., 2016; Ricardo N. Pereira, Souza, Cerqueira, Teixeira, & Vicente, 2010; Rodrigues et al., 2015b) but the specific influence of EF on protein`s structure and interactions has not yet been clarified and very few experimental works exist in literature about the topic. Driven by the potential knowledge and applications resulting from the influence of EF on proteins, the working plan of this thesis was elaborated, aiming at understanding and ultimately mastering these effects associated with moderate electric field (MEF) processing technology. It was our intention to apply this knowledge for the development of whey protein systems with distinctive properties, thus opening perspectives for new and innovative

applications. A larger body of research is needed to fully address the role of MEF on protein electrostatics, conformation and protein-protein interactions. The understanding and control of MEF effects on proteins may bring novel insights for the fabrication of protein-based systems with tailored functional and technological properties.

1.2 RESEARCH AIMS

The main objectives of this project were to evaluate and characterize at the molecular level the influence that MEF exert on the structure of whey proteins, their potential to establish interactions with identical or other molecules and on the formation of supramolecular structures. The impact of MEF on the development of protein networks of pure and enriched fractions of whey proteins, aiming at the production of food-grade structures for application in the food, pharmaceutical and biomedical areas was also addressed.

The project integrated different activities distributed in two main topics:

1) Characterization of β-lg conformational changes and protein-protein interactions imposed by MEF

2) Exploring the development of β-lg and whey protein systems (e.g. hydrogels) under the application of MEF

The first main challenge was to understand the role of MEF in the conformation of individual β-lg molecules. It was expected that different MEF treatment conditions would influence conformational transitions of β-lg and consequently its interactions. Techniques such as circular dichroism (CD) and fluorescence spectroscopy were used to access structural changes and to follow the conformational disturbances induced by MEF.

The second major objective was the production of tailored whey protein hydrogels with distinctive properties. The application of MEF treatments were performed in order to influence the protein structure and interactions thus affecting the hydrogel network and functional properties. Light scattering, calorimetry, CD and evaluation of the sulfhydryl (SH) groups and hydrophobicity allowed to retrieve qualitative information regarding protein denaturation and aggregation processes. Techniques such as dynamic light scattering (DLS) and fluorescence spectroscopy were used to characterize the development of protein aggregates and the role of covalent and non-covalent

interactions between proteins, respectively. Other techniques, such as confocal laser scanning microscopy (CLSM), scanning electronic microscopy (SEM), and rheology were used to characterize the microstructure of the produced hydrogels.

The developed protein-structured systems with distinctive properties together with their full characterization should allow multiple applications, gathering the requirements to be used in the biotechnology, pharmaceutical and food industries

1.3 OUTLINE OF THE THESIS

Based on these main objectives, this thesis was organized in 8 chapters. In addition to the present chapter, Chapter 2 provides a general introduction for the subsequent chapters. Chapters 3 to 7 contain the main experimental results and in Chapter 8 are presented the general conclusions and future perspectives.

Chapter 2: In this chapter a general introduction to EF processing is provided, with a literature review on the EF effects in protein systems. The main technologies, processing conditions and observed effects in protein structure, activity and functional properties were described.

Chapter 3: Thermal effects in β-lg were characterized in detail. In order to establish the characterization methodology, several analytic techniques were applied in the study of protein structure and transitions. The unfolding mechanism of this protein was further elucidated and the critical temperature for structural transitions was assessed.

Chapter 4: Based on the critical temperature for β-lg`s structural transitions, established in Chapter 3, a series of thermo-electric treatments were implemented to evaluate structural changes imposed by the presence of MEF. Under low aggregation conditions (low protein concentration and low ionic strength), β-lg solutions at different pH values were heated by OH and by conventional heat exchange. This strategy aimed at proving MEF effects in β-lg structure and at determining the most favourable conditions for their further exploration.

Chapter 5: In this chapter, the effects of MEF during thermal unfolding of β-lg have been investigated. Electric variables such as EF strength and frequency were tested and their effects in structural transitions and secondary structure distribution were determined. The structural changes

resultant from the electric treatment were also evaluated through the protein`s interactions with ANS and retinol.

Chapter 6: With the establishment of the specific effects of MEF and its variables in protein structure and interactions, in this chapter these effects were explored in protein aggregation and gelation. Distinctive thermo-electric treatments were applied on the formation of hydrogels of WPI by the cold gelation technique. MEF effects were evaluated form the molecular scale (aggregation) to the network formation (gelation) and resultant physicochemical, mechanical and functional properties.

Chapter 7: The capacity of MEF to change protein functional properties was put to the test and evaluated on the formation of protein-based scaffolds for tissue engineering. MEF action was assessed during the scaffolds production method and functional properties. The scaffold´s performance and MEF resultant effects were evaluated on the adhesion and proliferation of human fibroblast cells.

Chapter 8: The general conclusions, final remarks and future perspectives are presented in this chapter.

1.4 REFERENCES

Baier, D., Purschke, B., Schmitt, C., Rawel, H. M., & Knorr, D. (2015). Effect of high pressure - Low temperature treatments on structural characteristics of whey proteins and micellar caseins. *Food Chemistry*, *187*, 354–363. https://doi.org/10.1016/j.foodchem.2015.04.049

Bryant, C. M., & McClements, D. J. (1998). Molecular basis of protein functionality with special consideration of cold-set gels derived from heat-denatured whey. *Trends in Food Science & Technology*, *9*(4), 143–151. https://doi.org/10.1016/S0924-2244(98)00031-4

Guo, M. (Ed.). (2019). *Whey Protein Production, Chemistry, Functionality, and Applications*. Chichester, UK: John Wiley & Sons, Ltd. https://doi.org/10.1002/9781119256052

Jambrak, A. R., Mason, T. J., Lelas, V., Herceg, Z., & Herceg, I. L. (2008). Effect of ultrasound treatment on solubility and foaming properties of whey protein suspensions. *Journal of Food Engineering*, *86*(2), 281–287. https://doi.org/10.1016/j.jfoodeng.2007.10.004

Nicolai, T., Britten, M., & Schmitt, C. (2011). β-Lactoglobulin and WPI aggregates: Formation, structure and applications. *Food Hydrocolloids*, *25*(8), 1945–1962. https://doi.org/10.1016/j.foodhyd.2011.02.006

Pereira, R. N., Rodrigues, R. M., Ramos, O. L., Malcata, F. X., Teixeira, J. A., & Vicente, A. A. (2016). Production of Whey Protein-Based Aggregates Under Ohmic Heating. *Food and Bioprocess Technology*, *9*(4), 576–587. https://doi.org/10.1007/s11947-015-1651-4

Pereira, R. N., Rodrigues, R. M., Ramos, Ó. L., Xavier Malcata, F., Teixeira, J. A., & Vicente, A. A. (2016). Production of Whey Protein-Based Aggregates Under Ohmic Heating. *Food and Bioprocess Technology*, *9*(4). https://doi.org/10.1007/s11947-015-1651-4

Pereira, R. N., Souza, B. W. S., Cerqueira, M. A., Teixeira, J. A., & Vicente, A. A. (2010). Effects of Electric Fields on Protein Unfolding and Aggregation: Influence on Edible Films Formation. *Biomacromolecules*, *11*(11), 2912–2918. https://doi.org/10.1021/bm100681a

Prehoda, K. E., Mooberry, E. S., & Markley, J. L. (1998). High Pressure Effects on Protein Structure. In *Protein Dynamics, Function, and Design* (pp. 59–86). Boston, MA: Springer US. https://doi.org/10.1007/978-1-4615-4895-9_5

Ramos, O. L., Pereira, R. N., Martins, A., Rodrigues, R., Fuciños, C., Teixeira, J. A., … Vicente, A. A. (2017). Design of whey protein nanostructures for incorporation and release of nutraceutical compounds in food. *Critical Reviews in Food Science and Nutrition*, *57*(7). https://doi.org/10.1080/10408398.2014.993749

Ramos, O. L., Pereira, R. N., Rodrigues, R. M., Teixeira, J. A., Vicente, A. A., & Malcata, F. X. (2015). *Whey and Whey Powders: Production and Uses*. *Encyclopedia of Food and Health*. https://doi.org/10.1016/B978-0-12-384947-2.00747-9

Rodrigues, R. M., Martins, A. J., Ramos, O. L., Malcata, F. X., Teixeira, J. A., Vicente, A. A., & Pereira, R. N. (2015a). Influence of moderate electric fields on gelation of whey protein isolate. *Food Hydrocolloids*, *43*, 329–339. https://doi.org/10.1016/j.foodhyd.2014.06.002

Rodrigues, R. M., Martins, A. J., Ramos, O. L., Malcata, F. X., Teixeira, J. A., Vicente, A. A., & Pereira, R. N. (2015b). Influence of moderate electric fields on gelation of whey protein

isolate. *Food Hydrocolloids*, *43*, 329–339. https://doi.org/10.1016/j.foodhyd.2014.06.002

Xiang, B. Y., Ngadi, M. O., Ochoa-Martinez, L. A., & Simpson, M. V. (2011). Pulsed Electric Field-Induced Structural Modification of Whey Protein Isolate. *Food and Bioprocess Technology*, *4*(8), 1341–1348. https://doi.org/10.1007/s11947-009-0266-z

Zhang, H., Claver, I. P., Zhu, K. X., & Zhou, H. (2011). The effect of ultrasound on the functional properties of wheat gluten. *Molecules*, *16*(5), 4231–4240. https://doi.org/10.3390/molecules16054231

CHAPTER 2.

EF EFFECTS IN PROTEIN STRUCTURE

2.1 INTRODUCTION

The EF effects and their biological implications is an enduring subject of interest by the scientific community. It has been reported for centuries and object of study in many fields of science. Yet it is remarkable how little we know about their fundamental interactions and effects in biological systems. The electric interaction with biological materials can be traditionally classified as thermal and non-thermal (Sastry, 2008). The thermal effects of electric or electromagnetic (EM) fields on matter arise from the heat generated by the absorption of electric or EM energy. This effects are well described at the macro scale and well exploited on applications as inductive or ohmic heating (R. N. Pereira & Vicente, 2010). During OH, heat is produced directly within the material itself by Joule effect as electric current (I) is passing through a conductive material of resistance (R), which is heated by molecular agitation from the motion of charges within the material. This effect can be described by equation 2.1.

$$q = E2\sigma \qquad (2.1)$$

where q is the internal energy generation rate ($W.m^{-3}$), E is the electric field strength ($V.cm^{-1}$), and σ is the electrical conductivity of the product ($S.m^{-1}$).

The particular interest in these thermal effects are related with food processing, biotechnology industries and research. The fast, homogenous and energetic efficient heating provided by Joule effect are of interest in aseptic processing of liquid-particulate mixtures, processing residues and extraction processes (Sastry, 2008). EF thermal effects were already addressed in an extended number of works works (El Darra, Grimi, Vorobiev, Louka, & Maroun, 2013; Machado, Pereira, Martins, Teixeira, & Vicente, 2010; Sastry, 2008). In recent years the awareness in non-thermal effects of EF arising from related phenomena of charges movement and dipole interferences are still gaining strength. Studies regarding EF non-thermal effect on biological systems have been addressed in several fields as biomedicine, molecular biology, processing engineering among others (Almohammed, Mhemdi, & Vorobiev, 2016; Bekard & Dunstan, 2014; Machado et al., 2010; Rodrigues et al., 2015; Sastry, 2008). The scale addressed to investigate these effects is also wide, covering entire cellular tissues, unicellular organisms, cellular components and bio-molecules.

In a general way, authors emphasize a distinction between thermal and non-thermal effects associated with the presence of EF, even so this dissociation is not straightforward. Some authors

suggest that certain EF related effects can result from the rapid and localized temperature rise at molecular level, making it non detectable by traditional techniques (Zhao & Yang, 2010). It is clear that even subtle localized temperature rises could lead to an increase of entropy within the molecular structure leading to the occurrence of conformational disturbances (Laurence, French, Lindner, & Mckenzie, 2000; Ricardo N. Pereira, Souza, Cerqueira, Teixeira, & Vicente, 2010).

Ultimately biological systems can be defined as an organized collection of bio-molecules, thus the study of EF effects at molecular scale is a fundamental step for the disclosure of such events. For several decades researchers have theorized and attempted to study EF effects on biological components (Hill, 1958; Sher, Kresch, & Schwan, 1970). A particular focus on this field is the study of proteins since not only they play an essential role in all biological systems as present important functional properties in medicine, pharmaceutics, bioengineering and food industries.

Protein function is strongly related with the specific conformation and its change at any level (i.e. primary, secondary, tertiary and quaternary) results in distress of its functionality (i.e. specificity, activity, unfolding, aggregation properties, among others) (Foegeding & Davis, 2011). Therefore, the conformational integrity of proteins, *in vivo* and *in vitro*, has being received substantial attention in the literature. However, the involved mechanisms, as well as the adequate monitoring techniques and experimental strategies remain elusive and present a major challenge for fundamental science research. In particular, the effect of EF on protein`s structure and interactions has not yet been clarified once very few experimental works and a lack of fundamental knowledge exist in literature.

A folded functional protein 3D structure is a result of numerous endogenous interactions between the amino acids of the protein as well as between the amino acids and the physical chemical environment. Hydrophobic, hydrophilic and electrostatic interactions are essential components in these types of interactions. Most protein structures are only marginally stable and the folded structure of a protein can be perceived as a frustrated energy state, where a large number of stabilizing and destabilizing interactions have found at least a local minimum (Henriksen et al., 2011). It is therefore understandable that proteins behave as latent unstable entities. It seems obvious that EF will be able to influence electrical charges as well as charge distributions in the protein.

Several approaches have been taken to study the EF effects on proteins although the high responsiveness of proteins to extrinsic factors have been posing difficulties to isolate and study these phenomena at the molecular scale and thus enlighten EF effects. In this section, it is intended

to address the effects of EF on protein´s stability, structure and interactions. To do so, the effects related with the predominant EF-bases processing technologies will be reviewed.

2.2 USE OF EF IN BIOPROCESSING

EF based technologies are proliferating on food, bioprocess and medical applications. Particularly PEF, but also MEF and OH applications have been a subject of fast development, applications and industrial implementation. Several effects have been reported as a consequence of the application of these technologies on biological systems and particularly on proteins. However, most of the reports regard changes on the functional or macroscopic properties of the processed products. These changes are the consequence of particular effects at the molecular scale, yet it is not clear the mechanisms involved as the particular the role of EF non-thermal effects. Additionally, the experimental data regarding those effects on proteins at molecular scale are limited. In order to better clarify the protein response mechanisms to EF influence, more and complete experimental data on the influence of EF based technologies on protein´s conformation, folding and interactions are necessary.

2.2.1 PEF processing

PEF is an essentially a non-thermal processing technology that consist on the application of electric pulses on the range of kV with the duration of micro or nanoseconds range. The success of PEF application on foods suggests it can become and alternative or a complement to thermal processing on the food industry (Zhao, Tang, Lu, Chen, & Li, 2014). PEF treatments have shown efficiency in inactivating microorganisms and enzymes as well as functionalizing food components (Mirmoghtadaie, Shojaee Aliabadi, & Hosseini, 2016; Zhao et al., 2012). PEF efficiency is mostly reported to depend of EF intensity, but parameters as pulse width, number, shape and frequency have demonstrated a crucial relevance (Zhao et al., 2014). As an novel technology PEF have already proven value not only on food processing but also in other areas as for example electroporation in bio-refinery and biomedicine (Almohammed et al., 2016; Geada et al., 2018; Henri, Ospital, & Teissié, 2015; Mahnič-Kalamiza, Vorobiev, & Miklavčič, 2014; Rocha et al., 2018). However, a lot is yet to disclosure about the particular effects of PEF on biomaterials and

their constituents. One particular case of interest, as well as one of the most studied is the PEF effects on food proteins and endogenous enzymes.

The effect of PEF on soy protein isolate (SPI) was studied by Xiang et al. (2011) by EF of 2.2 and 2.5 $kV.cm^{-1}$ and pulse numbers between 30 and 120. Results shown changes on the intrinsic and extrinsic fluorescence of SPI confirming modifications on the protein´s structure and surface hydrophobicity. PEF treatments above 30 $kV.cm^{-1}$ and treatment time of 280 μs demonstrated not only to affect SPI hydrophobicity but also free SH content as a result of induced denaturation and aggregation (Y. Li, Chen, & Mo, 2007). On a more detailed study Li (2012) demonstrated that such treatments induced an increase of β-sheet and random coil and a decrease of α-helix content in SPI. These results confirmed that PEF influenced not only protein´s tertiary (conformation) but also secondary structure.

PEF treatment on other protein matrices as WPI was also object of study and compared with thermal treatment. Sui et al. (2011) reported no aggregation, hydrophobicity or SH changes under the conditions tested (35 $kV.cm^{-1}$ and 30-75 °C) on WPI. However, the heat induced gels after PEF treatment suffered significant changes on gelation time and gel strength. On similar conditions as reported previously for SPI, Xiang et al. (2009) reported modifications of fluorescence on PEF treated WPI solutions, concluding that parameters as EF intensity and number of pulsed have influenced on WPI structure.

It is clear that PEF affects different proteins in different extents and ways according with protein's specific characteristics and process conditions applied. The conjugation of EF intensity and treatment time (dependent of the pulse length and number) seems to be decisive on the effects of PEF on proteins. Wu et al. (2014) found that PEF with an intensity of 25 $kV.cm^{-1}$ for 400 μs did not affect egg white physicochemical properties but treatment times exceeding 600 μs induced events such as aggregation, decrease of solubility and increase of free SH groups.

Egg white albumin and β-lg, were subjected to long length exponential decay pulses (2 – 2.2 ms) of 12.5 $V.cm^{-1}$. Structure modifications and partial denaturation was induced on both proteins with 10 pulses, resulting on aggregation, particularly on egg white. PEF also induced differences on the gelation of both proteins (Perez & Pilosof, 2004).

Protein structure and functions relationship was already emphasized. It is thus clear the importance of understanding the mechanisms involved on protein conformational changes. On investigating

PEF´s effects on lysozyme, Zhao et al. (2007) determined a first order model on the inactivation when subjected to an EF of 35 $kV.cm^{-1}$ and treatment time above 300 μs. The lysozyme unfolding was accompanied by the cleavage of disulphide bonds, aggregation and correlated with the loss of α-helix content. The comparison with thermally treated lysozyme with the same activity loss have shown different structural modifications between the treatment methods. This different actions of thermal and EF induced stress on the protein was later confirmed under similar conditions (Zhao & Yang, 2010). Under PEF treatment the conformation of disulphide bonds was changed, tryptophan (Trp) residues were exposed and tyrosine became buried into the structure promoting new hydrogen bonds. Thermal action, besides a different conformation of disulphide bonds distribution, resulted on a higher exposure of Trp and tyrosine on the surface of the protein. These results show that thermal actions are linked to a more complete unfolding of the protein while PEF action is more associated to a reorganization of the structure. Based on the results from the studies aforementioned a model mechanism was actually proposed (see Figure 2.1).

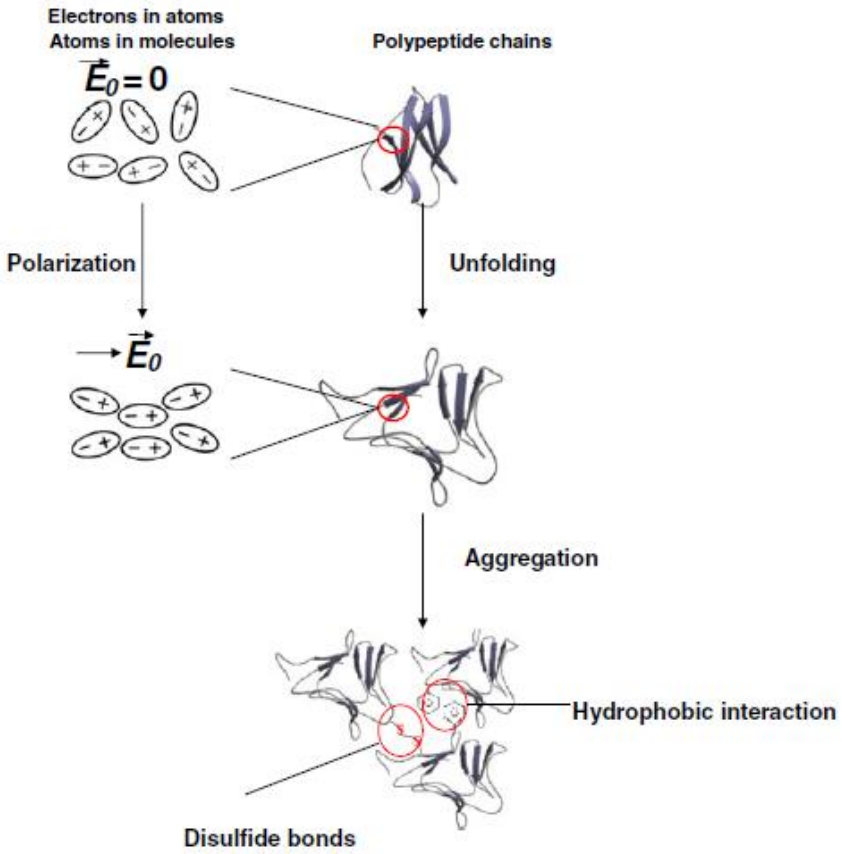

Figure 2.1: Diagram of PEF action in proteins (adapted from Zhao, et al. 2013).

This model involves the polarization of the protein molecule; dissociation of the quaternary structure by breaking non-covalent bonds; changes in protein structure that lead to the exhibition of

hydrophobic and thiol groups that were previously inside the protein core; and if the duration of electric pulse was high enough, the formation of aggregates.

PEF effects on protein´s structure reorganization brings important implications in protein´s stability and functionality, as is the particular case of enzyme activity. On the study of PEF effect on lipase activity, inactivation revealed to be more dependent of EF intensity, followed by frequency and pulse duration (Qian, Gu, Jiang, & Chen, 2014). Enzyme kinetics and thermo-stability were studied on ascorbic acid oxidase under low intensity and long pulse duration PEF (0.2 – 1.2 $kV.cm^{-1}$) (Leong & Oey, 2014), and both seemed to be affected by low EF intensities. Indeed, the energy applied, which is dependent of the field intensity and number of pulses, is a crucial factor. It is implicit then that lower EF and higher exposure times are able to produce equivalent effects of high intensity and short duration treatment.

2.2.2 Moderate Electric Field processing

OH is getting increasing attention and implementation on the food industry because of its fast homogeneous and efficient heating (Sakr & Liu, 2014). OH works under the specifications of MEF, where a EF of relatively low intensity (arbitrarily defined between 1 and 1000 $V.cm^{-1}$) and generally sine wave are applied (Machado et al., 2010). On the MEF´s field intensity range other applications besides heating have been developed like permeabilization of cellular membrane aiming extraction, microbial inactivation, tumour cells destruction among other non-thermal effects (Kirson et al., 2004; Machado et al., 2010; Sensoy & Sastry, 2004).

In fact, EF in the MEF range has been predominant in technological application for decades and the first on to be considered on biological effects, particularly non-thermal (Hill, 1958; Kaur & Singh, 2016). Some of the first reports of EF induced non-thermal effects are related with displacement or rearrangement on any scale, from molecular to macroscopic, of charged materials. Electrophoretic movements and pearl chain effects are classic study cases, long ago reported (Hill, 1958; Longsworth & MacInnes, 1939; Schwan, 1982; Sher et al., 1970) and responsible for further investigation on the EF effects on biological systems. The same basic principles involved are still object of study on applications as proteins nucleation and protein biofilms formation (Ferreira, Camargo, & Benelli, 2015; Pan et al., 2015). On other examples, MEF effects involve microbial inactivation and cellular permeabilization either by synergetic or

independent effects with temperature (Machado et al., 2010; Sensoy & Sastry, 2004; Won, Chungyung, Ki-Myung, & Cherl-Ho, 2002).

The great interest on OH by the food industry has been responsible for the major reports of EF effects on proteins and protein-based material. Enzyme inactivation was naturally one of the first topic addressed on the area. Inactivation kinetics under similar conditions of OH (10 – 90 $V.cm^{-1}$) and exchange heating revealed interesting results. The presence of an EF did not cause an enhanced inactivation to alkaline phosphatase, pectinase, and β-galactosidase. Yet, lipoxygenase and polyphenoloxidase, both containing metal ions, were significantly affected by the EF, increasing their inactivation kinetics (Castro, Macedo, Teixeira, & Vicente, 2006). This clearly demonstrated at least a synergetic EF and thermal effects and that is not verified on all enzymes. The increase of food enzymes inactivation was reported in other studies, but the EF effect on the enzyme structure was not confirmed. Also, the possibility of the effect coming from an environment modification by the EF was suggested as an alternative to structural modifications (Icier, Yildiz, & Baysal, 2006; Jakób et al., 2010).

Recently Samaranayake and Sastry (2016) studied the effects of frequency associated with MEF on the activity of endogenous enzymes. Operating at pectin methylesterase maximum activity temperature (65 °C), which is generally the threshold temperature for its thermal inactivation, a very low EF of 0.4 $V.cm^{-1}$ and frequencies between 0 (DC) and 1 MHz were applied. It was demonstrated that the low electrical frequencies (<60 Hz) can affect enzyme activity. Using molecular motion simulations, it was proposed the EF effects and frequency dependence arises from the amplitude of motion and resulting displacements due to reversal of the AC field.

MEF demonstrated to change gelation characteristics of protein-based foods and ingredients. Surimi and whey protein gels produced under OH presented differentiated mechanical properties and different gel structures (Rodrigues et al., 2015; Tadpitchayangkoon, Park, & Yongsawatdigul, 2012). Changes in gel properties are the result of MEF interference with protein unfolding pathways, which in turn leads to different denaturation and aggregation patterns (R.N. Pereira et al., 2016; Rodrigues et al., 2015). This effects are thermal related, but on the range of 75 to 90 °C it was demonstrated less dependency on temperature increase and lower denaturation of whey proteins under the presence of MEF (R. N. Pereira, Teixeira, & Vicente, 2011). The protein´s structure and nature of the interaction established between proteins was also affected under MEF resulting in lower incidence of free SH groups and increment of β-sheet content (Ricardo N. Pereira,

Souza, Cerqueira, Teixeira, & Vicente, 2010). All these works were conducted under MEF intensities between 2 and 25 $V.cm^{-1}$, electrical frequencies from 50 Hz to 25 kHz and temperatures above proteins denaturation point (> 70 °C).

On other approach Bekard and Dunstan (2014) investigated EF effects on the conformation of bovine serum albumin (BSA) and lysozyme in solution using structural techniques as intrinsic fluorescence and CD. Without significant temperature increase, the application of EF from 0.78 to 5 $V.cm^{-1}$, electrical frequencies of 10 and 500 Hz (sine wave) and long exposure times (i.e. up to 3 h), demonstrated significant effect on protein´s conformation. It was found that the electric force applied during EF exposure was significant to perturb hydrogen bonds, stabilizing the native structure of both protein systems. Both proteins' tertiary structures were affected by the application of EF at 3 $V.cm^{-1}$ and 10 Hz while only lysozyme suffered secondary structure changes. They also proposed a model whereby the electrophoretic motion of the proteins caused by the EF, leads to a frictional force resulting in protein unfolding.

It seems clear that MEF has an effect on proteins. However more detailed studies have to be conducted in order to clarify the dependence or not of thermal effects, the structural disturbances, and to evaluate the specific mechanisms involved and the role of some other electrical factors such as wave shape and frequency. EF effects on proteins and its implications are no doubt a fascinating topic, holding great potential as offering new possibilities on enzymatic properties modification and tailoring functionalities of proteins in general. On Table 2.1, the reported effects of EF through application of PEF and MEF technologies on proteins are resumed.

A great deal is yet to explore, new and deepen studies along with new or revised methodologies must be conducted to fully address this subject. The use of new tools can make a great contribution on the prospect, confirmation or expansion of experimental knowledge.

Table 2.1: Summary of reported effects on proteins induced by EF under multiple experimental approaches.

Method	Conditions tested	Protein	Effects reported	Reference
PEF	24-34 °C, 2.2 to 2. 50 kV.cm^{-1}, 0.5 Hz, 30 to 120 exp. decay pulses	SPI	Structure modification and surface hydrophobicity increase	(Xiang, Ngadi, Ochoa-Martinez, & Simpson, 2011)
	25 °C, 0 to 40 V.cm^{-1}, 0 to 547 µs, 500 Hz, square bipolar pulses of 2 µs	SPI	Increase of solubility, SH content, and hydrophobicity; induced dissociation, denaturation and aggregation	(Y. Li et al., 2007)
	25 °C, 30 V.cm^{-1}, 0 to 547 µs, 400 Hz, square bipolar pulses of 2 µs	SPI	Changes of tertiary and secondary structure	(Y.-Q. Li, 2012)
	≤34 °C, 120 to 2000 V.cm^{-1}, 0.5 Hz, 10 to 30 exp. decay pulses	WPI	Structure modification and surface hydrophobicity increase	(Xiang et al., 2011)
	30 to 75 °C, 30 to 35 kV.cm^{-1}, 19.2-211 µs, 100 to 400 Hz, square bipolar pulses of 2µs	WPI	Reductions in gel strength and increased gelation times	(Sui, Roginski, Williams, Versteeg, & Wan, 2011)
	≤18 °C, 25 kV.cm^{-1}, 100 Hz, 200 to 800 µs, square pulses of 2 µs	Egg white proteins	Induced aggregation, decreased solubility, increase free SHF content	(Wu, Zhao, Yang, & Chen, 2014)
	≤35 °C, 12.5 V.cm^{-1}, 1 to 10 exp. decay pulses of 2 µs	Egg white proteins and β-lg concentrate	Partially unfolding of the native structure, thermal stability changes, induced aggregation and differences in gelation	(Perez & Pilosof, 2004)
	60 °C, 35 kV.cm^{-1}, 0 to 1200 µs, 1000 Hz, square bipolar pulses of 2 µs	Lysozyme	Unfolding, secondary structure change, cleavage of disulphide bonds and aggregation.	(Zhao, Yang, Lu, Tang, & Zhang, 2007)
	≤20 °C, 35 kV.cm^{-1}, 300 to 1200 µs, 1000 Hz, square bipolar pulses of 2 µs	Lysozyme	Conformation changes, changes on disulphide and hydrogen bonds, secondary structure shifts (conversion of α-helix to β-sheet and random coil),	(Zhao & Yang, 2010)
	20 °C, 200 to 1200 V.cm^{-1}, 130 to 9000 µs, 5 to 300 Hz, square bipolar pulses of 20 µs	Ascorbic acid oxidase	Change conversion kinetic parameters and thermo-stability	(Leong & Oey, 2014)

MEF	85 °C, 10 V.cm^{-1}, 50 Hz, sine wave	WPI	Conformation changes, increase of β-Sheet content	(Ricardo N Pereira et al., 2010)
	75-90 °C, 2 to 220 V.cm^{-1}, 50 Hz sine wave	WPI	Alteration of denaturation kinetics	(R N Pereira et al., 2011)
	85 °C, 4 to 20 V.cm^{-1}, 25 kHz, sine wave	WPI	Free SH decrease, lower rates of denaturation and aggregation, degrease of storage and loss modules on the gel	(Rodrigues et al., 2015)
	Room temperature, 0.78 to 5 V.cm^{-1} ,10 and 500 Hz, sine wave	BSA and lyzozime	Tertiary and secondary structure changes. Hydrogen bonds perturbation	(Bekard & Dunstan, 2014)
	90 °C, 6.7 to16.7 V.cm^{-1}, 10 kHz,	Surimi (fish meat)	Free SH decrease, increased gel strength	(Tadpitchayangkoon et al., 2012)
	60 to 90°C, 20 to 90 V.cm^{-1}, 50 Hz, sine wave	Lipoxygenase and polyphenoloxidase	Inactivation kinetics increase	(Castro et al., 2006)
	30 to100 °C,30 to50 V.cm^{-1}, 50 Hz	Peroxidase	Inactivation kinetics increase	(Icier et al., 2006)
	65 °C, 0.4 V.cm^{-1}, 0 (DC) to 1 MHz, sine wave	Pectin methylesterase	Increased inactivation (between 1 and 60 Hz)	(Samaranayake & Sastry, 2016)
	60 °C, 1 V.cm^{-1}, 1 Hz to1MHz, sine wave	α-amylase	Enzyme activities control	(Samaranayake & Sastry, 2018)

2.3 CONCLUSIONS AND PERSPECTIVES

EF effects on several proteins have been reported by different methods and in different conditions. Observations of these effects on proteins, regardless of the timescale, field intensity and dependence of synergetic effects as thermal, are irrefutable and progressively more detailed. The reorientation of specific groups, tertiary structure rearrangement and disruption, secondary structure modifications and bonds shift (particularly hydrogen bonds), seems to be a common point between reports. A time dependent cumulative effect appears to be of major relevance regarding manifestation of the EF effects. The number of reports is still limited and they lack of common criteria, unable to present categorical conclusions. Further study of the subject is needed, particularly aiming the comprehension of all variables involved as the field intensity, time varying of the EF, pulse/wave shape, frequency, and incidence time among others.

Despite many uncertainties, EF effects are a reality and hold the potential for controlling proteins' structure and interactions, opening perspectives for protein tailored functionality. Enzymatic activity can be enhanced or reduced, allergens can be inhibited, wrong conformations corrected, controlled aggregation among many other possibilities.

2.4 REFERENCES

Almohammed, F., Mhemdi, H., & Vorobiev, E. (2016). Pulsed electric field treatment of sugar beet tails as a sustainable feedstock for bioethanol production. *Applied Energy*, *162*, 49–57. https://doi.org/10.1016/j.apenergy.2015.10.050

Bekard, I., & Dunstan, D. E. (2014). Electric field induced changes in protein conformation. *Soft Matter*, *10*(3), 431–437. https://doi.org/10.1039/c3sm52653d

Castro, I., Macedo, B., Teixeira, J. A., & Vicente, A. A. (2006). The Effect of Electric Field on Important Food-processing Enzymes: Comparison of Inactivation Kinetics under Conventional and Ohmic Heating. *Journal of Food Science*, *69*(9), C696–C701. https://doi.org/10.1111/j.1365-2621.2004.tb09918.x

El Darra, N., Grimi, N., Vorobiev, E., Louka, N., & Maroun, R. (2013). Extraction of Polyphenols from Red Grape Pomace Assisted by Pulsed Ohmic Heating. *Food and Bioprocess Technology*, *6*(5), 1281–1289. https://doi.org/10.1007/s11947-012-0869-7

Ferreira, C. F. D. G., Camargo, P. C., & Benelli, E. M. (2015). Formation of Organized Protein Thin Films with External Electric Field. *Journal of Physical Chemistry B*, *119*(39), 12561–12567. https://doi.org/10.1021/acs.jpcb.5b04952

Foegeding, E. A., & Davis, J. P. (2011). Food protein functionality: A comprehensive approach. *Food Hydrocolloids*, *25*(8), 1853–1864. https://doi.org/10.1016/j.foodhyd.2011.05.008

Geada, P., Rodrigues, R., Loureiro, L., Pereira, R., Fernandes, B., Teixeira, J. A., ... Vicente, A. A. (2018). Electrotechnologies applied to microalgal biotechnology – Applications, techniques and future trends. *Renewable and Sustainable Energy Reviews*, *94*, 656–668. https://doi.org/10.1016/j.rser.2018.06.059

Henri, P., Ospital, R., & Teissié, J. (2015). Content Delivery of Lipidic Nanovesicles in Electropermeabilized Cells. *The Journal of Membrane Biology*, *248*(5), 849–855. https://doi.org/10.1007/s00232-015-9789-6

Henriksen, S. B., Mortensen, R. J., Geertz-Hansen, H. M., Neves-Petersen, M. T., Arnason, O., Söring, J., & Petersen, S. B. (2011). Hyperdimensional Analysis of Amino Acid Pair Distributions in Proteins. *PLoS ONE*, *6*(12), e25638. https://doi.org/10.1371/journal.pone.0025638

Hill, T. L. (1958). Some Possible Biological Effects of an Electric Field Acting on Nucleic Acids or Proteins 1. *Journal of the American Chemical Society*, *80*(9), 2142–2147. https://doi.org/10.1021/ja01542a028

Icier, F., Yildiz, H., & Baysal, T. (2006). Peroxidase inactivation and colour changes during ohmic blanching of pea puree. *Journal of Food Engineering*, *74*(3), 424–429. https://doi.org/10.1016/j.jfoodeng.2005.03.032

Jakób, A., Bryjak, J., Wójtowicz, H., Illeová, V., Annus, J., & Polakovič, M. (2010). Inactivation kinetics of food enzymes during ohmic heating. *Food Chemistry*, *123*(2), 369–376. https://doi.org/10.1016/j.foodchem.2010.04.047

Kaur, N., & Singh, A. K. (2016). Ohmic Heating: Concept and Applications—A Review. *Critical Reviews in Food Science and Nutrition*, *56*(14), 2338–2351. https://doi.org/10.1080/10408398.2013.835303

Kirson, E. D., Gurvich, Z., Schneiderman, R., Dekel, E., Itzhaki, A., Wasserman, Y., ... Palti, Y.

(2004). Disruption of Cancer Cell Replication by Alternating Electric Fields. *Cancer Research*, *64*(9), 3288–3295. https://doi.org/10.1158/0008-5472.CAN-04-0083

Laurence, J. A., French, P. W., Lindner, R. A., & Mckenzie, D. R. (2000). Biological effects of electromagnetic fields - Mechanisms for the effects of pulsed microwave radiation on protein conformation. *Journal of Theoretical Biology*, *206*(2), 291–298. https://doi.org/10.1006/jtbi.2000.2123

Leong, S. Y., & Oey, I. (2014). Effect of pulsed electric field treatment on enzyme kinetics and thermostability of endogenous ascorbic acid oxidase in carrots (Daucus carota cv. Nantes). *Food Chemistry*, *146*, 538–547. https://doi.org/10.1016/j.foodchem.2013.09.096

Li, Y.-Q. (2012). Structure Changes of Soybean Protein Isolates by Pulsed Electric Fields. *Physics Procedia*, *33*, 132–137. https://doi.org/10.1016/j.phpro.2012.05.040

Li, Y., Chen, Z., & Mo, H. (2007). Effects of pulsed electric fields on physicochemical properties of soybean protein isolates. *LWT - Food Science and Technology*, *40*(7), 1167–1175. https://doi.org/10.1016/j.lwt.2006.08.015

Longsworth, L. G., & MacInnes, D. A. (1939). Electrophoresis of Proteins by the Tiselius Method. *Chemical Reviews*, *24*(2), 271–287. https://doi.org/10.1021/cr60078a006

Machado, L. F., Pereira, R. N., Martins, R. C., Teixeira, J. A., & Vicente, A. A. (2010). Moderate electric fields can inactivate Escherichia coli at room temperature. *Journal of Food Engineering*, *96*(4), 520–527. https://doi.org/10.1016/j.jfoodeng.2009.08.035

Mahnič-Kalamiza, S., Vorobiev, E., & Miklavčič, D. (2014). Electroporation in Food Processing and Biorefinery. *The Journal of Membrane Biology*, *247*(12), 1279–1304. https://doi.org/10.1007/s00232-014-9737-x

Pan, W., Xu, H., Zhang, R., Xu, J., Tsukamoto, K., Han, J., & Li, A. (2015). The influence of low frequency of external electric field on nucleation enhancement of hen egg-white lysozyme (HEWL). *Journal of Crystal Growth*, *428*, 35–39. https://doi.org/10.1016/j.jcrysgro.2015.07.018

Pereira, R. N., Rodrigues, R. M., Ramos, Ó. L., Xavier Malcata, F., Teixeira, J. A., & Vicente, A. A. (2016). Production of Whey Protein-Based Aggregates Under Ohmic Heating. *Food and Bioprocess Technology*, *9*(4). https://doi.org/10.1007/s11947-015-1651-4

Pereira, R. N., Souza, B. W. S., Cerqueira, M. A., Teixeira, J. A., & Vicente, A. A. (2010). Effects of Electric Fields on Protein Unfolding and Aggregation: Influence on Edible Films Formation. *Biomacromolecules*, *11*(11), 2912–2918. https://doi.org/10.1021/bm100681a

Pereira, R. N., Souza, B. W. S., Cerqueira, M. A., Teixeira, J. A., & Vicente, A. A. (2010). Effects of Electric Fields on Protein Unfolding and Aggregation: Influence on Edible Films Formation. *Biomacromolecules*, *11*(11), 2912–2918. https://doi.org/10.1021/bm100681a

Pereira, R. N., Teixeira, J. A., & Vicente, A. A. (2011). Exploring the denaturation of whey proteins upon application of moderate electric fields: a kinetic and thermodynamic study. *J Agric Food Chem*, *59*(21), 11589–11597. https://doi.org/10.1021/jf201727s

Pereira, R. N., & Vicente, A. A. (2010). Environmental impact of novel thermal and non-thermal technologies in food processing. *Food Research International*, *43*(7), 1936–1943. https://doi.org/10.1016/j.foodres.2009.09.013

Perez, O. E., & Pilosof, A. M. R. (2004). Pulsed electric fields effects on the molecular structure and gelation of β-lactoglobulin concentrate and egg white. *Food Research International*, *37*(1), 102–110. https://doi.org/10.1016/j.foodres.2003.09.008

Qian, J. Y., Gu, Y. P., Jiang, W., & Chen, W. (2014). Inactivating effect of pulsed electric field on lipase in brown rice. *Innovative Food Science and Emerging Technologies*, *22*, 89–94. https://doi.org/10.1016/j.ifset.2014.01.010

Rocha, C. M. R., Genisheva, Z., Ferreira-Santos, P., Rodrigues, R., Vicente, A. A., Teixeira, J. A., & Pereira, R. N. (2018). Electric field-based technologies for valorization of bioresources. *Bioresource Technology*, *254*. https://doi.org/10.1016/j.biortech.2018.01.068

Rodrigues, R. M., Martins, A. J., Ramos, O. L., Malcata, F. X., Teixeira, J. A., Vicente, A. A., & Pereira, R. N. (2015). Influence of moderate electric fields on gelation of whey protein isolate. *Food Hydrocolloids*, *43*, 329–339. https://doi.org/10.1016/j.foodhyd.2014.06.002

Sakr, M., & Liu, S. (2014). A comprehensive review on applications of ohmic heating (OH). *Renewable and Sustainable Energy Reviews*, *39*, 262–269.

https://doi.org/10.1016/j.rser.2014.07.061

Samaranayake, C. P., & Sastry, S. K. (2016). Effect of moderate electric fi elds on inactivation kinetics of pectin methylesterase in tomatoes : The roles of electric fi eld strength and temperature. *Journal of Food Engineering*, *186*, 17–26. https://doi.org/10.1016/j.jfoodeng.2016.04.006

Samaranayake, C. P., & Sastry, S. K. (2018). LWT - Food Science and Technology In-situ activity of α -amylase in the presence of controlled-frequency moderate electric fi elds. *LWT - Food Science and Technology*, *90*(October 2017), 448–454. https://doi.org/10.1016/j.lwt.2017.12.053

Sastry, S. (2008). Ohmic Heating and Moderate Electric Field Processing. *Food Science and Technology International*, *14*(5), 419–422. https://doi.org/10.1177/1082013208098813

Schwan, H. P. (1982). Nonthermal cellular effects of electromagnetic fields AC-field induced ponderomotoric forces. *The British Journal of Cancer. Supplement*, *5*, 220–4. Retrieved from http://www.ncbi.nlm.nih.gov/pubmed/6950764

Sensoy, I., & Sastry, S. K. (2004). Extraction Using Moderate Electric Fields. *Journal of Food Science*, *69*(1), 7–13. https://doi.org/10.1111/j.1365-2621.2004.tb17861.x

Sher, L. D., Kresch, E., & Schwan, H. P. (1970). On the Possibility of Nonthermal Biological Effects of Pulsed Electromagnetic Radiation. *Biophysical Journal*, *10*(10), 970–979. https://doi.org/10.1016/S0006-3495(70)86346-9

Sui, Q., Roginski, H., Williams, R. P. W., Versteeg, C., & Wan, J. (2011). Effect of pulsed electric field and thermal treatment on the physicochemical and functional properties of whey protein isolate. *International Dairy Journal*, *21*(4), 206–213. https://doi.org/10.1016/j.idairyj.2010.11.001

Tadpitchayangkoon, P., Park, J. W., & Yongsawatdigul, J. (2012). Gelation characteristics of tropical surimi under water bath and ohmic heating. *LWT - Food Science and Technology*, *46*(1), 97–103. https://doi.org/10.1016/j.lwt.2011.10.020

Won, Y. S., Chungyung, J. L., Ki-Myung, K., & Cherl-Ho, L. (2002). Leakage of cellular materials from Saccharomyces cerevisiae by ohmic heating. *Journal of Microbiology and Biotechnology*, *12*(2), 183–188.

Wu, L., Zhao, W., Yang, R., & Chen, X. (2014). Effects of pulsed electric fields processing on stability of egg white proteins. *Journal of Food Engineering*, *139*, 13–18. https://doi.org/10.1016/j.jfoodeng.2014.04.008

Xiang, B. Y., Ngadi, M. O., Ochoa-Martinez, L. A., & Simpson, M. V. (2011). Pulsed Electric Field-Induced Structural Modification of Whey Protein Isolate. *Food and Bioprocess Technology*, *4*(8), 1341–1348. https://doi.org/10.1007/s11947-009-0266-z

Zhao, W., Tang, Y., Lu, L., Chen, X., & Li, C. (2014). Review: Pulsed Electric Fields Processing of Protein-Based Foods. *Food and Bioprocess Technology*, *7*(1), 114–125. https://doi.org/10.1007/s11947-012-1040-1

Zhao, W., & Yang, R. (2010). Experimental study on conformational changes of lysozyme in solution induced by pulsed electric field and thermal stresses. *Journal of Physical Chemistry B*, *114*(1), 503–510. https://doi.org/10.1021/jp9081189

Zhao, W., Yang, R., Lu, R., Tang, Y., & Zhang, W. (2007). Investigation of the mechanisms of pulsed electric fields on inactivation of enzyme: Lysozyme. *Journal of Agricultural and Food Chemistry*, *55*(24), 9850–9858. https://doi.org/10.1021/jf072186s

Zhao, W., Yang, R., & Zhang, H. Q. (2012). Recent advances in the action of pulsed electric fields on enzymes and food component proteins. *Trends in Food Science & Technology*, *27*(2), 83–96. https://doi.org/10.1016/j.tifs.2012.05.007

CHAPTER 3.

BETA-LACTOGLOBULIN`S THERMAL TRANSITIONS

3.1 INTRODUCTION

β-lg is the most abundant protein in whey, dominating its functional properties (Ramos et al., 2015). This small globular protein with 162 amino acids holds a central calix and has the ability to bind small hydrophobic molecules (Considine, Patel, Singh, & Creamer, 2005). Due to its industrial relevance, it has been the focus of many studies regarding its conformation and thermal stability. Consequently β-lg is a well-studied protein and often referred to as a model for globular protein´s behaviour, either on molecular stability and conformation as in aggregation and supramolecular structure formation (Kontopidis, Holt, & Sawyer, 2004). Extensive studies deal with β-lg interactions with other proteins, fatty acids, biopolymers and micronutrients; additionally its self-interactions are of major importance and result on the formation of diverse structures as self-supporting gels and several types of aggregates as nano and micro spherical aggregates and fibrillary amyloid-like structures (Kontopidis et al., 2004; Loveday, Anema, & Singh, 2017; Nicolai, Britten, & Schmitt, 2011). β-lg behaviour and stability change significantly with environmental conditions such as temperature, pH and salt content. Most reports refer to pH values close to neutral and relatively low ionic strength once these are the most physiologically relevant conditions (Bhattacharjee & Das, 2000). Its thermal denaturation involves multiple steps, comprehending a sequence of changes in tertiary and secondary structure. These phenomena may not take place simultaneously but rather sequentially or triggering each other (Burgos, Dassie, Villarreal, & Fidelio, 2012; Loveday, 2016; Seelig & Schönfeld, 2016). It is generally recognised that β-lg starts undergoing structural changes above 60 °C, and that these changes can become irreversible between 70 and 140 °C (Loveday, 2016). Despite the extensive literature on the subject, the sequence and extent of thermally induced structural changes and their impact on β-lg functionality are often inconsistent. One of the reasons for these inconsistencies arises from the fact that different reports use different sets of characterization techniques and experimental conditions, evaluating different aspects and effects of the thermally induced transition. Furthermore, in dairy science, protein denaturation is often evaluated indirectly by measuring consequences of the structural changes – i.e. reactivity of disulphide groups, surface hydrophobicity, change in elution time, solubility loss, aggregation – and not by evaluating the *in situ* unfolding events. Indeed, the temperature effects on protein structure result from several phenomena and they can only be characterized by a systematic series of studies using a set of complementary techniques. The use of "online" techniques, characterizing the events as they occur is fundamental way to disclose the complex unfolding pathways and reversible events.

The biophysical characterization of a protein as function of the temperatures is crucial to understand and control its conformation, biological activities and functional properties (Privalov & Gill, 1988; Thirumalai, Liu, O'Brien, & Reddy, 2013). Protein unfolding results in a rearrangement of the tertiary and secondary structure causing a protein to undergo a transition from a well-defined native state conformation to a partially or completely unfolded state (Rees & Robertson, 2001). In its simplest form, proteins' thermally induced transition is addressed by a two-step model in which the protein assumes only the folded and the unfolded states. In this model the temperature at which 50% of the protein molecules undergo unfolding is referred to as the melting temperature (T_m) (Ibarra-Molero, Naganathan, Sanchez-Ruiz, & Muñoz, 2016; Rees & Robertson, 2001). More recently, various multi-step models for protein unfolding have been suggested, as for many proteins thermal unfolding occurs through a progressive sequence of partially unfolded states (Bhattacharyya & Varadarajan, 2013; Seelig & Schönfeld, 2016). The intermediates that occur during protein folding-unfolding equilibrium can provide valuable information about the complex structural transition pathways and can be assessed through differential scanning calorimetry (DSC) and *in situ* spectroscopic techniques, such as CD, fluorescence spectroscopy and light scattering.

The aim of this chapter was to study β-lg thermally induced transitions using a new approach by monitoring the conformational and structural transitions involved during temperature increase. Data from thermodynamic and structural stability, obtained from DSC and CD, were correlated with auto-fluorescence (AF), fluorescent probe binding and static light scattering (SLS) providing a novel strategy to establish a more complete picture of the thermally induced events even below denaturation temperature. It is expected that this improved characterisation of the β-lg´s thermal unfolding can contribute to identify critical transition points and structural events, allowing to study MEF actions on the following chapter. Furthermore, this knowledge may contribute to milk and whey processing as for their technological applications aiming an *in situ* functionalization.

3.2 MATERIAL AND METHODS

3.2.1 Protein preparation

β-lg was purified from commercial whey protein isolate (Lacprodan DI-9212, Arla Foods, Viby, Denmark). The purification was performed by salting out method using the procedure of Maté and Krochta (1994) adapted according to Konrad, Lieske and Faber (2000) and finally freeze dried. Purity and conformation were checked by SDS-PAGE, HPLC, CD and fluorescence, matching in all

criteria a commercial β-lg from Sigma-Aldrich (lyophilized powder ≥ 90% PAGE). The complete characterization of the purified protein is presented in the supplementary material section.

β-lg solutions were prepared in 2.5 x 10^{-2} mol.L^{-1} phosphate buffer at pH 7.0. The solutions were kept under stirring for 2 h to ensure full solubilisation. The pH was then readjusted if needed with 1 mol.L^{-1} HCl or NaOH. For the DSC experiments, β-lg solutions of different concentrations were prepared in the same buffer just prior to the respective experiment and used immediately after full solubilisation. For the spectroscopic techniques, β-lg concentration was maintained at 1 x 10^{-4} mol.L^{-1} (0.184 mg.mL^{-1}). The protein concentration chosen was substantially lower than the critical association concentration reported for β-lg (Baussay, Bon, Nicolai, Durand, & Busnel, 2004; Mehalebi, Nicolai, & Durand, 2008), in an attempt to reduce association and aggregation to a neglectable extent. This allowed focusing on conformational and structural changes, otherwise hindered by association phenomena.

All chemicals were of analytic grade and purchased form Sigma-Aldrich (Steinheim, Germany). The water used for buffer preparation was purified through Milli-Q Ultrapure water purification system (Millipore, Bedford MA. USA)

3.2.2 Differential scanning calorimetry

After β-lg solution preparation, protein concentration was confirmed by UV-absorbance (absorbance at 280 nm, absorbance coefficient =0.9565 $m^2.g^{-1}$) and then transferred to the DSC cell after degassing for 15 min in the ThermoVac (Microcal/Malvern). DSC analysis was performed in a MicroCal VP-DSC microcalorimeter from Malvern (Worcestershire, UK). Blank experiments with phosphate buffer in both cells were performed overnight prior to sample loading, for subsequent blank correction. Samples were ran against the buffer in the reference cell, performing two successive heating and cooling scans for each sample, at a scanning rate of 1.5 °C min^{-1}, over the temperature range from 20 to 110 °C. In order to ascertain possible association/dissociation events, denaturation scans were performed at different concentrations, namely 4.98 x 10^{-4}, 1.57 x 10^{-4} and 4.7 x 10^{-5} mol.L^{-1}. All procedures regarding sample preparation and handling (lag time at low temperature, temperature scan rate, gain and filter period) were kept constant in all experiments, to ensure that all samples had the same thermal history. In all cases, the reported DSC curves were corrected for the respective blank experiment.

3.2.3 Circular dichroism measurements

CD measurements were performed on a Chirascan plus circular dichroism detector (Applied Photophysics, Leatherhead, U.K.). The samples were placed in a quartz cuvette with 1 cm light path, the temperature control was ensured by the Peltier element on the cuvette holder and magnetically stirred at 200 rpm to ensure homogeneity. CD spectra were obtained in the far-UV range (260-200 nm) and the CD signal at a fixed wavelength (208 nm) was collected as a function of temperature from 20 to 90 °C. Here and in all spectroscopic determinations, a scanning rate of 1 °C min^{-1} was used during the spectroscopic determinations. That scanning rate is a standard for low gradient scans, allowing the direct comparison of these results with those published in several literature reports. Furthermore, it has been stated that for β-lg the T_m obtained at this scanning rate (and below) is almost constant and close to the T_m value obtained when extrapolating the modelled results to scanning rates asymptotically approaching 0 °$C.min^{-1}$, thus eliminating kinetic effects (de Jongh, Gröneveld, & de Groot, 2001; Relkin & Mulvihill, 1996).

3.2.4 Steady-state fluorescence spectroscopy and static light scattering

All measurements were conducted on a PTi fluorescence RTC 2000 spectrometer (Photon Technology International, Ontario, Canada) with a T-configuration, using a 75-W Xenon arc lamp coupled to a monochromator. The samples were placed in a quartz cuvette with 1 cm light path and magnetically stirred at 200 rpm to ensure homogeneity. Illumination power was set at 5.5 μW for all determinations except where otherwise mentioned. Thermal effects on β-lg were followed on the RTC 2000 spectrometer using the Peltier element as a temperature control device and a water bath as heat sink. Temperature was scanned from cycles from 20 °C to 90 °C at a heating/cooling rate of 1 °$C.min^{-1}$. This procedure was adopted for all the determinations described below.

Time-based fluorescent emission kinetic traces (emission fixed at 350 nm) were obtained during the thermal ramps at a continuous 295 nm excitation. Before and after each thermal ramp session, excitation and emission spectra were acquired for both the protein (excitation 295 nm, emission 350 nm) and for the aromatic amino acids photoproducts (excitation 320 and 360 nm, emission 405 and 435 nm) (Correia, Neves-Petersen, Jeppesen, Gregersen, & Petersen, 2012).

8-anilino-1-naphthalenesulfonic acid (ANS) was used as a conformational probe. ANS stock solution (1.2×10^{-2} $mol.L^{-1}$) was prepared in methanol and stored in the dark at 4 °C. Final concentration

of ANS used in the protein solution was 5 x 10^{-4} mol.L^{-1} and after excitation at 370 nm the fluorescence emission at 480 nm was recorded.

SLS experiments were performed by illuminating the sample at 532 nm, and collecting the light scattered at the same wavelength at 90° with respect to the light source.

3.2.5 Data analysis

All data analysis, plotting and fitting procedures were performed on Origin 8.1 software (OriginLab Corporation, Northampton, MA, USA). In the case of DSC, Origin 7 with the dedicated DSC module was used in data analysis. All spectroscopic determinations were obtained at least in triplicate and presented as average of the several accumulations. All intensity profiles were smoothed using a 10 points adjacent averaging filter and normalized by dividing each data point by the initial intensity value of the fresh sample.

For the DSC experiments, the protein scan was corrected to the buffer-buffer scan, the data normalized to the protein concentration in each case, and data curves treated with different models.

3.3 RESULTS AND DISCUSSIO

3.3.1 Differential scanning calorimetry

DSC measures directly the heat absorbed during the conformational transitions and is therefore a essential method for a complete thermodynamic analysis of the unfolding process. The DSC curve for the experiment performed at 4.98 x10^{-4} mol.L^{-1} is shown in Figure 3.1. It is clear from the asymmetry and width of the curve that the protein does not denature through a simple 2-state transition nor is it a highly cooperative transition. In fact, attempts to adjust a 2-state model gave a very poor representation of the denaturation curve. Therefore, models considering multiple transitions state were attempted. These multi-step models involve the increase in flexibility of the protein chains, followed by the collapse of some groups, culminating on energetically significant structural transitions (Bhattacharjee & Das, 2000; Semisotnov et al., 1991). The optimal results were obtained for the model considering that protein denaturation proceeds via three transitions (four-state unfolding). The deconvolution of the original curve into three Gaussian curves can be seen in Figure 3.1 with an excellent agreement between the original curve and the total fitted curve.

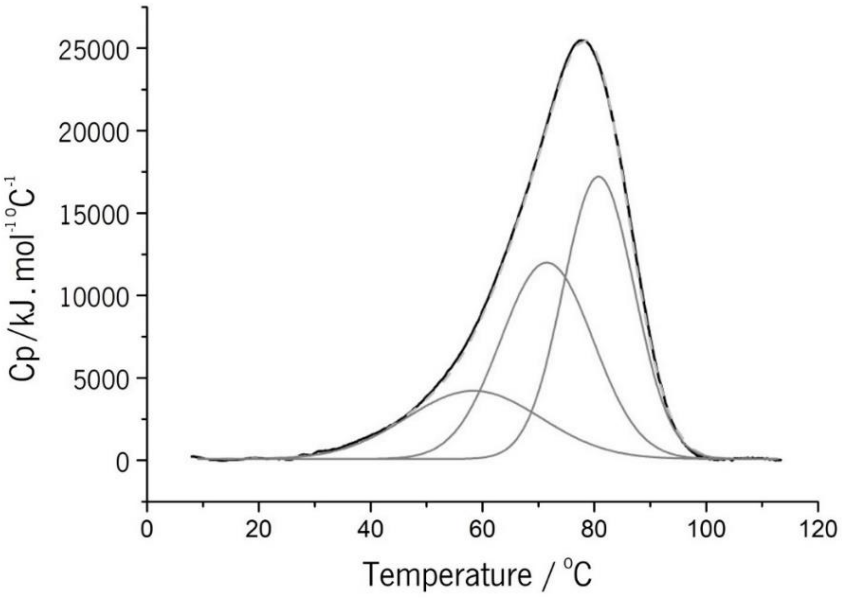

Figure 3.1: DSC profile (black line) for the denaturation of β-lg with concentration 4.98 x 10^{-4} mol.L^{-1} in 2.5 x 10^{-2} mol.L^{-1} phosphate buffer at pH 7.0; three curves resulting from the deconvolution to a three-state transition (grey lines) and the total fitted curve (dashed line).

The experimental curve was integrated to retrieve the calorimetric enthalpy, leading to a value of 525 kJ mol^{-1}. The parameters for the four-state unfolding are T_1 = 61.0 °C, H_1 = 101 kJ.mol^{-1}, T_2 = 72.7 °C, H_2 = 201 kJ.mol^{-1} and T_3 = 81.0 °C, H_3 = 223 kJ.mol^{-1}. It should be noted that although the four-state model did provide the best results, the fitting to a 3-state unfolding (2 transitions) also resulted on a rather acceptable fitting of the DSC results (results not shown). In any case, these results show that β-lg does not follow a single cooperative unfolding – rather indicate that different segments of the molecule may melt independently of one another.

The occurrence of possible association/dissociation events during the thermal scans can interfere with the DSC results. In order to validate the obtained results, the DSC experiments were repeated at lower concentrations (i.e. 1.57 x 10^{-4} and 4.7 x 10^{-5} mol.L^{-1}) and check if the transition temperatures changed with concentration. The denaturation profiles were similar at the three studied concentrations, and only the fitting to a 4-state unfolding model (three transitions) provided good results in all cases; only the transition temperatures changed, increasing somewhat with the decrease in protein concentration. This effect has been previously reported in similar conditions (Qi, Brownlow, Holt, & Sellers, 1995). Further DSC studies and refined models that cope with association upon denaturation are needed to fully disclosure this concentration dependence.

3.3.2 Circular dichroism

CD spectroscopy on the far-UV range was used to follow the structural changes of β-lg upon heating (Figure 3.2). From the spectra of the protein, plotted between 260 and 200 nm, for 20 °C, 90 °C and after cooling back to 20 °C (see Figure 3.2A), significant structural changes can be noticed. During the heating cycle as the decrease in ellipticity, especially below 210 nm, can be interpreted as the collapse of the secondary structure of β-lg at 90 °C (Griffin, Griffin, Martin, & Price, 1993).

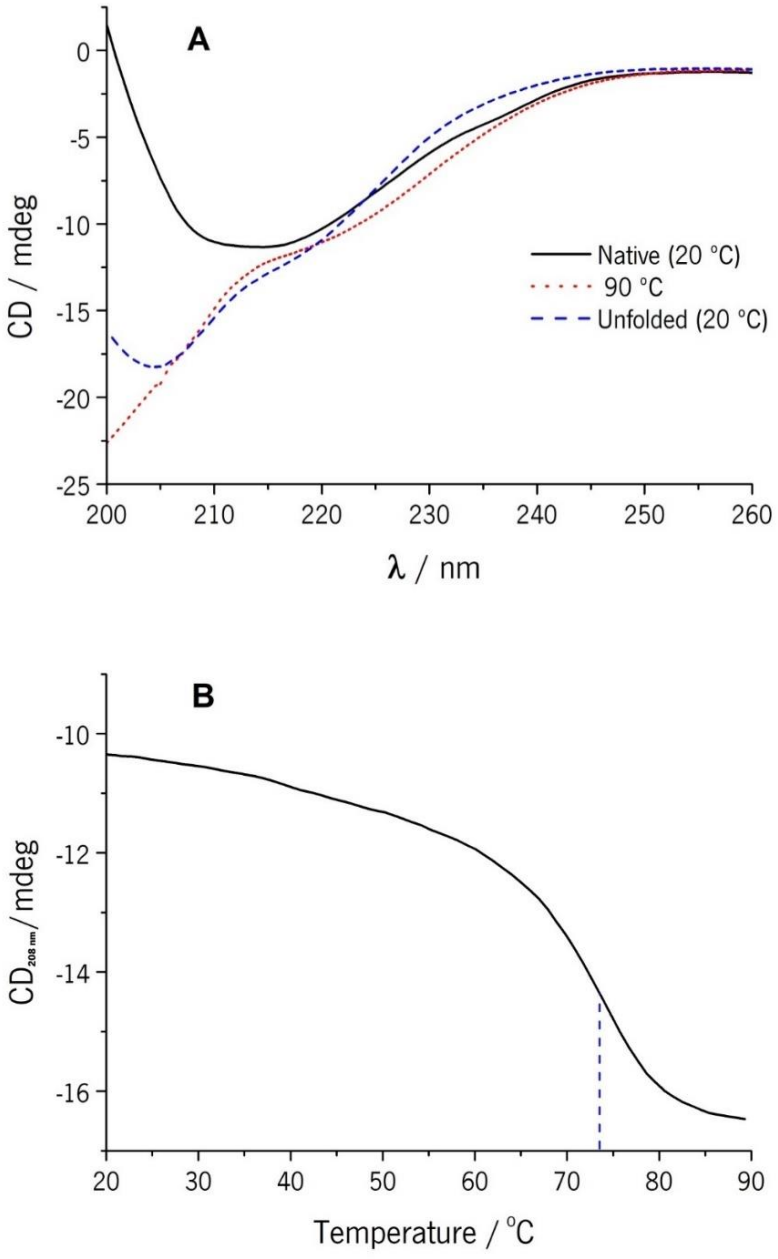

Figure 3.2: A - CD spectra of β-lg at 20 °C, at 90 °C and cooled down back to 20 °C; B - CD signal at 208 nm during heating until 90 °C (vertical line indicates the middle point of the transition given by the first derivative of the curve).

As expected, the spectra collected at 20 °C before and after heating to 90 °C are different, showing that heating to 90 °C causes irreversible denaturation of at least part of the protein. The difference between the spectra at 20 °C after cooling from 90 °C from the one collected at 90 °C indicates that the protein suffered a partial refolding during the cooling down process. It is well established that many proteins do not unfold completely after T_m, retaining a significant fraction of secondary structure and conformation or partially refolding into a different conformation once the temperature is decreased. The occurrence of these partially unfolded/refolded species with loss of tertiary structure, maintaining significant fractions of secondary structure, are often referred to as "molten globules" (Bhattacharyya & Varadarajan, 2013; Semisotnov et al., 1991).

Considering the changes in the β-lg's CD spectra, the variations of ellipticity at 208 nm were tracked during the heating cycle and used as an indicator of the structural changes occurring during the process. From Figure 3.2B it is clear that a transition takes place, particularly between 60 °C and 80 °C, which can be related with the secondary structure transition of the protein (Greenfield, 2007). Taking the derivative of the CD signal, the middle point of the structural transition can be determined, given by the temperature value at the inflexion point. This transition takes place at 73.8 °C (marked on the figure by the vertical dashed line).

3.3.3 Assessment of conformational changes

β-lg AF intensity is mostly resultant from the two Trp residues and therefore in this study, β-lg fluorescence was obtained in conditions specific to follow Trp exposure (excitation 295 nm, emission 350 nm). It is generally accepted that the microenvironment of Trp on the protein affects its relative fluorescence, thus factors resulting from conformational modifications such as solvent exposure or changes in the distance to neighbouring amino acids result in fluorescence changes (Busti, Scarpeci, Gatti, & Delorenzi, 2002). Protein association and aggregation is possible to occur at temperatures above 60 °C and can also contribute to fluorescence intensity modifications. However these phenomena were prevented by carrying the experiments below the reported critical association concentration, further their absence was also corroborated by SLS data presented further on this section.

Several studies identified fluorescence intensity reduction during the thermal increase of protein solution, attributing these changes to the occurrence of structural modifications on the protein

(Bhattacharjee & Das, 2000; Cairoli, Iametti, & Bonomi, 1994; Fessas, Iametti, Schiraldi, & Bonomi, 2001). Fluorescence emission is expected to decay with temperature increase due to collisional quenching (Lakowicz, 2006). This is the result of entropy increase, causing an intensification in collisions between excited state fluorophores and other molecules in solution leading to their deactivation. In order to differentiate structural modification form collisional quenching and establish a base-line for the fluorescence decay resulting from collisional quenching, the fluorescence of pure Trp solution was followed on the same conditions (i.e. molar ratio, buffer, heating rate and light intensity) as for β-lg. The comparison between the fluorescence scan of Trp solutions and β-lg can be seen in Figure 3.3A. The β-lg's fluorescence scan during temperature increase and decrease for samples for a series of heating cycles between 20 and 50, 60, 70 or 90 °C is shown in Figure 3.3B.

A single exponential decay model (Eq.3.1) was fitted to the data of Trp fluorescence intensity profile as function of temperature, where the fluorescence intensity (F) is described by the pre-exponential factor A_0, the decay constant τ, and the temperature T.

$$F = A_0 . e^{(-\tau . T)} \qquad (3.1)$$

The values obtained from this model have shown an excellent fit ($R^2 > 0.999$). This is in agreement with the described model for fluorescence decay involved in collisional quenching (Gratton, Jameson, Weber, & Alpert, 1984; Lakowicz, 2006). Adjusting the same model to the β-lg's fluorescence data only, resulted in a satisfactory fit for the temperature range 20-50 °C; above this temperature the fluorescence intensity drifts form the Trp collisional quenching profile. Fluorescence intensity may suffer variations due to a) conformational changes resulting in Trp re-positioning, b) changes in neighbouring amino acids or c) modified solvent exposure (Bhattacharjee & Das, 2000).

Fluorescence scans were performed cyclically, from 20 °C up to four different temperatures and back to 20 °C, namely: 20 °C → 90 °C → 20 °C, 20 °C → 70 °C → 20 °C, 20 °C → 60 °C → 20 °C and 20 °C → 50 °C → 20 °C (see Figure 3.3B). For all the cases, the ascending temperature scans overlapped perfectly, whereas for the descending scans, they diverged according with the denaturation degree and reversible/irreversible nature of the structural changes induced by the treatment. Therefore, in the 50-75 °C interval the changes observed in the fluorescence profile were caused by structural changes associated with a partial loss of tertiary

structure. At the temperature of 75 °C a second shift in the fluorescence profile was observed, and until 90 °C the fluorescence decays again on a profile consistent with collisional quenching.

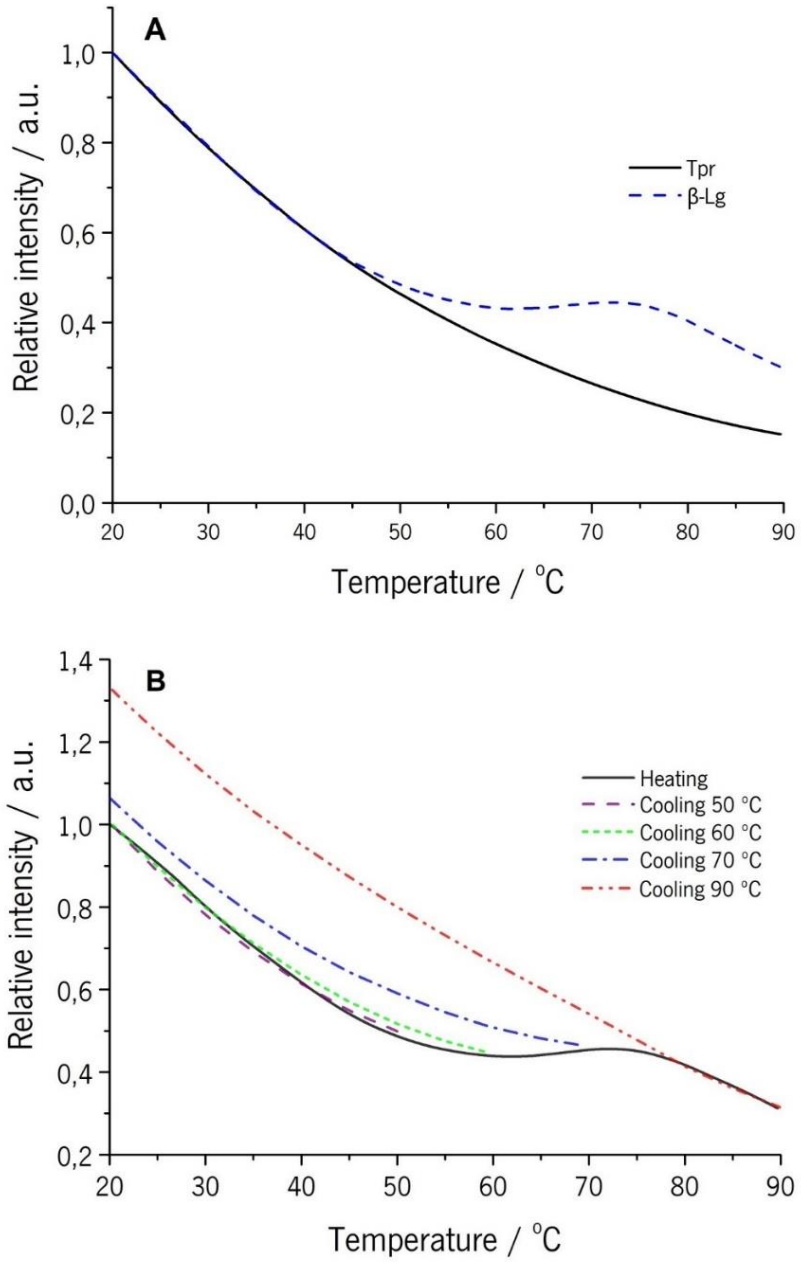

Figure 3.3: A - Fluorescence intensity of Trp and β-lg at excitation of 295 nm and emission of 350 nm, as function of temperature; B - Fluorescent intensity profiles for heating up to 90 ° and cooling from 50 °C, 60°C, 70 °C and 90 °C.

In the cycle reaching 90 °C, the heating and cooling fluorescence scans overlap above ≈78 °C. This behaviour is consistent with collisional quenching of the Trp signal by the solute molecules and suggests that no further significant changes on the Trp microenvironment take place in this

temperature range, thus the transition is complete above 78 °C. As the temperature descends to 20 °C again, the fluorescence intensity is substantially higher than the initial value, indicating large modifications in the protein structure. On the scans descending from 70 °C to 20 °C the fluorescence profile immediately diverges from the corresponding heating scan, also suggesting the irreversibility of the modifications in the protein's conformation. The fluorescence scanning descending from 60 °C to 20 °C is slightly different from the corresponding heating scan, eventually merging for temperatures below ≈ 35 °C. This indicates that the changes occurred until 60 °C are reversible. The fluorescence profiles obtained during the temperature cycling from 20 °C to 50 °C and back to 20 °C overlap – and so does the pure Trp scan – indicating that only collisional quenching is occurring. This means that no rearrangement on Trp positioning and thus no significant structural changes took place within this temperature interval. The reversibility of the structural changes occurring in β-lg below 60 °C has been established by previous studies (Bhattacharjee & Das, 2000; Cairoli et al., 1994; Tolkach & Kulozik, 2007). However, this approach is unique in exploring these phenomena *in situ*, during the thermal scans and with a series of heating cycles between different temperatures. Further, the existing studies did not consider the effects of collisional quenching, often attributing the decrease of fluorescence to structural changes or self-quenching or even reversible structural modifications, while in some of the cases collisional quenching could be the main reason for the observed behaviour. With presented methodology, it was possible to differentiate these phenomena occurring simultaneously and precisely pinpoint the thermally-induced transitions.

The use of the extrinsic fluorescent probe ANS offers additional possibilities for protein characterization and thermal transitions' determination. This extrinsic dye interacts with proteins mainly via non-specific hydrophobic interactions, (although electrostatic interactions can also be involved) and are sensitive to conformational changes and to hydrophobic pockets' accessibility (Hawe, Sutter, & Jiskoot, 2008). ANS binds to β-lg in its native form by interacting mainly with the opening of the hydrophobic calix, involving low energy values - i.e. -26 to -23 $kJ.mol^{-1}$ (Collini et al., 2003; Collini, D'Alfonso, & Baldini, 2000). Due to the non-specific interaction nature of ANS binding and the dynamics of the protein structure, changes in the protein conformation will impact its affinity to ANS (D'Alfonso, Collini, & Baldini, 1999). Figure 3.4 shows the fluorescence profile of ANS in the presence of β-lg for the thermal cycles (from 20 °C to 90 °C, 70 °C, 60 °C or 50 °C and back to 20 °C) as described previously. The binding of ANS to native β-lg was confirmed

through the control sample performed without the protein (ANS in buffer solution). The fluorescence intensity in the presence of β-lg increased about 5 times and a substantial blue shift was observed.

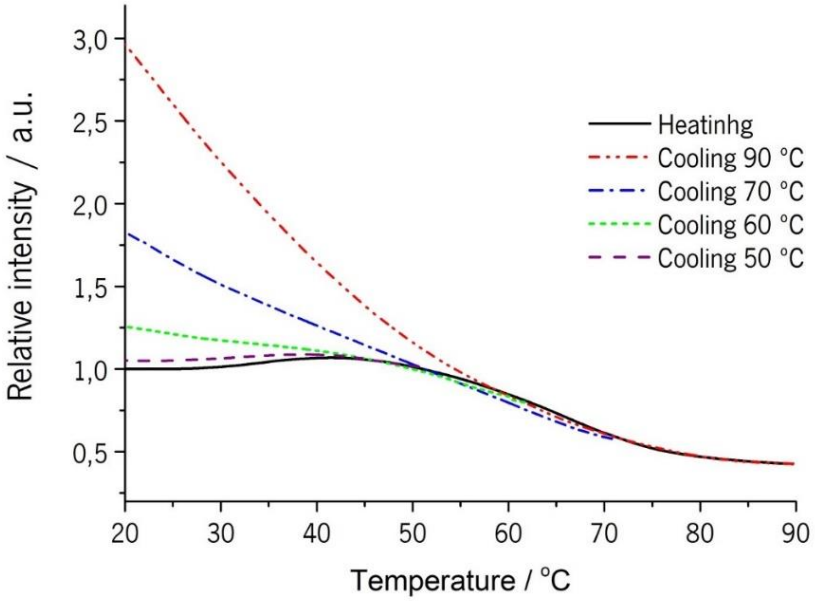

Figure 3.4: Fluorescence intensity of hydrophobic dye ANS during heating to 90 °C (continuous line), and cooling from 50 °C, 60°C, 70 °C and 90 °C in the different dashed lines.

ANS fluorescence was constant between 20 °C to 30 °C suggesting that the binding to β-lg and the microenvironment is unchanged. From 30 °C to 45 °C, an increase of 10% in ANS fluorescence was observed, possibly caused by the increase of the protein structural dynamics (i.e. side-chains and loops flexibility or structure swelling), thus facilitating the access of the probe to the opening of the calix (Collini et al., 2000). It is expected that the exposure of the hydrophobic sites occurs during heating, as conformational and structural changes take place. This exposure would result in an increased binding of ANS to the protein. However the ANS fluorescence decreases above 45 °C, attenuating around 75 °C and remaining almost constant above this temperature. Despite of the occurrence of structural changes and the exposure of potential ANS binding sites, the probe is actually detaching from the protein. Due to the low energy involved in ANS binding and the entropy increase during heating, the binding equilibrium must be limited by free energy associated with the entropy increase, overcoming the affinity between the protein and ANS. During the cooling stage of the thermal cycles, the fluorescence profiles partially follow the inverse path of the heating profiles until a point where the profiles diverge. These diverging points must coincide with the temperature where the probe affinity overcomes the entropy of the system and ANS binds again to

the protein. In all the thermal cycles, with exception of the one reaching 50 °C, the fluorescence intensity increases substantially with the temperature reduction. The points at which the fluorescence profiles during cooling diverge from the fluorescence profiles during heating are positively correlated with the maximum temperature attained in each cycle. This suggests that the increase in exposure temperature - and the consequent structural changes - results in the creation of more binding sites and/or in a concomitant higher affinity to ANS. It is interesting to notice that contrasting with the AF determinations, the increased binding of ANS to β-lg exposed to 60 °C suggests the occurrence of irreversible conformational changes. This either supports that ANS is more sensitive to transient states in protein conformation (Hawe, Sutter, & Jiskoot, 2008) or that it impairs the refolding process by disturbing the hydrophobic interactions. For the fluorescence scanning cycling between 20 °C to 50 °C and back to 20 °C again, the ANS fluorescence remains at levels near the maximum observed at 45 °C, suggesting that besides the increase in the access to the calix, no further binding sites were created nor the affinity increased by exposure at 50 °C.

The progressive increase in flexibility and disorder of the protein structure caused by thermal stress also results in the unpacking of the structure and increase of the radius of the hydrated protein, thus allowing this process to be followed by light scattering techniques (Xu, 2015). The scattering profile of β-lg solution at 532 nm during the heating and cooling cycle between 20 to 90 °C is presented in Figure 3.5. It is clear that the hydrodynamic radius of β-lg increases in response to the temperature increase. These observations agree with the multistep model for protein unfolding, where the increase in flexibility of the peptide chain and loss of tertiary and secondary structures, lead to the unpacking of protein conformation. It is clear that the hydrodynamic radius of β-lg increases in response to the temperature increase. These observations agree with the multistep model for protein unfolding, where the increase in flexibility of the peptide chain and loss of tertiary and secondary structures, lead to the unpacking of protein conformation. This process culminates with protein melting, reaching a maximum hydration radius. In the temperature range 30-40 °C the SLS intensity starts to increase, correlating with the observation of an increase in ANS fluorescence. This corroborates the hypothesis of the initial expansion in this temperature range, facilitating access of ANS to the central calix. The plateau reached during 75 °C to 90 °C corresponds to a structural stabilization after the unfolding took place. This is the confirmation that after the transition culminating at 75 °C, no further significant changes occur in the protein conformation in the interval of temperatures tested. The stabilization of the scattering intensity after denaturation also supports the inexistence of association phenomena, as the scattering intensity

would substantially increase if higher molecular weight species were formed. By following the cooling processes, a decrease in SLS intensity between 90 °C and 70 °C is indicative of a partial refolding, corroborating the observation in the CD spectra presented above.

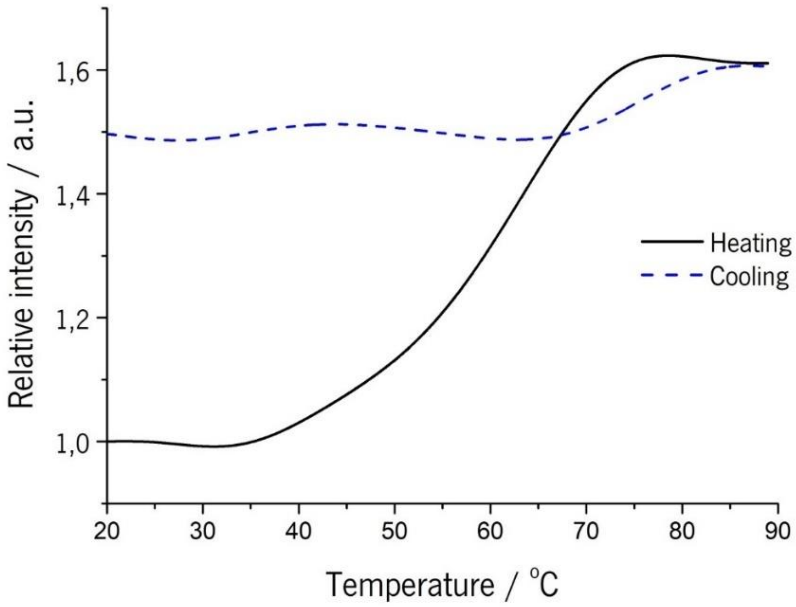

Figure 3.5: Scattering intensity of β-lg during heating and cooling.

3.3.4. Unfolding mechanism

The use of different "online" techniques has shown to be productive, as all of them allowed obtaining information about structural features and thermally induced effects and transitions. Correlating the data obtained from the different determinations allows stablishing the sequence and a clear understanding of the events involved in β-lg thermal unfolding. Table 3.1 presents the midpoint transition temperatures obtained by each technique.

Table 3.1: Transition points of β-lg given by different techniques.

Technique	**DSC**	**CD**	**Fluorescence (AF)**	**ANS**	**SLS**
Transition point (°C)	61.0, 72.7 and 81.0	73.8	67.5 and 83.7	34.9 and 66.3	66.5

It is generally accepted a multistep mechanism in β-lg thermal unfolding, (de Wit, 2009; Fessas et al., 2001; Loveday, 2016). Classically protein-unfolding events are characterized by the energetic and structural transitions obtained by DSC and CD analysis. The CD midpoint transition is concordant with the second of the three discreet transitions observed by DSC and it would be safe to consider this as the denaturation temperature of the protein, in the context of a two-state unfolding model. Nonetheless the other two transitions detected by DSC and the complementary data from AF, ANS binding and SLS provide additional information about other structural and local conformational events resulting from the temperature increase and denaturation. In literature, it is often reported that at 60 °C β-lg starts to undergo structural changes. The great majority of these reports involve methodologies where denaturation is typically measured by indirect effects (i.e. aggregation, solubility change, chromatography, among others) or by spectroscopic observations after cycling the temperature from room temperature to a target temperature and back to room temperature again. As consequence of these methods being performed "offline", they are only able to detect irreversible changes in the proteins structure (Loveday, 2016). Only a few authors addressed the existence of reversible thermal changes in β-lg, however limitations in real-time monitoring and the absence of quenching considerations impaired an accurate characterization of these events. In the present work, real time monitoring during thermal scanning allowed to observe early and reversible conformational changes as they occurred, and to establish a more detailed sequence of events during β-lg unfolding, resulting on the proposed mechanism presented in figure 3.6. The results obtained reveal reversible conformational changes occurring above 35 °C and irreversible above 60 °C. The earlier event during thermal increase is an expansion of the protein´s hydrodynamic radius detected by SLS and coincident with an increase of ANS florescence. Above 50 °C the Trp fluorescence shift suggests changes in local positioning of Trp and neighbour amino acids and over 60 °C these changes become irreversible. These events are consistent with the fist energetic transition detected by DSC which corroborates the permanent character of the structural changes above this temperature.

Between 66.3 and 67.5 °C were obtained the midpoint of the AF, ANS and SLS transitions, implying significant structural changes affecting not only the proteins hydrodynamic radius, but also Trp solvent exposure and ANS affinity. Some authors have reported that the partial loss of secondary structure, particularly α-helical content, occurs between 60 and 70 °C (de Wit, 2009; Ql et al., 1997). This would contribute to the disruption of the globular conformation, increase the hydrodynamic radius of the protein and increase the exposure of Trp and hydrophobic sites, being

consistent with the observations reported here. DSC and AF detect a later transition above 80 °C and above this temperature the profiles obtained by CD, auto-fluorescence, ANS and SLS remain unchanged. This can be interpreted as a stabilization of the remaining protein´s fold and the culmination of the thermal induced effects in the temperature range studied.

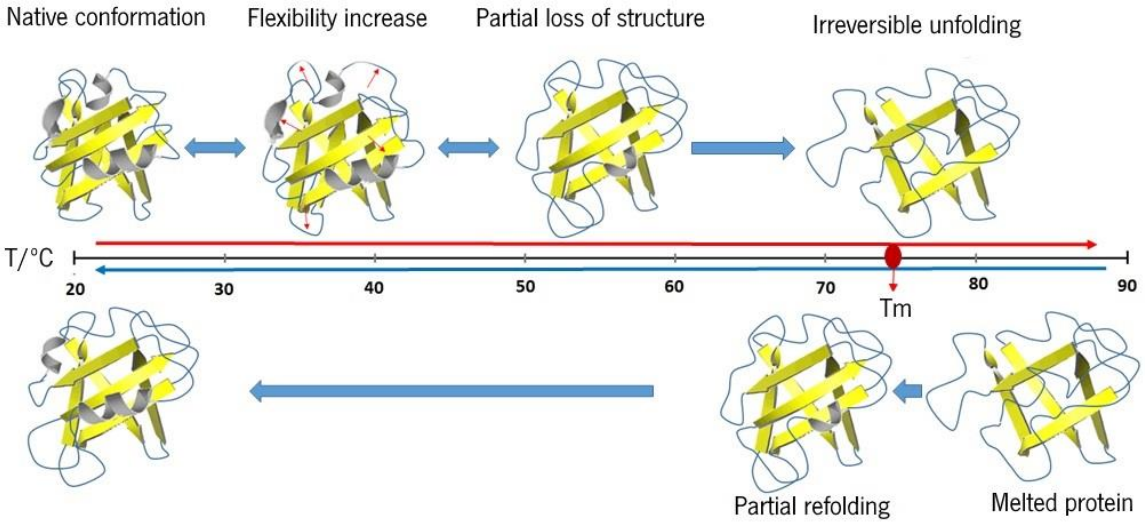

Figure 3.6: Proposed unfolding/refolding mechanism of β-lg.

β-lg presents a highly dynamic structural behaviour as a function of factors such as pH or ionic strength, allowing the protein to undergo several transitions and assume different conformations. These structural dynamics are associated with the presence of a central hydrophobic cavity instead of a compact hydrophobic core (Gutiérrez-Magdaleno, Bello, Portillo-Téllez, Rodríguez-Romero, & García-Hernández, 2013). The free-energy associated with this is compensated by a rigid β-barrel forming the core of the structure and by the entropy associated to changes in the flexible loops at the barrel extremities (Jameson, Adams, & Creamer, 2002). The observations made in this study reflect the dynamic structural properties as a function of temperature. The multi-step thermal transition corroborated by several techniques confirms the complexity of the thermally induced effect on the protein´s structure. The reversible structural changes observed below the first thermal transition (35-60 °C) are a clear sign of a high dynamic behaviour of β-lg, usually not addressed in research, nor considered in industrial applications. The methodology used allowed a more precise and detailed description of the unfolding/refolding pathways of β-lg. This contributes to a better understanding of these complex phenomena and represents one more step towards improving and controlling protein functionality.

3.4 CONCLUSIONS

In the work presented in this Chapter, the thermal stability of β-lg was assessed using calorimetric and spectroscopic techniques through an *in-situ* approach. The interpretation of complementary information obtained by each technique allowed unravelling some of the very complex structural dynamics in terms of three discrete thermal transitions. The existence of reversible conformational changes occurring at low temperatures (35-60 °C) were confirmed and differentiated from the quenching phenomenon. The methodology defined here is a simple and efficient way to characterize proteins' thermally-induced transitions. The observed conformational changes and complex transition behaviour upon thermal stress is a key to understand and control β-lg's functionality and thus the improved characterization of these phenomena is one more step towards new approaches in future research and applications involving β-lg and whey protein systems. This knowledge is crucial to establish a background for the study of MEF effects during thermo-electric treatments addressed on the following chapter of this thesis.

3.5 REFERENCES

Baussay, K., Bon, C. Le, Nicolai, T., Durand, D., & Busnel, J.-P. (2004). Influence of the ionic strength on the heat-induced aggregation of the globular protein β-lactoglobulin at pH 7. *International Journal of Biological Macromolecules*, *34*(1–2), 21–28. https://doi.org/10.1016/j.ijbiomac.2003.11.003

Bhattacharjee, C., & Das, K. P. (2000). Thermal unfolding and refolding of β-lactoglobulin. *European Journal of Biochemistry*, *267*(13), 3957–3964. https://doi.org/10.1046/j.1432-1327.2000.01409.x

Bhattacharyya, S., & Varadarajan, R. (2013). Packing in molten globules and native states. *Current Opinion in Structural Biology*, *23*(1), 11–21. https://doi.org/10.1016/j.sbi.2012.10.010

Burgos, I., Dassie, S. A., Villarreal, M. A., & Fidelio, G. D. (2012). Thermodynamic and structural analysis of homodimeric proteins: Model of β-lactoglobulin. *Biochimica et Biophysica Acta - Proteins and Proteomics*, *1824*(2), 383–391. https://doi.org/10.1016/j.bbapap.2011.11.005

Busti, P., Scarpeci, S., Gatti, C., & Delorenzi, N. (2002). Use of fluorescence methods to monitor unfolding transitions in β-lactoglobulin. *Food Research International*, *35*(9), 871–877. https://doi.org/10.1016/S0963-9969(02)00096-0

Cairoli, S., Iametti, S., & Bonomi, F. (1994). Reversible and irreversible modifications of β-lactoglobulin upon exposure to heat. *Journal of Protein Chemistry*, *13*(3), 347–354. https://doi.org/10.1007/BF01901568

Collini, M., D'Alfonso, L., & Baldini, G. (2000). New insight on β-lactoglobulin binding sites by 1-anilinonaphthalene-8-sulfonate fluorescence decay. *Protein Science*, *9*(10), 1968–1974. https://doi.org/10.1110/ps.9.10.1968

Collini, M., D'Alfonso, L., Molinari, H., Ragona, L., Catalano, M., & Baldini, G. (2003). Competitive binding of fatty acids and the fluorescent probe 1-8-anilinonaphthalene sulfonate to bovine β-lactoglobulin. *Protein Science*, *12*(8), 1596–1603. https://doi.org/10.1110/ps.0304403

Considine, T., Patel, H. a, Singh, H., & Creamer, L. K. (2005). Influence of Binding of Sodium Dodecyl Sulfate, All- trans -retinol, Palmitate, and 8-Anilino-1-naphthalenesulfonate on the Heat-Induced Unfolding and Aggregation of β-Lactoglobulin B. *Journal of Agricultural and Food Chemistry*, *53*(8), 3197–3205. https://doi.org/10.1021/jf0481756

Correia, M., Neves-Petersen, M. T., Jeppesen, P. B., Gregersen, S., & Petersen, S. B. (2012). UV-Light Exposure of Insulin: Pharmaceutical Implications upon Covalent Insulin Dityrosine Dimerization and Disulphide Bond Photolysis. *PLoS ONE*, *7*(12), e50733. https://doi.org/10.1371/journal.pone.0050733

D'Alfonso, L., Collini, M., & Baldini, G. (1999). Evidence of heterogeneous 1-anilinonaphthalene-8-sulfonate binding to β-lactoglobulin from fluorescence spectroscopy. *Biochimica et Biophysica Acta (BBA) - Protein Structure and Molecular Enzymology*, *1432*(2), 194–202. https://doi.org/10.1016/S0167-4838(99)00105-3

de Jongh, H. H. J., Gröneveld, T., & de Groot, J. (2001). Mild Isolation Procedure Discloses New Protein Structural Properties of β-Lactoglobulin. *Journal of Dairy Science*, *84*(3), 562–571. https://doi.org/10.3168/jds.S0022-0302(01)74508-0

de Wit, J. N. (2009). Thermal behaviour of bovine β-lactoglobulin at temperatures up to 150°C. a

review. *Trends in Food Science & Technology*, *20*(1), 27–34. https://doi.org/10.1016/j.tifs.2008.09.012

Fessas, D., Iametti, S., Schiraldi, A., & Bonomi, F. (2001). Thermal unfolding of monomeric and dimeric β-lactoglobulins. *European Journal of Biochemistry*, *268*(20), 5439–5448. https://doi.org/10.1046/j.0014-2956.2001.02484.x

Gratton, E., Jameson, D. M., Weber, G., & Alpert, B. (1984). A model of dynamic quenching of fluorescence in globular proteins. *Biophysical Journal*, *45*(4), 789–794. https://doi.org/10.1016/S0006-3495(84)84223-X

Greenfield, N. J. (2007). Using circular dichroism collected as a function of temperature to determine the thermodynamics of protein unfolding and binding interactions. *Nature Protocols*, *1*(6), 2527–2535. https://doi.org/10.1038/nprot.2006.204

Griffin, W. G., Griffin, M. C. A., Martin, S. R., & Price, J. (1993). Molecular basis of thermal aggregation of bovine β-lactoglobulin A. *J. Chem. Soc., Faraday Trans.*, *89*(18), 3395–3405. https://doi.org/10.1039/FT9938903395

Gutiérrez-Magdaleno, G., Bello, M., Portillo-Téllez, M. C., Rodríguez-Romero, A., & García-Hernández, E. (2013). Ligand binding and self-association cooperativity of β-lactoglobulin. *Journal of Molecular Recognition*, *26*(2), 67–75. https://doi.org/10.1002/jmr.2249

Hawe, A., Sutter, M., & Jiskoot, W. (2008). Extrinsic Fluorescent Dyes as Tools for Protein Characterization. *Pharmaceutical Research*, *25*(7), 1487–1499. https://doi.org/10.1007/s11095-007-9516-9

Ibarra-Molero, B., Naganathan, A. N., Sanchez-Ruiz, J. M., & Muñoz, V. (2016). Modern Analysis of Protein Folding by Differential Scanning Calorimetry. In *Methods in Enzymology* (Vol. Volume 567, pp. 281–318). https://doi.org/10.1016/bs.mie.2015.08.027

Jameson, G. B., Adams, J. J., & Creamer, L. K. (2002). Flexibility, functionality and hydrophobicity of bovine β-lactoglobulin. *International Dairy Journal*, *12*(4), 319–329. https://doi.org/10.1016/S0958-6946(02)00028-6

Kontopidis, G., Holt, C., & Sawyer, L. (2004). Invited Review: β-Lactoglobulin: Binding Properties, Structure, and Function. *Journal of Dairy Science*, *87*(4), 785–796. https://doi.org/10.3168/jds.S0022-0302(04)73222-1

Lakowicz, J. R. (2006). *Principles of Fluorescence Spectroscopy*. (J. R. Lakowicz, Ed.), *Principles of fluorescence spectroscopy, Springer, New York, USA, 3rd edn, 2006.* Boston, MA: Springer US. https://doi.org/10.1007/978-0-387-46312-4

Loveday, S. M. (2016). β-Lactoglobulin heat denaturation: A critical assessment of kinetic modelling. *International Dairy Journal*, *52*, 92–100. https://doi.org/10.1016/j.idairyj.2015.08.001

Loveday, S. M., Anema, S. G., & Singh, H. (2017). β-Lactoglobulin nanofibrils: The long and the short of it. *International Dairy Journal*, *67*, 35–45. https://doi.org/10.1016/j.idairyj.2016.09.011

Mehalebi, S., Nicolai, T., & Durand, D. (2008). Light scattering study of heat-denatured globular protein aggregates. *International Journal of Biological Macromolecules*, *43*(2), 129–135. https://doi.org/10.1016/j.ijbiomac.2008.04.002

Nicolai, T., Britten, M., & Schmitt, C. (2011). β-Lactoglobulin and WPI aggregates: Formation, structure and applications. *Food Hydrocolloids*, *25*(8), 1945–1962. https://doi.org/10.1016/j.foodhyd.2011.02.006

Privalov, P. L., & Gill, S. J. (1988). Stability of Protein Structure and Hydrophobic Interaction. In *Advances in Protein Chemistry* (Vol. 39, pp. 191–234). https://doi.org/10.1016/S0065-3233(08)60377-0

Qi, X. L., Brownlow, S., Holt, C., & Sellers, P. (1995). Thermal denaturation of β-lactoglobulin: effect of protein concentration at pH 6.75 and 8.05. *Biochimica et Biophysica Acta (BBA) - Protein Structure and Molecular Enzymology*, *1248*(1), 43–49. https://doi.org/10.1016/0167-4838(94)00225-6

QI, X. L., HOLT, C., MCNULTY, D., CLARKE, D. T., BROWNLOW, S., & JONES, G. R. (1997). Effect of temperature on the secondary structure of β -lactoglobulin at pH 6.7, as determined by CD and IR spectroscopy: a test of the molten globule hypothesis. *Biochemical Journal*, *324*(1), 341–346. https://doi.org/10.1042/bj3240341

Ramos, O. L., Pereira, R. N., Rodrigues, R. M., Teixeira, J. A., Vicente, A. A., & Malcata, F. X. (2015). *Whey and Whey Powders: Production and Uses*. *Encyclopedia of Food and Health*. https://doi.org/10.1016/B978-0-12-384947-2.00747-9

Rees, D. C., & Robertson, A. D. (2001). Some thermodynamic implications for the Thermostability of Proteins. *Protein Science*, (3), 1187–1194. https://doi.org/10.1110/ps.180101.

Relkin, P., & Mulvihill, D. M. (1996). Thermal unfolding of β-lactoglobulin, α-lactalbumin, and bovine serum albumin. A thermodynamic approach. *Critical Reviews in Food Science and Nutrition*, *36*(6), 565–601. https://doi.org/10.1080/10408399609527740

Seelig, J., & Schönfeld, H.-J. (2016). Thermal protein unfolding by differential scanning calorimetry and circular dichroism spectroscopy Two-state model versus sequential unfolding. *Quarterly Reviews of Biophysics*, *49*(July), e9. https://doi.org/10.1017/S0033583516000044

Thirumalai, D., Liu, Z., O'Brien, E. P., & Reddy, G. (2013). Protein folding: from theory to practice. *Current Opinion in Structural Biology*, *23*(1), 22–29. https://doi.org/10.1016/j.sbi.2012.11.010

Tolkach, A., & Kulozik, U. (2007). Reaction kinetic pathway of reversible and irreversible thermal denaturation of β-lactoglobulin. *Le Lait*, *87*(4–5), 301–315. https://doi.org/10.1051/lait:2007012

Xu, R. (2015). Light scattering: A review of particle characterization applications. *Particuology*, *18*, 11–21. https://doi.org/10.1016/j.partic.2014.05.002

CHAPTER 4

MEF EFFECTS ON BETA-LACTOGLOBULIN DENATURATION

4.1 INTRODUCTION

β-lg presents a dynamic structural behaviour strongly governed by the environmental pH, which influences the monomer-dimer equilibrium, access to the central hydrophobic barrel or exposure of surface hydrophobic sites (Collini et al., 2003; Taulier & Chalikian, 2001). Furthermore, by controlling other physicochemical factors, such as protein concentration, ionic strength, temperature or pressure, it is possible to tailor the properties and functionality of whey protein systems (Bryant & McClements, 1998). Often the functionalization of proteins is achieved through denaturation, as the unfolding of the proteins results on exposure of its hydrophobic groups and free thiols (de Wit, 2009). The exposure of these groups increases protein reactivity towards the formation of new intra- and inter-molecular interactions, establishing the basis for aggregation and network formation (Nicolai, Britten, & Schmitt, 2011). Thermal denaturation is by far the predominant method to achieve protein functionalization; this strategy has been extensively reviewed and commonly used in the food industry. The use OH and its MEF effects have been highlighted in previous sections (see chapter 2) and several works have been exploring MEF effects on the properties of whey protein network systems (Pereira et al., 2016; Pereira, Teixeira, & Vicente, 2011; Rodrigues et al., 2015). It was demonstrated that MEF can interfere with aggregation kinetics and gelation of whey proteins, possibly due to conformational disturbances. However, the way how the EF interacts with protein structure is far from being understood. In fact, all these works were carried in complex (i.e. WPI) and highly concentrated protein systems, which favour extensive aggregation during thermal treatment. These conditions do not allow disclosing the electrical effects involved, because complex interactions between one or several different proteins occurring during thermal aggregation can hinder structural transitions or local conformational changes. Actually it is not clear if MEF effects are the result of protein conformational changes or of impairment of the aggregation process due to electrostatic disturbances (Rodrigues et al., 2015). It is therefore necessary to study MEF effect on pure fractions of proteins, in conditions that allow confirming their influence on protein denaturation and conformation.

The objective of this chapter was to evaluate the effect of MEF during OH of purified fractions of β-lg at different physicochemical conditions of pH and temperature. It is expected that under low aggregation conditions and without the influence of other whey constituents, the impact of MEF on proteins' structural features upon thermal denaturation can be confirmed and comprehensively elucidated.

4.2 MATERIALS AND METHODS

4.2.1 Protein solutions

β-lg was obtained by the purification method descried in chapter 3 and was used to prepare protein solutions at 1 x 10^{-5} mol.L^{-1} in 2.5 x10^{-2} mol.L^{-1} sodium phosphate buffer at pH values of 7.0, 5.7, 4.3 and 3. The solutions were stirred for 2 h to ensure full solubilisation and then the pH was checked and adjusted if needed with 1 mol.L^{-1} HCl or NaOH. The conditions established, as previously mentioned in chapter 3, aimed to minimize protein aggregation and optimize the analytic technique used.

4.2.2 Thermal treatments

Thermal treatments were performed at target temperatures of 50, 60, 70, 80 and 90 °C for a total of 10 min. The treatment time included the come-up time (5 to 7 min according to the target temperature) and the holding time for the remaining period. Additionally, fractions of β-lg solutions (unheated and not exposed to MEF) were used as control solutions in all determinations. The electric field applied ranged from 80 V.cm^{-1} during heating to 20 V.cm^{-1} during holding time. The electric frequency was set at 20 kHz, once the use of frequencies on the kHz range (i.e. <17 kHz) effectively eliminates the electrochemical effects as electrolysis and electrode oxidation (Jaeger et al., 2016; Pataro et al., 2014). To evaluate the influence of MEF on protein unfolding, conventional (Cov) heating treatments without presence of electric field were performed under the same heating conditions in order to evaluate non-thermal effects of OH. At the end of the treatments, samples were transferred to screw cap glass tubes, placed in a melting ice bath (≈15 min), and after reaching room temperature, the samples were analysed.

4.2.3 Heating unit

Experiments were conducted on a double-jacketed glass cylinder containing stainless steel electrodes at each edge (see figure 4.1), as described by Machado *et al.* 2010.

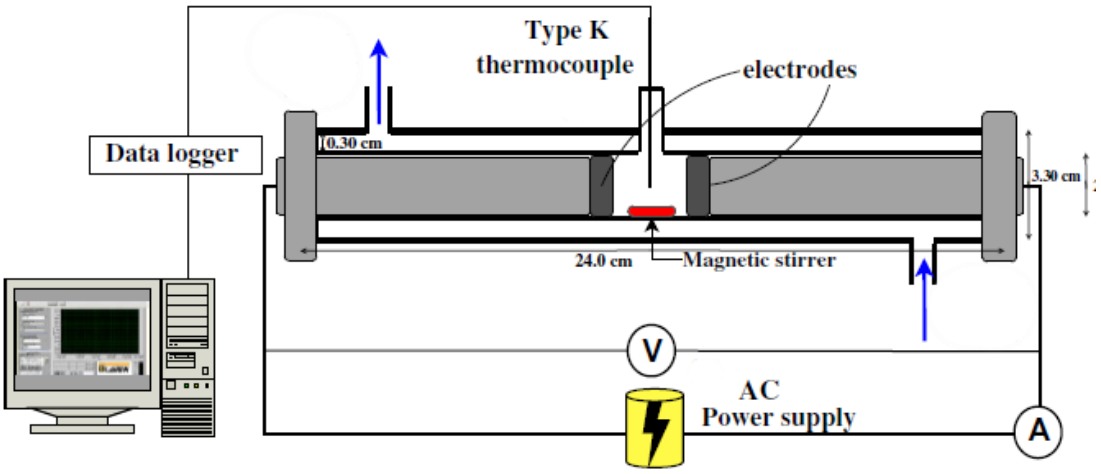

Figure 4.1: Ohmic heating installation (adapted from Machado, Pereira, Martins, Teixeira, & Vicente, 2010)

For the OH treatments, the temperature was controlled by regulating the voltage output of a function generator (Agilent 33220A, Penang, Malaysia) and then amplified on an amplifier system (Peavey CS3000, Meridian, MS, USA). For conventional treatments, the temperature was controlled by circulating water on the reactor´s jacket with a circulating thermo-stabilized water bath. Temperature was measured with a type K thermocouple (Omega Engineering, Inc., Stamford, CT, USA), connected to a data logger (USB-9161, National Instruments Corporation, Austin, TX, USA). During the treatments the samples were gently stirred (with a magnetically stirrer) to ensure homogeneity.

4.2.4 Fluorescence determinations

Florescence determinations were performed on the fluorescence instrument Aqualog (HOBIBA-Jobin Yvon, Inc. Japan). Intrinsic fluorescence of β-lg was determined by Trp on the samples at 295 nm and recording the emission from 300 to 450 nm. Hydrophobic sites accessibility was determined using ANS fluorescent probe, according with the methodology described in Chapter 3.

4.2.5 CD spectroscopy

CD spectra were recorded on a Jasco J-1500 CD spectrophotometer (Jasco Inc., Tokyo, Japan) between 250 and 190 nm at 20 °C, using a 1 mm quartz cuvette. The experimental parameters were as follows: band width, 1 nm; data pitch, 0.5 nm; scanning speed, 50 $nm.min^{-1}$, response

D.I.T. 1 s; accumulations, 5; the CD spectrum of the blank was subtracted from each of the recorded spectra.

CD spectra analysis was performed using DICHROWEB software, allowing to estimate the fractions of secondary structure elements of the protein (Whitmore & Wallace, 2008), before and after thermo-electric treatments. The analysis program used was CONTIN with the reference set 4, optimized for the wavelength interval ranging from 190 to 240 nm.

4.2.6 Determination of Accessible Sulfhydryl Groups

Determination of the free SH was performed using Ellman's DTNB (5.5′-dithiobis-(2-nitrobenzoicacid)) method (Ellman, Courtney, Andres, & Featherstone, 1961) with some modifications. Briefly, a DTNB solution at 5 x 10^{-3} mol.L^{-1} was prepared in phosphate buffer, 0.1 mol.L^{-1}, pH 8 and stored at 4 °C, protected from light. On a glass test tube 2.5 mL of phosphate buffer (0.1 mol.L^{-1}, pH 8), 0.5 mL of protein solution and 100 μL of DTNB solution were mixed and allowed to react for 1 h at room temperature. The absorbance at 412 nm was determined on a UV-VIS spectrophotometer (V-560, Jasco Inc., Tokyo, Japan). All determinations were performed in triplicate and the absorbance of the blank (using buffer instead of protein solution) were subtracted on each sample´s absorbance. The total amount of thiol groups was determined using a positive control produced as described above, but using an 8 mol.L^{-1} urea solution at pH 8 instead of the phosphate buffer. The results were expressed as percentage of the total amount of free SH.

All chemicals were of analytic grade and purchased form Sigma-Aldrich (Steinheim, Germany). Double distilled water was used for the preparation of all solutions.

4.2.7 Data analysis

The statistical analyses of the experimental data were executed using Origin 8.1 software (OriginLab Corporation, Northampton, MA, USA) applying an analysis of variance to estimate any statistically significant differences at a confidence level of 95%. Unless otherwise stated, all experiments were run at least in triplicate. For the Principal Component Analysis (PCA) the average values of the determined variables (i.e maximum fluorescence intensity for both Trp and ANS, percentage of the SH groups and the ellipticity at 208 from DC) were used after being normalized and scaled.

4.3 RESULTS AND DISCUSSION

4.3.1 Effects of physicochemical conditions

The aim of this work was to determine the influence of MEF on a wide-ranging spectrum of conditions. In this sense, Cov and OH treatments were performed at different temperatures and pH conditions, establishing the treatment type as the only variable of analysis. Nonetheless, the temperatures of 80 and 90 °C for the pH values of 4.3 and 5.7 were not considered on the analysis. Under these conditions, the treated samples presented high turbidity and, in some cases, the protein precipitated, indicating excessive and uncontrolled aggregation. These insoluble aggregates are not suited for the analytic methods used in this work and do not fulfilled the requirement of the intended study of structural features. The appearance of these insoluble aggregates is explained by the proximity of the isoelectric point of the protein, and therefore the low charge and the consequent low repulsion occurring in these conditions. This, along with exposure to temperatures above denaturation, caused the reported aggregation even at such low protein concentration (Chi, Krishnan, Randolph, & Carpenter, 2003; Majhi et al., 2006). In all the other treatment conditions, the solutions remained clear and the absence of substantial aggregation was verified by the dynamic light scattering technique (DLS).

Variability on the CD spectra, Trp and ANS fluorescence intensities and exposure of SH groups can be used to evaluate changes in conformation and structure of proteins. Using these data, a principal component analysis (PCA) was performed to determine the overall behaviour of the samples under the treatments applied. This analysis is a dimension-reduction tool that decreases a large set of variables in to a smaller set that contains most of the information in the original. Figure 4.2 shows the PCA of the determinations performed and the corresponding projection of each treatment point. According to the analysis, the two main principal components, the first (horizontal axis) and second (vertical axis), accounted for 94.61 % of the variability found in measured data, showing that the analysis by a bivariate dimension is satisfactory.

The samples dispersion resulted in four groups correspond to the intervals of the four pH values tested, each of them represented by the 95 % confidence ellipses. The differentiation of these groups by the vertical factor is caused by the pH variation and the factor value is zero near the isoelectric point of the protein (i.e. 5,1). The vertical separation of the samples is more influenced by the fluorescence determination, suggesting the pH effect to be related with the conformation of the protein (i.e. hydrophobic sites accessibility and Trp exposure and micro-environment) and not

with extreme structural changes, that could be determined by SH groups exposure and significant changes in the secondary structure. On the other hand, the distribution along the horizontal axis is caused by the temperature increase and reflects structural events. This is the result of irreversible conformational changes occurring once the denaturation temperature was overcome.

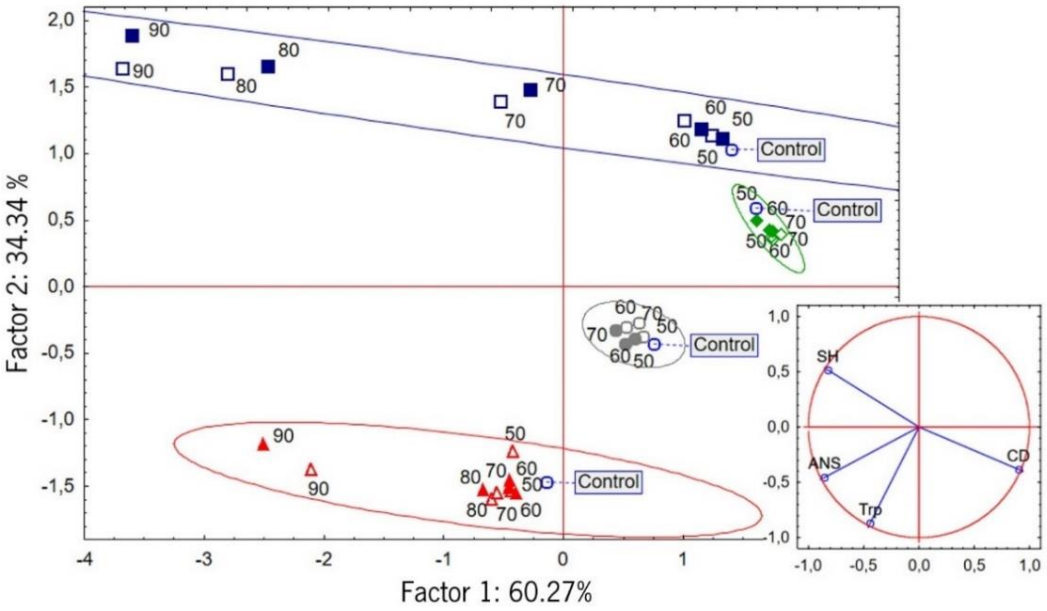

Figure 4.2: Principal component analysis of measurements performed in ohmic and conventionally treated samples. The colours red, grey, green and blue represent the samples at pH 3, 4.3, 5.7 and 7 respectively and the ellipses represent a 95 % confidence interval for each pH group. The open symbols represent conventional treatments and the closed ones represent OH. The corresponding treatment temperatures are placed next to the respective symbol. Figure insert shows the projection and correlations between variables measured.

For pH 3, despite a general tendency of the treated samples to be located to the left of the unheated sample, only the samples treated at 90 °C present a clear differentiation. Under these pH conditions, β-lg thermal stability is increased (Kella & Kinsella, 1988) and structural changes were only appreciable at the highest temperature tested. At pH of 4.3, there was little differentiation of the samples, although a tendency for small conformational changes (as the samples moved left and up from the unheated control) is apparent for increasing treatment temperatures. In contrast, at pH 5.7 the tendency is the opposite, as the samples move to the right and down. For pH 7 the clearest tendencies and higher differentiation between samples are found. A strong displacement to the left and along the vertical axis is caused by the increase of treatment temperature (≥70 °C). This indicates that at neutral pH β-lg is more susceptible to thermally-induced structural changes.

In any case, whenever the thermal treatment induces higher structural changes, the samples heated under OH show a clear differentiation from the Cov ones. With the clear differentiation of the samples into four groups, reflecting the environment pH, the subsequent analysis of the results and MEF effects, was then carried for each group individually by comparing only Cov and OH treatments. For the further discussion and aiming at focussing in the MEF effects on β-lg unfolding, only the treatments that presented statistical significance from the unheated samples and between treatment types will be considered, namely pH 3 at 90 °C and pH 7 at 70 °C, 80 °C and 90 °C. The complete data set containing the average values, standard deviation and statistical significance analysis of the determined variables for all the treatment performed is presented as supplementary material.

4.3.2 MEF effects in conformation and structure of unfolded β-lg

4.3.2.1 Secondary structure

CD spectra analysis presented in Table 1 shows that unheated samples, corresponding to the native conformation of the proteins, presented small differences in secondary structure fractions according to the environmental pH. β-sheet content was slightly higher at pH 7 than at pH 3, at which α-helix was favoured.

Table 4.1: Comparison of the percentage of secondary structures of β-lg from CD spectra analysis.

pH	Sample	α-helix	β-sheet	Turn	Random coil
pH 7	Unheated	13.0 ± 0.7	42.0 ± 0.7	22.4 ± 0.6	22.6 ± 0.9
	Cov 70	14.6 ± 0.9	34.8 ± 0.5	22.5 ± 1.0	28.1 ± 0.6
	OH 70	15.4 ± 0.5	31.4 ± 0.8	23.7 ± 0.6	29.5 ± 1.6
	Cov 80	16.4 ± 0.9	26.3 ± 0.6	21.2 ± 0.9	36.2 ± 0.4
	OH 80	20.8 ± 0.8	20.4 ± 1.0	19.7 ± 0.5	39.1 ± 0.8
	Cov 90	20.5 ± 0.8	21.0 ± 0.7	21.3 ± 1.2	37.2 ± 0.3
	OH 90	16.2 ± 0.4	24.4 ± 0.5	23.0 ± 0.8	36.5 ± 1.1
pH 3	Unheated	16.8 ± 0.3	40.7 ± 0.5	22.4 ± 1.3	20.1 ± 1.7
	Cov 90	20.1 ± 0.6	31.3 ± 1.5	21.5 ± 0.6	27.1± 1.5
	OH 90	19.2 ± 0.8	35.1 ± 1.1	23.3 ± 1.0	22.5 ± 1.6

After thermal treatments, changes in the secondary structure of β-lg attributed to the loss of secondary structural elements were verified. These changes potentiated by the temperature increase, were characterized by a progressive loss of β-sheet, a slight increase in α-helix content and increase of random coil. Nonetheless, the overall loss of secondary structural elements was not radical, once substantial fractions of β-sheet were preserved and α-helix content was increased. This may indicate that the main structural features of β-lg, namely the central barrel, is preserved at least partially, resulting on a non-native forms known as molten globule (Bhattacharyya & Varadarajan, 2013; Croguennec, Mollé, Mehra, & Bouhallab, 2004). At pH 7 the secondary structural changes are more extensive and start at 70 °C. Samples treated by OH present different structural features than the Cov, presenting lower content of β-sheet, higher of α-helix and random coil in 70 °C and 80 °C treatments. For treatments at 90 °C the behaviour inverts and OH treated samples display higher content of β-sheet, α-helix and random coil than the Cov. Interestingly samples treated by OH at 80 °C, present secondary structural features similar to the Cov at 90 °C, being the most distant from the native conformation, reaching changes up to 22 % in β-sheet loss, 7 % increase of α-helix content and 17 % increase in random coil. At pH 3, a similar behaviour among OH and Cov treatments was found, nonetheless with lower changes in magnitude, as treatments at 90 °C result in a distribution of secondary structural elements similar to the treatments at pH 7 and 70 °C. Again, OH at 90 °C results in higher β-sheet and lower α-helix and random coil content.

4.3.2.2 Free SH group relativity

SH reactivity is not only dependent on the accessibility of cystein (Cys) 121 but also on the disulphide bond brake and disulphide interchange, usually occurring above 80 °C, resulting on the reactivity of other Cys residues buried in the protein structure (Halder, Chakraborty, Das, & Bose, 2012). In figure 4.3 is presented the SH reactivity for all the treatments at pH 3 and 7. Untreated samples (at 20 °C) exhibit similar SH reactivity in both pH values. The higher reactivity of SH groups at pH 7 was favoured by the higher structural changes observed and for the increased access to the central barrel known as the Tanford transition. SH reactivity increased significantly above 60 °C for treatments at pH 7, supporting literature reports which confirm this temperature as starting point to make Cys 121 accessible (de Wit, 2009; QI et al., 1997). With higher treatment

temperatures, the amount of free thiols also increased, reaching more than 50 %, and OH treated samples consistently presented a lower amount of reactive SH.

At pH 3, along with all the other determinations, SH reactivity increases only for treatments at 90 °C, contrasting with much earlier response at pH 7. Also, the SH reactivity reached fractions of 21 % and 17 % for Cov and OH treatments respectively, smaller than the observed in the treatments at neutral pH, which reached about 25 % already at 70 °C treatments. Interestingly, samples treated at 90 °C by OH present higher SH reactivity than the equivalent Cov treatments. SH reactivity correlates with the structural changes occurring upon thermal stress. However, the presence of MEF seems to promote different actions in pH 3 and 7. The favouring or restriction of SH reactivity imposed by MEF on the reported conditions can be resultant on the different conformations imposed by the pH conditions and inherent changes in charge distribution, which should be able to promote rearrangements in structural elements or even influence intramolecular disulphide exchanges.

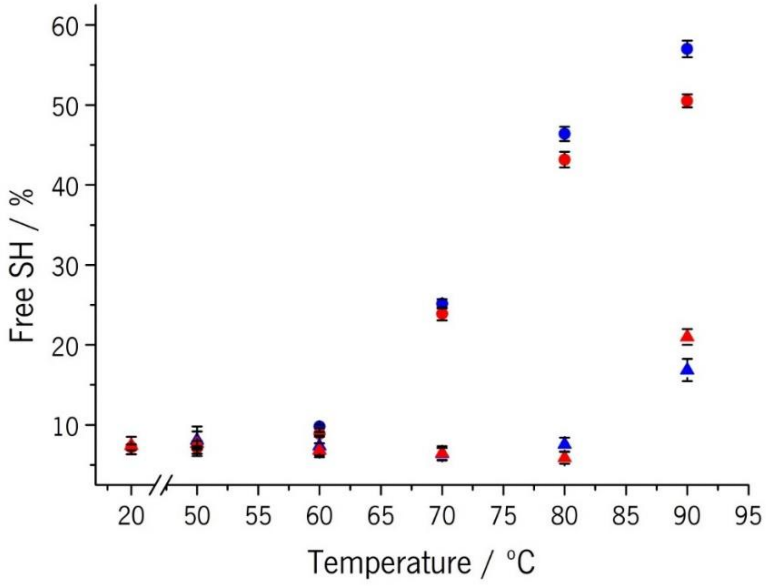

Figure 4.3: Reactivity of SH for treatments at pH 3 (triangles) and pH 7 (circles). Red markers represent OH treatments and the blue ones the Cov treatments.

4.3.2.3 Intrinsic fluorescence

β-lg's fluorescence is attributed mainly to the Trp 19 residue, placed deep inside the hydrophobic barrel (Albani, Vogelaer, Bretesche, & Kmiecik, 2014) while the Trp 61 is mostly quenched by the

nearby Cys66-Cys160 bond and solvent exposure (Croguennec et al., 2004). Therefore, variations in Trp fluorescence intensity and shifts in fluorescence peak and spectra shape can contribute with valuable information about protein conformation and intramolecular changes. In Figure 4.4 are presented illustrative fluorescence spectra of Trp in β-lg under different conditions.

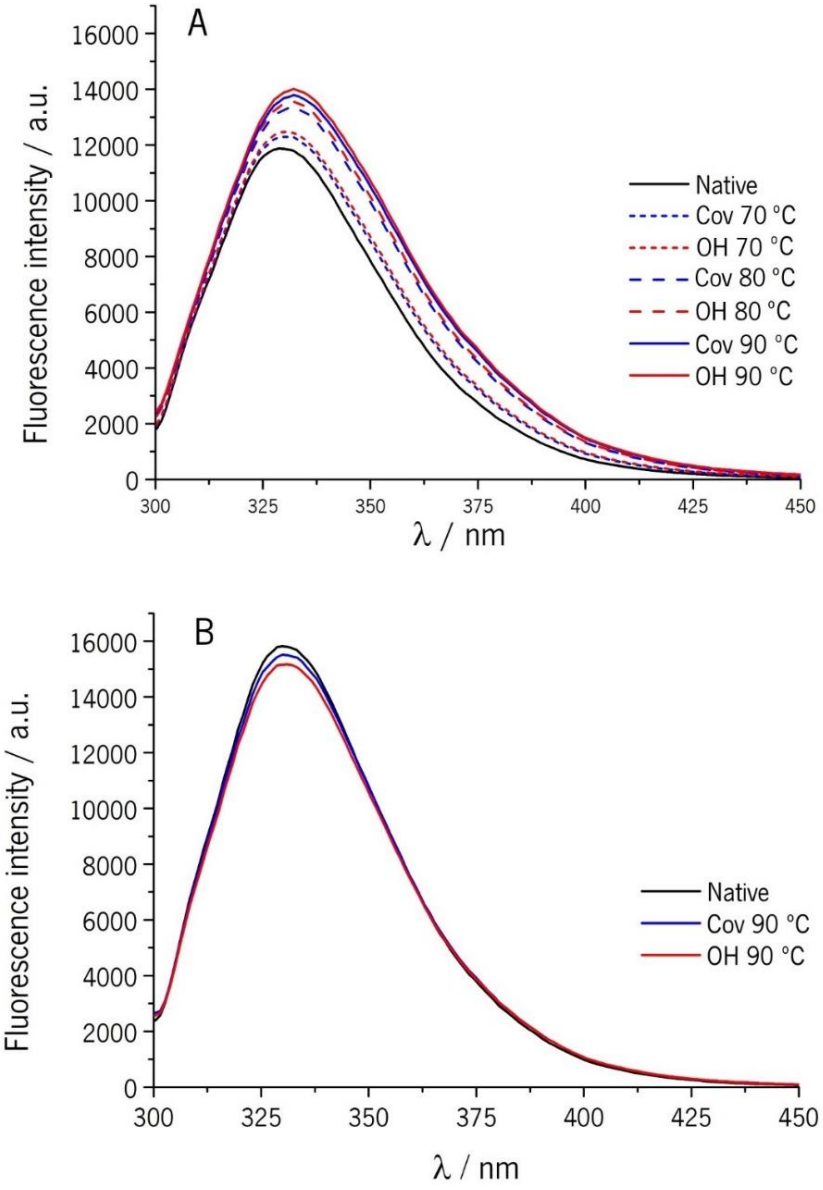

Figure 4.4: Trp florescence spectra of native and treated β-lg samples at pH 7 (A) and pH 3 (B). Excitation wavelength was 295 nm.

At pH 7 the unfolded proteins shows an increase in Trp fluorescence, as well as a red shift (≤ 5 nm) in the maximum fluorescence and an elongation of the spectra to the right, indicating a change from an apolar to a more polar Trp microenvironment (Halder et al., 2012; Sahihi, Ghayeb, &

Bordbar, 2012). The OH samples from 70 to 90 °C present small but significantly higher intensities than Cov, indicating changes in Trp exposure or quenchers accessibility. At pH 3, the Trp fluorescence is considerably higher than the observed at pH 7 because in acid environments β-lg presents a closed conformation and displacement of some structural element´s orientation as the long α-helix (Uhrínová et al., 2000). This more compact conformation may result on the shielding of the Trp19, which becomes less susceptible to be quenched by the solvent molecules and thus increasing the effective florescence. In these conditions, Trp fluorescence suffered few changes, decreasing the maximum intensity for 90 °C treatments and presenting a smaller red shift of 2 nm; again, OH treated samples presented higher changes than the Cov treated samples. This decrease in Trp fluorescence intensity is opposite to the observed at pH 7, also the red shift observed is smaller in the treatments at different pH values. This may be correlated with the reactivity of SH and disulphide bonds distribution. The interchange of any of the two disulphide bonds among them or with Cys 121 would result on different quenching equilibrium of the two Trp residues. An interchange in Cys66-Cys160, leaving any of these Cys free would cause a reduced quenching in Trp 61, resulting on a higher contribution of this residue, increasing the fluorescence intensity and also the red shift. On the other hand, an exchange in Cys106-Cys119 bond with Cys 121 would position de disulphide bond closer to the Trp19, causing an increased quenching and reduce the fluorescence intensity. Once this Trp is located inside the β-barrel the microenvironment is not expected to suffer substantial changes and thus lower shift would be expected. Other disulphide interchange and SH exposures mechanism may take place and probably several of them occur simultaneously in molecules of the same sample. However, the processing methods and environmental conditions may favour some mechanisms against others, but the two scenarios described are consistent with the observations reported, where after thermo-electric treatments at pH 7 the Trp fluorescence increases with a larger red shift than at pH 3 where the Trp florescence diminishes and lower shift was observed.

In both pH values, the presence of MEF induced higher changes in Trp fluorescence intensities; however, no apparent shift on the maximum intensity or distortion of the spectra were observed between treatment types. This suggests that no differences in Trp positioning were induced by the presence of MEF.

4.3.2.4 ANS binding

ANS fluorescence intensity suffers major variations depending on the pH value. These modifications relate with conformational changes induced by protonation/deprotonation of some groups and overall surface charge of the protein (Sakurai, Konuma, Yagi, & Goto, 2009; Taulier & Chalikian, 2001). The main binding site of ANS to β-lg is on the opening of the central hydrophobic barrel, but at low pH a second binding site at the surface has been also reported (Collini et al., 2003; Collini, D'Alfonso, & Baldini, 2000). Figure 4.5 shows ANS fluorescence spectra of untreated samples and samples treated at 90 °C for pH 3 and at 70, 80 and 90 °C for pH 7.

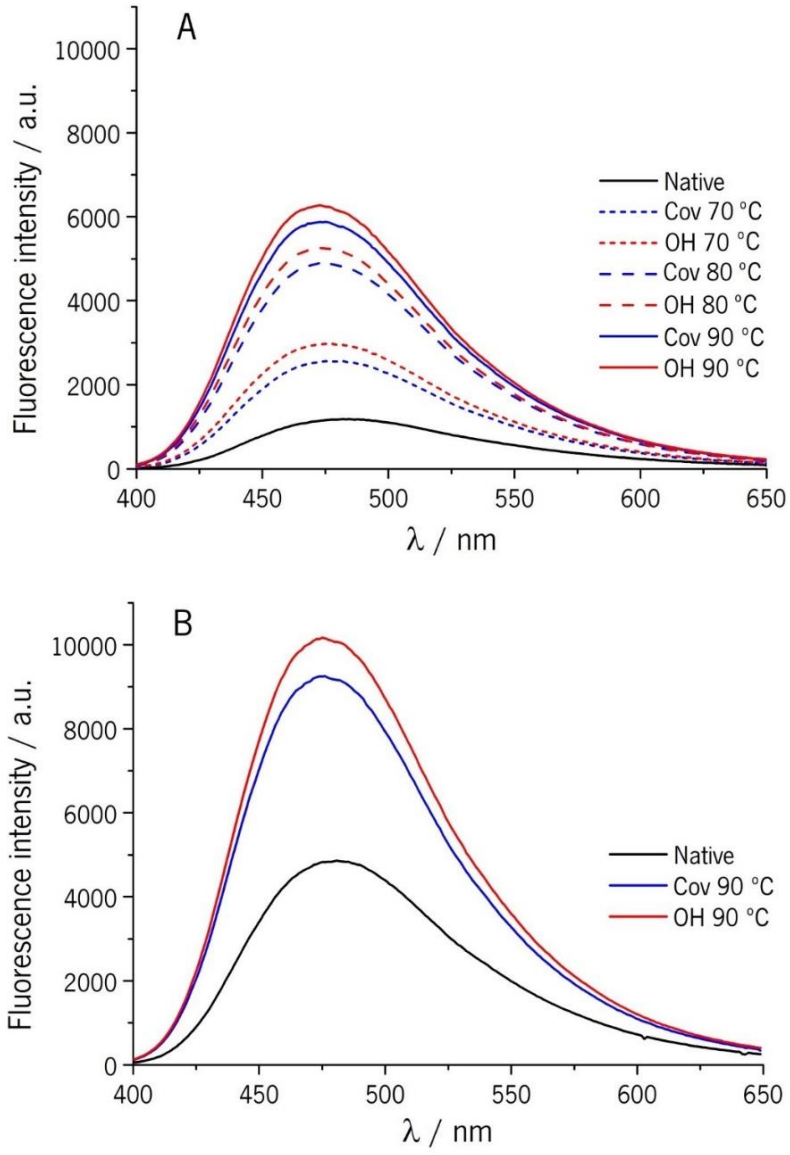

Figure 4.5: ANS-β-lg florescence spectra of native and treated samples at pH 7 (A) and pH 3 (B). Excitation wavelength was 370 nm.

The higher ANS fluorescence at pH 3 results from the availability of the external binding site, that is not available at higher pH values. At pH 7, ANS fluorescence suffers the largest relative increase (related to the unheated sample at the same pH) with increasing treatment temperatures. This agrees with the secondary structure analysis that suggests a partial unfolding with the conservations of substantial fractions of the β-barrel, resulting on an enhancement of the access to the barrel. For all the OH treated samples, regardless of the environmental pH value, ANS florescence was higher than the correspondent Cov treatment, which demonstrates that MEF action increased hydrophobic groups accessibility. The capability of MEF to affect hydrophobic and SH groups disposition implies important consequences in functionality, as the interactions established by these groups define protein aggregation and association with other compounds as drugs or bioactives (Mudgal, Daubert, & Foegeding, 2011; Vetri & Militello, 2005).

4.3.3 MEF mechanism in protein unfolding

The effects of MEF in proteins have been reported previously and demonstrated to change structure and activity of proteins. These reports used MEF at room temperature (without thermal effects) for long exposure periods or probed enzymatic activity, associates with a specific temperatures of activation and deactivation (Bekard & Dunstan, 2014; Samaranayake & Sastry, 2016b, 2018). It was proposed that the effects of an external EF are related with molecular motions induced from oscillatory behaviour of the EF and the consequent energy dissipation through frictional drag. In fact Samaranayake & Sastry (2016) propose that the action of MEF is related with the increase energy dissipation and consistent with an apparent elevation of temperature on the protein molecules. The level of energy involved in these motions was estimated to be equivalent or greater to the hydrogen bonds that stabilize the protein fold and thus they are susceptible of being destabilize or disrupted. These effects are more effective at low frequencies, where the oscillatory motions have greater amplitude or even induce full rotation. Higher frequencies, as the ones used in this study, induce vibrational motion, more chaotic with unstable and aperiodic motion (Kouzaev, 2013). The conditions used in this study involved low exposition time to MEF and the use of high frequencies, which must have limited the effectiveness of electric effects, thus explaining the absence of observed effects at low temperature treatments. However, results demonstrate that the presence of MEF during OH influenced the structural features in non-native forms of β-lg. For higher treatment temperatures, the increased entropy imposed and the disruption of the protein native

fold may allow the vibrational effects and additional energy dissipation to effectively induce changes in conformation upon rearrangement of the structural elements.

The proposed mechanism of MEF action is supported by the experimental data where the differentiation of OH and Cov treated samples was only evident in conditions were substantial structural changes were induced by thermal action. Furthermore, the conformational rearrangements imposed by the environmental pH greatly affects the specific action of MEF. Upon thermal unfolding, the MEF presence resulted in significant changes in secondary structural elements, Trp fluorescence, hydrophobic sites accessibility, SH reactivity and possibly different disulphide rearrangement. These facts are consistent with an additional energy dissipation resultant form the molecular motion induced by the EF. None of the reported MEF effects represents a disruptive behaviour when compared to the Cov treatments, but results show an evidence of local conformational changes that should not be overlooked once can impact functional and technological properties of β-lg. In this sense, the understanding of the specific effects and mechanisms involved in MEF action are fundamental to control protein functionality - i.e. complex formation or aggregation in nanostructures and gel systems- and further investigation should be carried out to better understand these mechanisms in β-lg, and proteins in general.

4.4 CONCLUSIONS

In this Chapter, the effects of MEF on the unfolding of β-lg have been demonstrated through structural and conformational characterization by differentiation in the far-UV CD spectra, reactivity of SH groups, Trp and ANS florescence. Despite the previously reported effects of MEF in protein structure, this is the first time that MEF influence was verified at molecular level in thermal processing treatments. Results have shown that MEF effects are limited to unfolded forms of the protein, suggesting that in the conditions used (i.e. electric field strength, frequency and time of exposure) the disturbances imposed are not sufficient to disrupt the protein fold and MEF effects are therefore synergic with the thermal effects. Furthermore, their specific action and extent was dependent of pH, which may be a result of the dynamic β-lg conformation in response to the environmental conditions. MEF effects were most noticeable at pH 7, establishing these conditions as the most promising to proceed with further studies of MEF action on protein structure and network formation. These results corroborated the hypothesis postulated in previous works, where MEF effects were proven to influence aggregation and gelation of whey proteins. These findings

contribute also to a more comprehensive understanding of the pathways involved in the dynamic behaviour of this protein and to define MEF as technological tool to control protein functionality and unravel potential interactions with other bioactive molecules.

4.5 REFERENCES

Albani, J. R., Vogelaer, J., Bretesche, L., & Kmiecik, D. (2014). Tryptophan 19 residue is the origin of bovine β-lactoglobulin fluorescence. *Journal of Pharmaceutical and Biomedical Analysis*, *91*, 144–150. https://doi.org/10.1016/j.jpba.2013.12.015

Bekard, I., & Dunstan, D. E. (2014). Electric field induced changes in protein conformation. *Soft Matter*, *10*(3), 431–437. https://doi.org/10.1039/c3sm52653d

Bhattacharyya, S., & Varadarajan, R. (2013). Packing in molten globules and native states. *Current Opinion in Structural Biology*, *23*(1), 11–21. https://doi.org/10.1016/j.sbi.2012.10.010

Chi, E. Y., Krishnan, S., Randolph, T. W., & Carpenter, J. F. (2003). No Title. *Pharmaceutical Research*, *20*(9), 1325–1336. https://doi.org/10.1023/A:1025771421906

Collini, M., D'Alfonso, L., & Baldini, G. (2000). New insight on β-lactoglobulin binding sites by 1-anilinonaphthalene-8-sulfonate fluorescence decay. *Protein Science*, *9*(10), 1968–1974. https://doi.org/10.1110/ps.9.10.1968

Collini, M., D'Alfonso, L., Molinari, H., Ragona, L., Catalano, M., & Baldini, G. (2003). Competitive binding of fatty acids and the fluorescent probe 1-8-anilinonaphthalene sulfonate to bovine β-lactoglobulin. *Protein Science*, *12*(8), 1596–1603. https://doi.org/10.1110/ps.0304403

Croguennec, T., Mollé, D., Mehra, R., & Bouhallab, S. (2004). Spectroscopic characterization of heat-induced nonnative beta-lactoglobulin monomers. *Protein Science : A Publication of the Protein Society*, *13*(5), 1340–6. https://doi.org/10.1110/ps.03513204

de Wit, J. N. (2009). Thermal behaviour of bovine β-lactoglobulin at temperatures up to 150°C. a review. *Trends in Food Science & Technology*, *20*(1), 27–34. https://doi.org/10.1016/j.tifs.2008.09.012

Ellman, G. L., Courtney, K. D., Andres, V., & Featherstone, R. M. (1961). A new and rapid colorimetric determination of acetylcholinesterase activity. *Biochemical Pharmacology*, *7*(2), 88–95. https://doi.org/10.1016/0006-2952(61)90145-9

Halder, U. C., Chakraborty, J., Das, N., & Bose, S. (2012). Tryptophan dynamics in the exploration of micro-conformational changes of refolded β-lactoglobulin after thermal exposure: A steady state and time-resolved fluorescence approach. *Journal of Photochemistry and Photobiology B: Biology*, *109*, 50–57. https://doi.org/10.1016/j.jphotobiol.2012.01.005

Jaeger, H., Roth, A., Toepfl, S., Holzhauser, T., Engel, K. H., Knorr, D., ... Steinberg, P. (2016). Opinion on the use of ohmic heating for the treatment of foods. *Trends in Food Science and Technology*, *55*, 84–97. https://doi.org/10.1016/j.tifs.2016.07.007

Kella, N. K., & Kinsella, J. E. (1988). Enhanced thermodynamic stability of beta-lactoglobulin at low pH. A possible mechanism. *The Biochemical Journal*, *255*(1), 113–8.

Kouzaev, G. A. (2013). *Applications of Advanced Electromagnetics* (Vol. 169). Berlin, Heidelberg: Springer Berlin Heidelberg. https://doi.org/10.1007/978-3-642-30310-4

Machado, L. F., Pereira, R. N., Martins, R. C., Teixeira, J. A., & Vicente, A. A. (2010). Moderate electric fields can inactivate Escherichia coli at room temperature. *Journal of Food Engineering*, *96*(4), 520–527. https://doi.org/10.1016/j.jfoodeng.2009.08.035

Majhi, P. R., Ganta, R. R., Vanam, R. P., Seyrek, E., Giger, K., & Dubin, P. L. (2006). Electrostatically Driven Protein Aggregation: β-Lactoglobulin at Low Ionic Strength. *Langmuir*, *22*(22), 9150–9159. https://doi.org/10.1021/la053528w

Mudgal, P., Daubert, C. R., & Foegeding, E. A. (2011). Kinetic study of β-lactoglobulin thermal aggregation at low pH. *Journal of Food Engineering*, *106*(2), 159–165. https://doi.org/10.1016/j.jfoodeng.2011.04.025

Nicolai, T., Britten, M., & Schmitt, C. (2011). β-Lactoglobulin and WPI aggregates: Formation, structure and applications. *Food Hydrocolloids*, *25*(8), 1945–1962. https://doi.org/10.1016/j.foodhyd.2011.02.006

Pataro, G., Barca, G. M. J., Pereira, R. N., Vicente, A. A., Teixeira, J. A., & Ferrari, G. (2014). Quantification of metal release from stainless steel electrodes during conventional and

pulsed ohmic heating. *Innovative Food Science and Emerging Technologies*, *21*, 66–73. https://doi.org/10.1016/j.ifset.2013.11.009

Pereira, R. N., Rodrigues, R. M., Ramos, Ó. L., Xavier Malcata, F., Teixeira, J. A., & Vicente, A. A. (2016). Production of Whey Protein-Based Aggregates Under Ohmic Heating. *Food and Bioprocess Technology*, *9*(4), 576–587. https://doi.org/10.1007/s11947-015-1651-4

Pereira, R. N., Teixeira, J. A., & Vicente, A. A. (2011). Exploring the denaturation of whey proteins upon application of moderate electric fields: A kinetic and thermodynamic study. *Journal of Agricultural and Food Chemistry*, *59*(21), 11589–11597. https://doi.org/10.1021/jf201727s

QI, X. L., HOLT, C., MCNULTY, D., CLARKE, D. T., BROWNLOW, S., & JONES, G. R. (1997). Effect of temperature on the secondary structure of β -lactoglobulin at pH 6.7, as determined by CD and IR spectroscopy: a test of the molten globule hypothesis. *Biochemical Journal*, *324*(1), 341–346. https://doi.org/10.1042/bj3240341

Rodrigues, R. M., Martins, A. J., Ramos, O. L., Malcata, F. X., Teixeira, J. A., Vicente, A. A., & Pereira, R. N. (2015). Influence of moderate electric fields on gelation of whey protein isolate. *Food Hydrocolloids*, *43*, 329–339. https://doi.org/10.1016/j.foodhyd.2014.06.002

Sahihi, M., Ghayeb, Y., & Bordbar, A. K. (2012). Fluorescence spectroscopic study on interaction of retinol with ??-lactoglobulin in the presence of cetylpyridinium chloride. *Spectroscopy*, *27*(1), 27–34. https://doi.org/10.3233/SPE-2012-0565

Sakurai, K., Konuma, T., Yagi, M., & Goto, Y. (2009). Structural dynamics and folding of β-lactoglobulin probed by heteronuclear NMR. *Biochimica et Biophysica Acta (BBA) - General Subjects*, *1790*(6), 527–537. https://doi.org/10.1016/j.bbagen.2009.04.003

Samaranayake, C. P., & Sastry, S. K. (2016a). Effect of moderate electric fields on inactivation kinetics of pectin methylesterase in tomatoes: The roles of electric field strength and temperature. *Journal of Food Engineering*, *186*(Supplement C), 17–26. https://doi.org/https://doi.org/10.1016/j.jfoodeng.2016.04.006

Samaranayake, C. P., & Sastry, S. K. (2016b). Effects of controlled-frequency moderate electric fields on pectin methylesterase and polygalacturonase activities in tomato homogenate.

Food Chemistry, *199*(Supplement C), 265–272. https://doi.org/https://doi.org/10.1016/j.foodchem.2015.12.010

Samaranayake, C. P., & Sastry, S. K. (2018). LWT - Food Science and Technology In-situ activity of α -amylase in the presence of controlled-frequency moderate electric fi elds. *LWT - Food Science and Technology*, *90*(October 2017), 448–454. https://doi.org/10.1016/j.lwt.2017.12.053

Sastry, S. (2008). Ohmic Heating and Moderate Electric Field Processing. *Food Science and Technology International*, *14*(5), 419–422. https://doi.org/10.1177/1082013208098813

Taulier, N., & Chalikian, T. V. (2001). Characterization of pH-induced transitions of β-lactoglobulin: ultrasonic, densimetric, and spectroscopic studies 1 1Edited by C. R. Matthews. *Journal of Molecular Biology*, *314*(4), 873–889. https://doi.org/10.1006/jmbi.2001.5188

Uhrínová, S., Smith, M. H., Jameson, G. B., Uhrín, D., Sawyer, L., & Barlow, P. N. (2000). Structural changes accompanying pH-induced dissociation of the β- lactoglobulin dimer. *Biochemistry*, *39*(13), 3565–3574. https://doi.org/10.1021/bi992629o

Vetri, V., & Militello, V. (2005). Thermal induced conformational changes involved in the aggregation pathways of beta-lactoglobulin. *Biophysical Chemistry*, *113*(1), 83–91. https://doi.org/10.1016/j.bpc.2004.07.042

Whitmore, L., & Wallace, B. A. (2008). Protein secondary structure analyses from circular dichroism spectroscopy: Methods and reference databases. *Biopolymers*, *89*(5), 392–400. https://doi.org/10.1002/bip.20853

CHAPTER 5.

EFFECTS OF MEF VARIABLES IN BETA-LACTOGLOBULIN THERMAL TRANSITION, STRUCTURE AND INTERACTIONS

5.1 INTRODUCTION

Based in literature reports and on the data presented in Chapter 3 of this thesis, it has been stablished that β-lg's thermal denaturation is a complex phenomenon. It follows a sequence of modifications in its tertiary and secondary structures that do not take place simultaneously, but somewhat successively or triggering each other (Cairoli, Iametti, & Bonomi, 1994; Loveday, 2016; Tolkach & Kulozik, 2007). Close to physiological conditions (near neutral pH and low ionic strength), β-lg's T_m is located around 74 °C. However, due to differences in thermal stability of different domains, this protein can present different denaturation levels below and above T_m, with more or less preservation of its structural features (Fessas, Iametti, Schiraldi, & Bonomi, 2001; Tolkach & Kulozik, 2007). In fact β-lg retains a significant fraction of its native structure even at temperatures of 90 °C, exiting in partially unfolded states, according with the molten globule model (Bhattacharyya & Varadarajan, 2013; Ql et al., 1997). In these partially unfolded forms, the protein presents thiol reactivity, increased Trp exposure and accessible hydrophobic patches (Bhattacharjee & Das, 2000; Cairoli et al., 1994). This modification result in functionality changes affecting for example, protein interactions. β-lg has the ability to bind small hydrophobic molecules, and a particular affinity to retinol has been documented. This affinity is highly specific and has an apparent association constant similar to the one from plasma retinol-binding protein, with which it shares homology (George Kontopidis et al., 2002; Papiz et al., 1986).

Significant work has been developed on the conjugation of thermal and electrical effects in protein systems (R. N. Pereira, Teixeira, & Vicente, 2011; R. N. Pereira, Souza, Cerqueira, Teixeira, & Vicente, 2010; Rodrigues et al., 2015), where the main focus has been in complex systems (i.e. WPI) and the impact in functional aspects such as aggregation and gelation. Despite the confirmation of the EF effects in β-lg's structure presented in the previous chapter, there is a lack of fundamental knowledge regarding the effects caused by MEF and its variables in protein structural transitions and intermolecular interactions – i.e. protein binding properties. The effects of MEF on protein conformation at non-denaturing temperatures have demonstrated effects even at low voltage gradients (Bekard & Dunstan, 2014; Samaranayake & Sastry, 2016b, 2016c, 2018). It was hypothesized that the presence of a MEF induces molecular motions resultant from the oscillatory behaviour of the EF applied. These motions are particularly effective at low electrical frequencies (< 100 Hz) and result in local energy dissipation, yielding as an apparent elevation of temperature on the protein molecules.

In Chapter 3 we have established the complex structural transitions of β-lg thermal unfolding, composed by a series of discreet transitions and in Chapter 4 the MEF effects during OH of β-lg solutions were confirmed. Following these findings, the objective of this chapter was to assess the influence of MEF and its variables (i.e. electric field strength, frequency and wave shape) during β-lg thermal unfolding. This was performed by using an *in situ* approach with CD thermal scan, which allowed to follow the changes in structural features imposed by thermal and electrical effects during MEF's treatments. Far-UV CD spectra analysis and fluorescence spectroscopy of the endogenous Trp were used to assess the possible occurrence of changes in structural features imposed by MEF; ligand binding studies with ANS and retinol were also performed aiming at demonstrating differentiated binding affinities, resulting from altered conformations imposed by the treatments applied.

5.2 MATERIALS AND METHODS

5.2.1 Protein solutions

The β-lg used was obtained by the purification method described in chapter 3. β-lg solutions at 1 x 10^{-5} mol.L^{-1} were prepared in sodium phosphate buffer (2.5 x 10^{-2} mol.L^{-1}) at pH 7.0. The solutions were stirred until full solubilisation and the pH was adjusted, if needed, with 1 mol.L^{-1} HCl or NaOH.

5.2.2 Structural changes upon thermo-electric treatments

CD spectra were collected on a Jasco J-1500 CD spectrophotometer (Jasco Inc., Tokyo, Japan) between 250 and 190 nm at 20 °C, using a 1 mm quartz cuvette. The experimental parameters were as follows: band width, 1 nm; data pitch, 1 nm; scanning speed, 50 nm.min^{-1}, response D.I.T. 1 s; accumulations, 5; the CD spectrum of the blank was subtracted from each of the recorded spectra. CD spectra analysis was performed using DICHROWEB software, in order to determine the fractions of secondary structure elements on the protein (Whitmore & Wallace, 2008). The analysis program CONTIN was used with the reference set 4, optimized for the wavelength interval of 190-240 nm.

For CD thermal shift assay, samples were placed into 1 mm path-length quartz cell equipped with a custom-built system with two platinum electrodes embedded on the cuvette cap (see Figure 5.1).

The electrodes fit the sidewalls of the cuvette in all its length with a constant electrode gap of 0.9 cm. The cell was placed on the thermostated holder and the temperature was monitored by a thermocouple placed inside the cuvette. CD spectra was collected at each 5 °C increment, at a heating rate of 1 °C.min^{-1} over the temperature range of 20 to 95 °C. After the target temperature was reached, the temperature was brought back to 20 °C and the spectra of the unfolded protein were collected. During the process, an EF was applied through the voltage output of a function generator (1 Hz to 25 MHz and 1 to 10 V; Agilent 33220A, Penang, Malaysia). For the control samples, similar setups were used but without the presence of the EF. Finally, the samples were collected and used for further analysis.

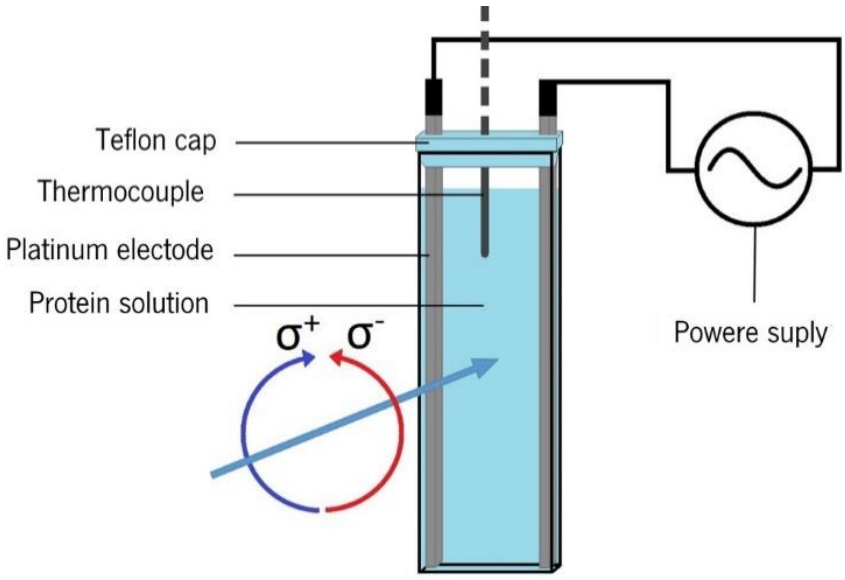

Figure 5.1: Representation of the experimental installation used for the CD thermal scan experiments.

As the frequency range used in this study included low frequencies, additional precautions were taken to minimize possible electrochemical reactions such as water electrolysis, electrode oxidation or erosion. These problems were minimized by using a low power system, preventing excessive energy dissipation, and by the use of platinum as electrode material (Rieger, 1994). The platinum stability and corrosion resistance minimize electrode oxidation and sample contamination. A visual inspection was performed before and after each test, confirming the absence of bubbling, electrode erosion or other signs of electrochemical reactions. For higher frequencies (i.e. > 17 kHz) the electrochemical phenomena are virtually inexistent (Pataro et al., 2014; C P Samaranayake, Sastry, & Zhang, 2005).

5.2.3 Fluorescence determinations

Determinations of intrinsic (Trp) and ANS fluorescence were conducted according to the methodology described in Chapter 4.

5.2.4 Quenching experiments

Retinol (all-trans-Retinol, 95%, ACROS Organics) solution was prepared in ethanol absolute (≥99.8%, AnalaR NORMAPUR® ACS) at 4 x 10^{-4} mol.L^{-1} and used immediately. The retinol solution was titrated manually into the cell using a micro-injector, allow to homogenise after each addition and then the Trp was excited at 295 nm and the resulting fluorescence spectra recorded. For the quenching analysis, absorption correction of the fluorescence values was conducted by the inner filter effect method (Keppler, Stuhldreier, Temps, & Schwarz, 2014; van de Weert, 2010).

5.2.5 Data processing, fitting and analyses

All the data analyses were performed in the software Origin 8.1 software (OriginLab Corporation, Northampton, MA, USA). All spectra presented is the result of at least three accumulations of independent determinations and further smoothed using a 10 points adjacent averaging. For CD spectra analysis to obtain secondary structure quantifications, CD transition profile analysis to estimate the T_m and for fluorescence quenching experiments, all fitting and calculations were performed individually for each spectroscopic determination and the results presented as average values with standard deviations.

5.3 RESULTS AND DISCUSSION

The rates of change in the secondary structure of a protein as a function of temperature can be followed by far-UV CD spectra (Greenfield, 2007). Figure 5.2 shows the changes in β-lg's CD spectra with the progressive increase of temperature, reflecting the protein structural changes. CD spectra changes are mostly detected in the region between 215 and 190 nm, were the θ values become progressively more negative and the spectra minimum shifts towards 204 nm. These changes are consistent with loss of β-sheet and increase of random coil fractions.

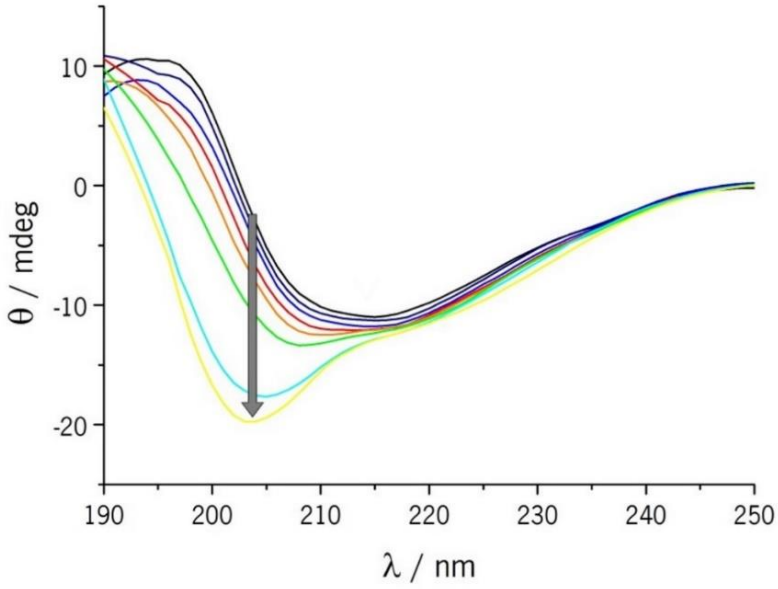

Figure 5.2: Far-UV CD spectra β-lg as function of temperatures. The black line represents the native protein at 20 °C and the coloured lines spectra collected at 10 °C increments until 90 °C (the arrow indicates the change of the magnitude of θ values at 204 nm as temperature is increased).

5.3.1 MEF effect in β-lg thermally induced transition

In order to determine the effects induced by MEF during the thermal unfolding of β-lg, variables such as electric frequency, EF strength ($V.cm^{-1}$) and wave shape (i.e. sine and square wave) were tested during preliminary experiments. The variation of the EF frequency and strength resulted in observable changes in the unfolding of β-lg. The use of sine and square wave resulted in similar thermal unfolding behaviour of β-lg and by this reason the following results refer only to experiments conducted using sine wave MEF.

By following the θ values at 204 nm (θ_{204nm}) it is possible to monitor the protein's secondary structure unfolding transition, assessing the protein's stability as a function of temperature and MEF applied. Figure 5.3 shows the unfolding profiles of β-lg exposed to different MEF frequencies. The control sample presented a lower initial change rate and higher values of θ_{204nm} after the transition when compared with all MEF treated samples. The most contrasting example of MEF effects is the transition profile produced at 50 Hz, where the decrease in θ_{204} was more pronounced on the initial stages of heating and with a more uniform slope. This suggests that the transition starts sooner and is more progressive than the control, until reaching a similar final θ_{204} value. For the other MEF

conditions tested the increasing frequency seems to produce a transition profile more similar to the control, but with a higher initial rate of change and reaching lower ellipticity levels at higher temperatures. Considering a two state unfolding mechanism, T_m was estimated by fitting a Boltzmann sigmoidal curve (Orwig & Lieberman, 2011). The insert in figure 5.3 shows T_m values as a function of the frequency applied. T_m for the control samples (not exposed to MEF) was determined to be 73.15 ± 1.07 °C, while for samples exposed to MEF, T_m values ranged from 51.21 ± 1.71 °C at 50 Hz to 75.23 ± 1.15 °C at 1 MHz. The very significant decrease of T_m caused by exposure to lower MEF frequencies (i.e. 50 and 200 Hz) contrasts with a slight increase caused by the higher frequencies (200 kHz and 1 MHz), whereas the intermediate frequencies present similar T_m values to the control samples. EF effects in T_m have been reported in β-lg exposed to PEF at 12.5 kV.cm^{-1} through DCS analysis, demonstrating a decrease of T_m up to 5 °C (Perez & Pilosof, 2004). In the present study, despite a different electric methodology was used - i.e. much lower EF strengths, longer treatment times and an assigned electrical frequency - the observed decrease in T_m was greater than 20 °C. This is probably related with the longer exposure times and with the higher temperatures (please recall that PEF are a so-called "non-thermal" technology, thus temperature increases are seldom relevant). Nonetheless, the EF effects contributing to a facilitated unfolding transition are evident in both studies.

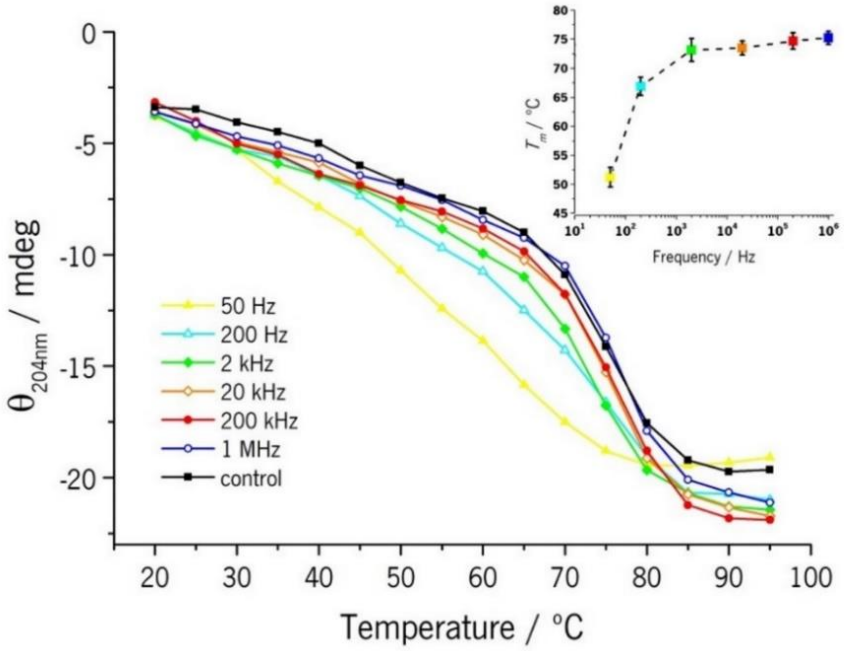

Figure 5.3: A - Changes in θ_{204} as a function of temperature for samples exposed to MEF of 10 V.cm^{-1} and different frequencies. Insert shows T_m for samples exposed to different electric frequencies.

Previous reports of MEF action upon properties of various proteins (i.e. conformational changes and enzymatic activity) have determined a higher influence when low frequencies were applied (Bekard & Dunstan, 2014; Chaminda P Samaranayake & Sastry, 2016a, 2016b, 2018). These observations are in line with our experimental data (where for the first time, thermal stability of β-lg under MEF were analysed): at lower frequencies, a decrease in T_m is clearly visible. In this sense, it can be concluded that at low frequencies, the presence of MEF can impose more substantial changes in β-lg's transition, whereas at high frequencies different structural features can be obtained although T_m remains practically unchanged. This will be more evident when looking at data of the secondary structure analysis (see Table 5.1).

Another relevant aspect of the MEF effects is the influence of the EF strength applied. The effect of this parameter could be determined adopting a similar procedure to the one used to evaluate the frequency effects, but now varying the MEF strength at a fixed frequency (i.e. 50 Hz). Figure 5.4 presents the transition profiles and T_m variation as a function of EF strength. An increased action of the MEF with the EF strength applied could be observed, resulting in a linear decrease of T_m and thus an early unfolding transition. The fact that this decrease is linear suggests a proportional action between the EF applied and the destabilization of the protein's structure.

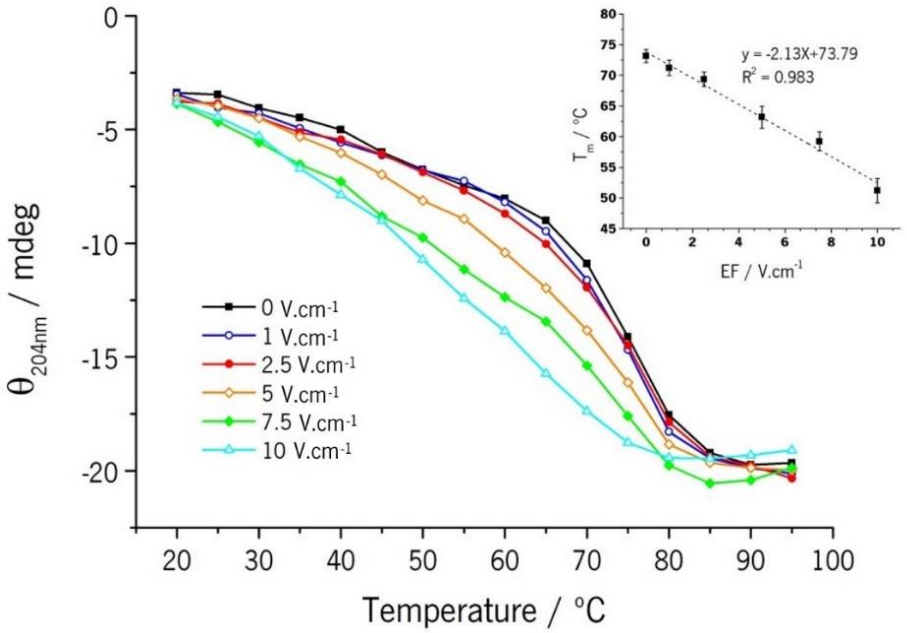

Figure 5.4: Changes in θ_{204} as a function of temperature for samples exposed to MEF at 50 Hz and different voltage gradients, insert shows T_m for samples exposed to different EF strength at 50 Hz.

A question often raised in EF-related applications is the possible occurrence of electrochemical reactions and their possible impacts. Apart from the precautions taken regarding the experimental apparatus and procedure, described in Materials and Methods, the linearity observed on the EF strength effects (see the Figure 5.4 insert) makes it reasonable to assume that if other contributions (e.g. electrolysis) were present, the behaviour observed would not be linear, especially at higher EF values.

5.3.2 Effects of MEF on structural features

Changes in β-lg structural features upon EF effects have been revealed by PEF treatments (again at different EF magnitudes, exposure time and without synergy with temperature), showing increased Trp exposure, increased ANS binding, secondary structure changes and differences in immunoglobulins binding (Xiang et al., 2011; Yang et al., 2018). After establishing the influence of EF strength and electrical frequency in β-lg unfolding profile and T_m, further experiments were focused on the determination of representative conditions in the assessment of structural changes induced by MEF - i.e. EF of 10 $V.cm^{-1}$ and frequencies of 50 Hz and 20 kHz, together with the control without the presence of MEF. Furthermore, considering the thermal transition profiles observed in CD results, it was decided to include the analysis of samples exposed to different temperatures, i.e. 50, 70 and 90 °C. These temperatures are just below the lower T_m and the higher T_m observed in this study and at a value where the thermal transition in all the conditions tested was complete. In this scenario, it was possible to evaluate EF effects at early stages of unfolding and after unfolding being completed.

The analysis of far-UV CD spectra of unfolded and refolded forms of the protein reveals different structural features, confirming that MEF can change protein secondary structure. Table 5.1 presents the data from structural analysis of representative samples. The major change in the structural features of β-lg caused by the temperature increase was the loss of β-strand content, accompanied by the increase of turns and random coil. The control samples and the samples exposed to MEF at 20 kHz experienced a loss of about half the β-strand content at 90 °C; however, it is important to note that this loss was higher for samples exposed to MEF. The use of MEF at 50 Hz lead to higher unfolding degree, resultant from a higher loss of β-strand, only preserving approximately a third of the native content when subjected to 90 °C treatment. The α-helix content suffered small decreases with increasing temperature values, comparable for all treatments up

until 70 °C. For the treatments at 90 °C, the α-helix content returns to levels similar to the native form both for the control and MEF at 20 kHz, while for MEF at 50 Hz treatments it continued to decrease.

Table 5.1: Secondary structure fractions of native β-lg and exposed in different thermo-electric conditions at temperatures of 50, 70 and 90 °C and respective refolded forms at 20 °C.

	α-helix	β-strand	Turn	Random coil
Native	17.4 ± 0.4	42.6 ± 1.0	19.8 ± 1.0	20.3 ± 0.7
Control at 50 °C	14.9 ± 0.7	34.2 ± 1.3	24.5 ± 1.1	26.2 ± 1.1
Control at 70°C	13.7 ± 0.3	31.8 ± 0.6	24.7 ± 0.4	29.7 ± 0.5
Control at 90°C	17.1 ± 0.1	22.1 ± 0.1	25.7 ± 1.1	34.9 ± 0.4
Control 50 °C refolded	15.8 ± 0.7	41.1 ± 0.8	20.8 ± 0.6	22.4 ± 1.0
Control 70 °C refolded	13.7 ± 0.4	39.1 ± 0.3	22.4 ± 0.2	24.9 ± 0.2
Control 90 °C refolded	15.2 ± 0.3	26.9 ± 0.4	24.1 ± 0.2	33.8 ± 0.8
EF 20 kHz at 50 °C	14.0 ± 00.4	34.4 ± 0.3	25.2 ± 0.9	26.5 ± 0.1
EF 20 kHz at 70 °C	12.6 ± 0.2	29.6 ± 1.2	25.9 ± 0.3	31.6 ± 1.3
EF 20 kHz at 90 °C	17.3 ± 0.8	19.1 ± 0.8	24.0 ± 0.6	39.2 ± 0.5
EF 20 kHz 50 °C refolded	11.7 ± 1.7	40.7 ± 0.7	22.2 ± 0.5	22.5 ± 0.7
EF 20 kHz 70 °C refolded	13.3 ± 00.8	38.2 ± 1.5	22.7 ± 0.6	26.0 ± 0.9
EF 20 kHz 90 °C refolded	14.8 ± 0.4	24.6 ± 0.6	25.6 ± 0.7	35.2 ± 0.4
EF 50 Hz at 50 °C	14.3 ± 0.6	27.7 ± 2.1	24.0 ± 1.6	33.9 ± 2.3
EF 50 Hz at 70 °C	13.7 ± 0.9	24.1 ± 1.8	25.0 ± 1.2	37.2 ± 2.4
EF 50 Hz at 90 °C	10.7 ± 0.4	12.4 ± 1.4	30.3 ± 0.9	46.0 ± 0.8
EF 50 Hz 50 °C refolded	14.2 ± 1.8	39.1 ± 1.5	21.7 ± 0.5	25.6 ± 2.3
EF 50 Hz 70 °C refolded	13.2 ± 0.7	27.4 ± 0.4	23.9 ± 0.8	35.5 ± 0.5
EF 50 Hz 90 °C refolded	10.5 ± 0.6	23.6 ± 0.7	24.6 ± 0.4	40.9 ± 0.8

After cooling back to 20 °C, all samples show a partial refolding, mostly evident by the recovery of β-strand content and decrease of random coil. Again, the samples exposed to MEF at 50 Hz stand out, maintaining the low α-helix content during refolding and a substantial recovery of β-strand content. Overall, these results allow concluding that different secondary structures' distributions

are imposed by the presence of MEF during β-lg thermal unfolding, as well as after a partial refolding for all the temperatures tested.

5.3.3 Fluorescence determinations

Heating at 50 °C resulted in a minor decrease in fluorescence when compared with the native protein, but there was no clear differentiation among the different treatments. However, for the temperatures of 70 and 90 °C a clear difference exists in the fluorescence measurements among the various EF conditions applied (see Figure 5.5).

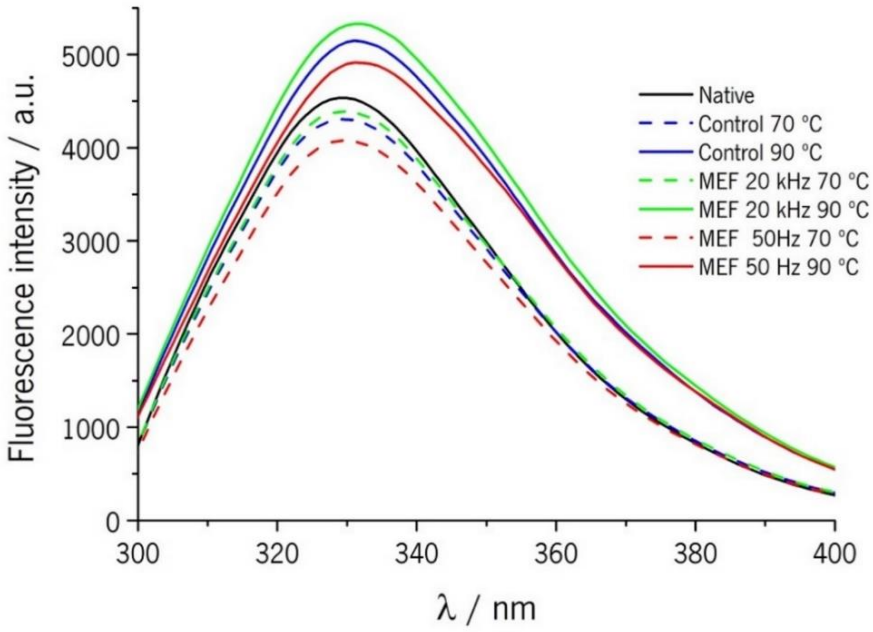

Figure 5.5: Fluorescence emission spectra (excitation at 295 nm) of native β-lg and exposed to temperatures of 70 and 90 °C by control treatments (without the presence of MEF) and MEF of 10 $V.cm^{-1}$ at 50 Hz and 20 kHz.

The exposure to temperatures of 70 °C resulted in a decrease in Trp fluorescence, which was more pronounced for the samples exposed to an EF of 50 Hz. The control samples and the one exposed to MEF at 20 kHz suffered smaller decreases and exhibited a comparable fluorescence profile, with a slightly higher intensity for the later. No shift in the fluorescence maximum was detected, indicating no change in the Trp microenvironment, thus the decrease in fluorescence observed must be the result of an increased quenching from the neighbour amino acids due to small conformation rearrangements or higher structural dynamics (Bhattacharjee & Das, 2000; Lakowicz, 2006). The exposure to temperatures of 90 °C resulted in an increase of Trp

fluorescence and a 4 nm red-shift on the fluorescence maximum with a broadening of the spectra to the right in the three conditions tested. These facts corroborate the occurrence of substantial structural changes resulting in different Trp local environment and solvent accessibility. The presence of MEF again, imposed higher fluorescence intensity for EF at 20 kHz, and lower for MEF at 50 Hz when compared with the control, confirming different protein conformations induced by the application of MEF at different frequencies.

The use of ANS hydrophobic fluorescent probe allows assessing the degree of structural changes and possible binding affinities of proteins (Collini, D'Alfonso, & Baldini, 2000; Hawe, Sutter, & Jiskoot, 2008). Similarly to the Trp fluorescence results, the experiments at 50 °C did not produce significant changes in the ANS fluorescence. The emission spectra of ANS - β-lg complex presented in Figure 5.6 show a fluorescence intensity increase and a blue shift with the exposure to temperatures of 70 and 90 °C. The intensity increase together with the observed peak shift indicates higher energy involved in the ANS-protein interaction, thus suggesting increased affinity towards the hydrophobic pocket (Hawe et al., 2008).

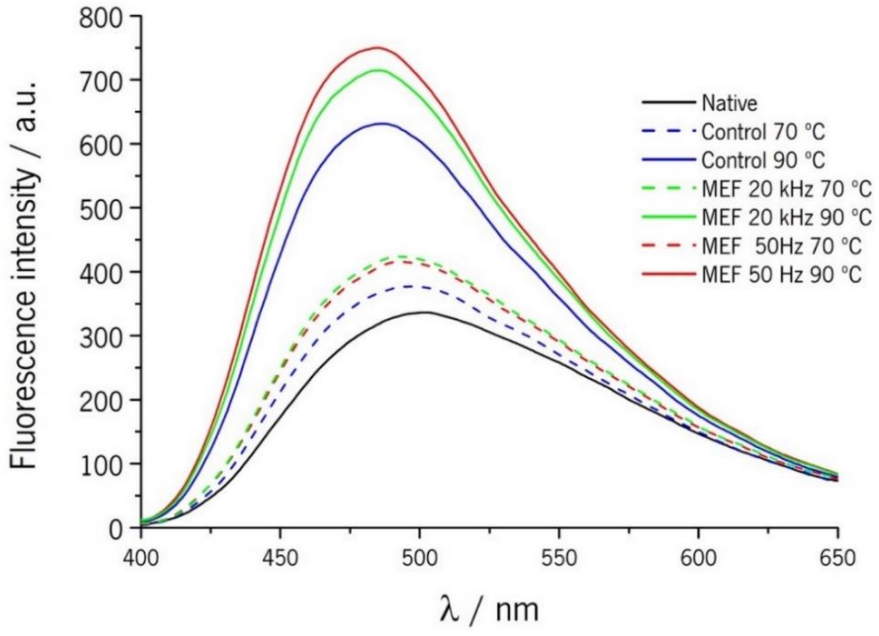

Figure 5.6.: ANS fluorescence emission spectra (excitation 370 nm) for native β-lg and exposed to temperatures of 70 and 90 °C by control treatments (without the presence of MEF) and MEF of 10 $V.cm^{-1}$ at 50 Hz and 20 kHz.

MEF-exposed samples display higher fluorescence intensities than the control, presumably resulting from an increased affinity of ANS. MEF samples at 70 °C show similar fluorescence intensities, while for 90 °C, MEF at 50 Hz presented higher ANS affinity than 20 kHz, being both clearly above the control. The β-lg - ANS affinity for MEF treatments at 50 Hz and 20 kHz is similar and clearly higher than the control. The increase in ANS florescence may arise from an increased binding affinity or from the exposure of more hydrophobic regions. Interestingly, ANS fluorescence data contrasts with preceding results, where electrical frequency substantially influences secondary structures' distribution and Trp exposure, while these events do not seem to be reflected in ANS binding. Instead, the presence of MEF during unfolding, regardless of the frequency applied, seems to be more relevant. An increased access to the hydrophobic barrel or an increase in the local hydrophobicity caused by MEF action, rather than the formation of new binding sites, could explain the observed behaviour. Further studies and the use of more advanced fluorescence techniques (e.g. synchronous and 3D fluorescence) are needed to fully disclose these phenomena and establish the origin of the ANS-β-lg fluorescence increase upon MEF treatments.

5.3.4 Quenching experiments

Binding experiments were conducted with retinol, using fluorescence-quenching method. The fluorescence quenching data were analysed with the Stern–Volmer equation (Lakowicz, 2006) – Equation 5.1:

$$F_0/F = 1 + k_q\tau_0[Q] = 1 + K_{SV}[Q] \quad (5.1)$$

The parameters F_0 and F are the relative fluorescence intensities in the absence and presence of quencher, respectively. K_{SV} is the Stern–Volmer quenching constant, $[Q]$ is the concentration of quencher, k_q is the quenching rate constant; and τ_0 is the average lifetime of the fluorophore in the excited state, which for Trp in β-lg is 1.28 ns (Liang, Tajmir-Riahi, & Subirade, 2008).

Fluorescence quenching is a process that leads to the decrease of fluorescence quantum yield from a fluorophore and it can be caused by molecular interactions involving dynamic or static mechanisms. Figure 5.7 represents the fluorescent quenching caused by retinol binding to the native β-lg. Retinol-β-lg form a stable complex where a static quenching mechanism is dominant (Agudelo, Bourassa, Bariyanga, & Tajmir-Riahi, 2017; Khorsand Ahmadi et al., 2015; G. Kontopidis et al., 2004). The experimental data presented a linear Stern-Volmer relation and the estimated k_q

value is substantially higher than the maximum collisional quenching constant ($2.0 \times 10^{10}\ M^{-1}\ s^{-1}$), confirming the formation of a stable complex between retinol and β-lg. Once the complex formation was verified, resulting from a static quenching mechanism, than K_{SV} can be interpreted as the association constant (Lakowicz, 2006).

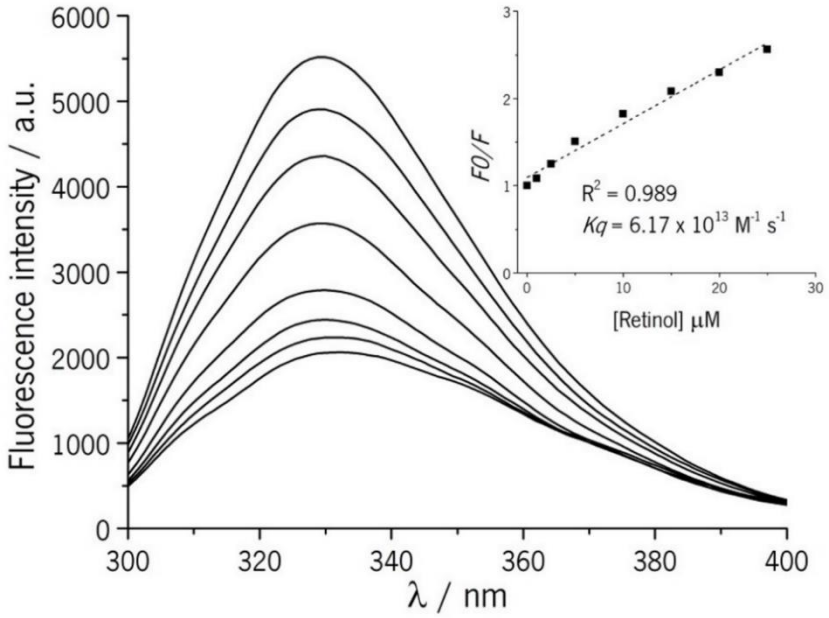

Figure 5.7: A- Fluorescence quenching spectra (excitation at 295 nm) of native β-lg in the presence of retinol ranging from 0 to 25 μM (Figure insert shows the Stern-Volmer plot for binding of retinol to native β-lg), B- K_{SV} of Retinol binding to β-lg in native form and after exposure to different thermo-electric treatments.

The same procedure was reproduced with the treated samples to determine the association constant of retinol, allowing to assess the influence of the different structural features imposed by MEF on β-lg binding properties (see Figure 5.8).

K_{SV} values decrease with the increasing temperature exposure, reflecting the lower accessibility of retinol to Trp in β-lg due to partial destruction of native structure. For control experiments, the decrease of K_{SV} is significant for the samples exposed to the three temperature levels. The samples exposed to MEF at 50 Hz and 20 kHz present no significant differences when treated at the same temperatures. K_{SV} values present a higher decrease for samples exposed to 50 °C, when compared with the control (in fact, K_{SV} values of MEF samples at 50 °C are comparable to those of control samples at 70 °C). Despite of the drop of K_{SV} values by the use of higher temperatures, they only become significant for MEF-exposed samples at 50 Hz and 90 °C. In general, MEF-exposed

samples presented lower variation of K_{SV} and retained higher affinity (in this case when exposed to higher temperatures) with retinol than control samples.

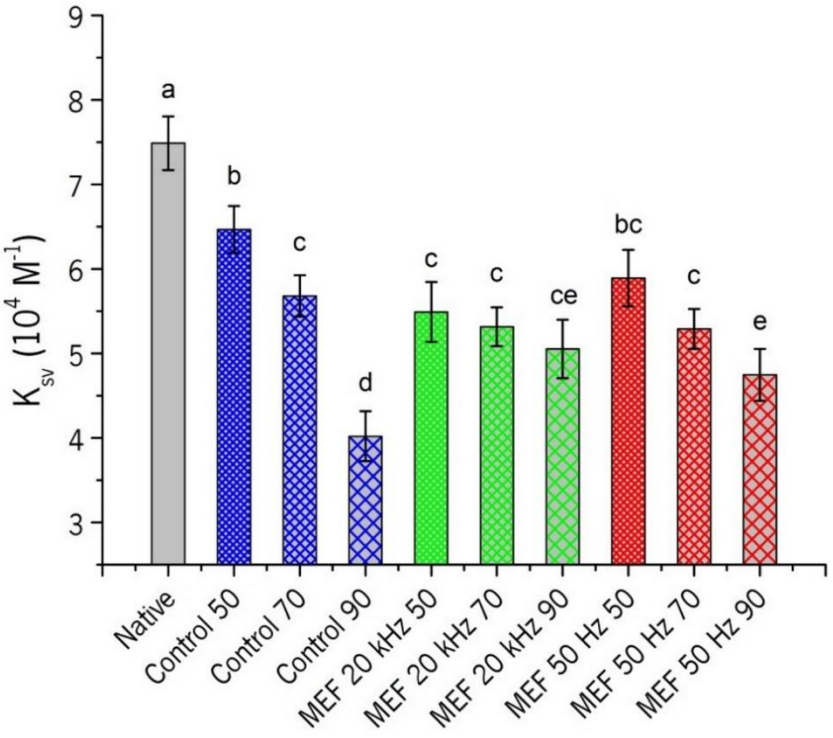

Figure 5.8: K_{SV} of retinol binding to β-lg in native form and after exposure to different thermo-electric treatments. For each column, different letters correspond to statistically significant differences ($p < 0.05$).

The samples exposed to MEF at 50 Hz and 20 kHz present no significant differences when treated at the same temperatures. K_{SV} values present a higher decrease for samples exposed to 50 °C, when compared with the control (in fact, K_{SV} values of MEF samples at 50 °C are comparable to those of control samples at 70 °C). Despite of the drop of K_{SV} values by the use of higher temperatures, they only become significant for MEF-exposed samples at 50 Hz and 90 °C. In general, MEF-exposed samples presented lower variation of K_{SV} and retained higher affinity (in this case when exposed to higher temperatures) with retinol than control samples.

Unlike to ANS results, where the binding substantially increases with the partial unfolding of β-lg, in the case of retinol the binding affinity suffers a decrease due to the protein's structural changes. This may be related with the nature of the interactions established by the two compounds. ANS interactions are of non-specific nature and thus ANS binds to any accessible hydrophobic patch, resultant from the unfolding process (Hawe et al., 2008). Retinol binding, however, occurs by specific interactions involving several amino acids in the interior of the β-barrel and at least one

hydrogen bond (George Kontopidis et al., 2002). Hence, it is expected that changes in protein conformation, particularly in the central barrel, would impact negatively the retinol-β-lg complex formation. Interestingly, and despite of the significant ($p < 0.05$) change in K_{SV} values imposed by the different thermo-electric treatments, K_{SV} values remain on same magnitude order demonstrating a stable complex formation. This implies the maintenance of a substantial retinol affinity to the partially unfolded forms of β-lg. The secondary structure analysis has demonstrated that the refolded forms of the protein still hold substantial fractions of secondary structure, particularly β-strand content, even after submitting the samples to 90 °C with or without MEF in different conditions. The retention of significant fractions of structural features is consistent with the existence of a molten globule form and thus the core, composed by the β-strands which form a hydrophobic cavity, may be (at least partially) preserved.

Identically to ANS experiments, samples exposed to MEF display a similar behaviour, resulting in a higher affinity of hydrophobic compounds when exposed to higher temperatures. This reaffirms the MEF effects in β-lg interactions and the ability to form complexes with small hydrophobic compounds.

5.4 CONCLUSION

The presence of MEF during β-lg's thermal unfolding resulted in changes in the estimated T_m values and in different structural features. The structural changes were observed at the target temperatures tested and upon partial refolding (after the samples have been cooled back to room temperature). The thermal transition and structural changes were largely influenced by the electrical frequency and by the EF strength applied. The presence of MEF was also reflected in the protein's Trp fluorescence and affinity to hydrophobic compounds. Contrasting with the thermal transitions and structural features, the affinity to hydrophobic compounds appeared to have little dependence on frequency. Interestingly the effects of MEF in unfolded forms of β-lg exposed to temperatures equal or higher to 70 °C, revealed to increase the affinity to ANS and maintain higher affinity to retinol. These results demonstrated that the use MEF along with thermal unfolding give rise to changes in structural and functional aspects of β-lg. This brings implications to the technological applications involving MEF – e.g. ohmic heating, electro filtration, dielectric separation – and it opens perspectives of new strategies to control protein technological properties.

5.5 REFERENCES

Agudelo, D., Bourassa, P., Bariyanga, J., & Tajmir-Riahi, H. A. (2017). Loading efficacy and binding analysis of retinoids with milk proteins: a short review. *Journal of Biomolecular Structure and Dynamics*, *1102*, 1–9. https://doi.org/10.1080/07391102.2017.1411833

Bekard, I., & Dunstan, D. E. (2014). Electric field induced changes in protein conformation. *Soft Matter*, *10*(3), 431–437. https://doi.org/10.1039/c3sm52653d

Bhattacharjee, C., & Das, K. P. (2000). Thermal unfolding and refolding of β-lactoglobulin. *European Journal of Biochemistry*, *267*(13), 3957–3964. https://doi.org/10.1046/j.1432-1327.2000.01409.x

Bhattacharyya, S., & Varadarajan, R. (2013). Packing in molten globules and native states. *Current Opinion in Structural Biology*, *23*(1), 11–21. https://doi.org/10.1016/j.sbi.2012.10.010

Cairoli, S., Iametti, S., & Bonomi, F. (1994). Reversible and irreversible modifications of β-lactoglobulin upon exposure to heat. *Journal of Protein Chemistry*, *13*(3), 347–354. https://doi.org/10.1007/BF01901568

Collini, M., D'Alfonso, L., & Baldini, G. (2000). New insight on β-lactoglobulin binding sites by 1-anilinonaphthalene-8-sulfonate fluorescence decay. *Protein Science*, *9*(10), 1968–1974. https://doi.org/10.1110/ps.9.10.1968

Fessas, D., Iametti, S., Schiraldi, A., & Bonomi, F. (2001). Thermal unfolding of monomeric and dimeric β-lactoglobulins. *European Journal of Biochemistry*, *268*(20), 5439–5448. https://doi.org/10.1046/j.0014-2956.2001.02484.x

Greenfield, N. J. (2007). Using circular dichroism collected as a function of temperature to determine the thermodynamics of protein unfolding and binding interactions. *Nature Protocols*, *1*(6), 2527–2535. https://doi.org/10.1038/nprot.2006.204

Hawe, A., Sutter, M., & Jiskoot, W. (2008). Extrinsic Fluorescent Dyes as Tools for Protein Characterization. *Pharmaceutical Research*, *25*(7), 1487–1499. https://doi.org/10.1007/s11095-007-9516-9

Keppler, J. K., Stuhldreier, M. C., Temps, F., & Schwarz, K. (2014). Influence of mathematical

models and correction factors on binding results of polyphenols and retinol with β-lactoglobulin measured with fluorescence quenching. *Food Biophysics*, *9*(2), 158–168. https://doi.org/10.1007/s11483-013-9328-x

Khorsand Ahmadi, S., Mahmoodian Moghadam, M., Mokaberi, P., Reza Saberi, M., & Chamani, J. (2015). A comparison study of the interaction between β-lactoglobulin and retinol at two different conditions: Spectroscopic and molecular modeling approaches. *Journal of Biomolecular Structure and Dynamics*, *33*(9), 1880–1898. https://doi.org/10.1080/07391102.2014.977351

Kontopidis, G., Holt, C., & Sawyer, L. (2002). The Ligand-binding Site of Bovine β-Lactoglobulin: Evidence for a Function? *Journal of Molecular Biology*, *318*(4), 1043–1055. https://doi.org/10.1016/S0022-2836(02)00017-7

Kontopidis, G., Holt, C., & Sawyer, L. (2004). Invited Review: β-Lactoglobulin: Binding Properties, Structure, and Function. *Journal of Dairy Science*, *87*(4), 785–796. https://doi.org/10.3168/jds.S0022-0302(04)73222-1

Lakowicz, J. R. (2006). *Principles of Fluorescence Spectroscopy*. (J. R. Lakowicz, Ed.), *Principles of fluorescence spectroscopy, Springer, New York, USA, 3rd edn, 2006.* Boston, MA: Springer US. https://doi.org/10.1007/978-0-387-46312-4

Liang, L., Tajmir-Riahi, H. A., & Subirade, M. (2008). Interaction of β-Lactoglobulin with resveratrol and its biological implications. *Biomacromolecules*, *9*(1), 50–56. https://doi.org/10.1021/bm700728k

Loveday, S. M. (2016). β-Lactoglobulin heat denaturation: A critical assessment of kinetic modelling. *International Dairy Journal*, *52*, 92–100. https://doi.org/10.1016/j.idairyj.2015.08.001

Orwig, S. D., & Lieberman, R. L. (2011). Biophysical Characterization of the Olfactomedin Domain of Myocilin, an Extracellular Matrix Protein Implicated in Inherited Forms of Glaucoma. *PLoS ONE*, *6*(1), e16347. https://doi.org/10.1371/journal.pone.0016347

Papiz, M. Z., Sawyer, L., Eliopoulos, E. E., North, A. C. T., Findlay, J. B. C., Sivaprasadarao, R., … Kraulis, P. J. (1986). The structure of β-lactoglobulin and its similarity to plasma retinol-binding protein. *Nature*, *324*(6095), 383–385. https://doi.org/10.1038/324383a0

Pataro, G., Barca, G. M. J., Pereira, R. N., Vicente, A. A., Teixeira, J. A., & Ferrari, G. (2014). Quantification of metal release from stainless steel electrodes during conventional and pulsed ohmic heating. *Innovative Food Science and Emerging Technologies*, *21*, 66–73. https://doi.org/10.1016/j.ifset.2013.11.009

Pereira, R. N., Souza, B. W. S., Cerqueira, M. A., Teixeira, J. A., & Vicente, A. A. (2010). Effects of Electric Fields on Protein Unfolding and Aggregation: Influence on Edible Films Formation. *Biomacromolecules*, *11*(11), 2912–2918. https://doi.org/10.1021/bm100681a

Pereira, R. N., Teixeira, J. A., & Vicente, A. A. (2011). Exploring the denaturation of whey proteins upon application of moderate electric fields: a kinetic and thermodynamic study. *J Agric Food Chem*, *59*(21), 11589–11597. https://doi.org/10.1021/jf201727s

Perez, O. E., & Pilosof, A. M. R. (2004). Pulsed electric fields effects on the molecular structure and gelation of β-lactoglobulin concentrate and egg white. *Food Research International*, *37*(1), 102–110. https://doi.org/10.1016/j.foodres.2003.09.008

QI, X. L., HOLT, C., MCNULTY, D., CLARKE, D. T., BROWNLOW, S., & JONES, G. R. (1997). Effect of temperature on the secondary structure of β -lactoglobulin at pH 6.7, as determined by CD and IR spectroscopy: a test of the molten globule hypothesis. *Biochemical Journal*, *324*(1), 341–346. https://doi.org/10.1042/bj3240341

Rieger, P. H. (1994). *Electrochemistry*. Dordrecht: Springer Netherlands. https://doi.org/10.1007/978-94-011-0691-7

Rodrigues, R. M., Martins, A. J., Ramos, O. L., Malcata, F. X., Teixeira, J. A., Vicente, A. A., & Pereira, R. N. (2015). Influence of moderate electric fields on gelation of whey protein isolate. *Food Hydrocolloids*, *43*, 329–339. https://doi.org/10.1016/j.foodhyd.2014.06.002

Samaranayake, C. P., & Sastry, S. K. (2016a). Effect of moderate electric fi elds on inactivation kinetics of pectin methylesterase in tomatoes : The roles of electric fi eld strength and temperature. *Journal of Food Engineering*, *186*, 17–26. https://doi.org/10.1016/j.jfoodeng.2016.04.006

Samaranayake, C. P., & Sastry, S. K. (2016b). Effects of controlled-frequency moderate electric

fields on pectin methylesterase and polygalacturonase activities in tomato homogenate. *Food Chemistry*, *199*(Supplement C), 265–272. https://doi.org/https://doi.org/10.1016/j.foodchem.2015.12.010

Samaranayake, C. P., & Sastry, S. K. (2018). LWT - Food Science and Technology In-situ activity of α -amylase in the presence of controlled-frequency moderate electric fi elds. *LWT - Food Science and Technology*, *90*(October 2017), 448–454. https://doi.org/10.1016/j.lwt.2017.12.053

Samaranayake, C. P., Sastry, S. K., & Zhang, H. (2005). Pulsed ohmic heating - A novel technique for minimization of electrochemical reactions during processing. *Journal of Food Science*, *70*(8), E460–E465. https://doi.org/10.1111/j.1365-2621.2005.tb11515.x

Tolkach, A., & Kulozik, U. (2007). Reaction kinetic pathway of reversible and irreversible thermal denaturation of β-lactoglobulin. *Le Lait*, *87*(4–5), 301–315. https://doi.org/10.1051/lait:2007012

van de Weert, M. (2010). Fluorescence Quenching to Study Protein-ligand Binding: Common Errors. *Journal of Fluorescence*, *20*(2), 625–629. https://doi.org/10.1007/s10895-011-0953-

Whitmore, L., & Wallace, B. A. (2008). Protein secondary structure analyses from circular dichroism spectroscopy: Methods and reference databases. *Biopolymers*, *89*(5), 392–400. https://doi.org/10.1002/bip.20853

Xiang, B. Y., Ngadi, M. O., Ochoa-Martinez, L. A., & Simpson, M. V. (2011). Pulsed Electric Field-Induced Structural Modification of Whey Protein Isolate. *Food and Bioprocess Technology*, *4*(8), 1341–1348. https://doi.org/10.1007/s11947-009-0266-z

Yang, W., Tu, Z., Wang, H., Zhang, L., Kaltashov, I. A., Zhao, Y., … Ye, W. (2018). The mechanism of reduced IgG/IgE-binding of β-lactoglobulin by pulsed electric field pretreatment combined with glycation revealed by ECD/FTICR-MS. *Food and Function*, *9*(1), 417–425. https://doi.org/10.1039/c7fo01082f

CHAPTER 6.

EFFECTS OF MEF IN WHEY PROTEIN GELATION

6.1 INTRODUCTION

The increase of consumer demands regarding high quality foods and environmental concerns has triggered the development of emergent technological approaches for food processing. OH is recognised as an emerging high-potential technology for tomorrow (De Vries et al., 2018), being the aim of a continued research and counting with a significant industrial interest (Priyadarshini, Rajauria, O'Donnell, & Tiwari, 2018). In the previous chapters, MEF action was established during β-lg thermal denaturation and confirmed to cause distinctive structural features in the unfolded protein. These changes were dependent of the electrical variables' magnitude used (i.e. electric field strength and electrical frequency), impacting functional properties such as protein interactions, SH and hydrophobic groups accessibility and molecular binding. These properties are fundamental to induce and control protein aggregation and gelation.

During protein gelation, the interactions established between protein molecules are fundamental to the network formation, plus their nature and extent define the final gel properties (Bryant & McClements, 1998; T. van Vliet, 2000). In order to potentiate protein interactions an initial denaturation step is often induced by thermal treatment. Once the protein structure is destabilized, reactive groups are exposed and interact with other proteins, starting aggregation and ultimately gelation (Ramos et al., 2014). If the protein denaturation and initial aggregation step is carried out at relative low protein concentration and with predominant electrostatic repulsive forces (i.e. pH far from isoelectric point and low salt concentration), the resultant unfolded proteins/aggregates remain soluble at room temperature. The electrostatic balance of these stable dispersions can be changed by modifying the solution's pH or by adding salts, resulting in protein/aggregates interactions and a network formation (Amin, Barnett, Pathak, Roberts, & Sarangapani, 2014; Chi, Krishnan, Randolph, & Carpenter, 2003). This process is known as cold gelation and has demonstrated potential to produce highly tuneable gels with distinctive characteristics and with the ability to incorporate thermal labile compounds (Ako, Nicolai, & Durand, 2010; Guo, 2019; Nicolai, Britten, & Schmitt, 2011). Furthermore, as aggregation and gelation take place separately, it is possible to study the relationship between aggregate and final gel properties (Alting, Hamer, De Kruif, & Visschers, 2003; Ton Van Vliet, Lakemond, & Visschers, 2004).

Changes in physical properties of gels affect their functional and sensorial properties, which are a complex function of the raw composition, established molecular interactions, microscopic and mesoscopic structures and ultimately the gel matrix rheological behaviour. The objective of this section was to study the MEF effects on the gelation mechanism and functional properties of WPI, from the molecular to

macroscopic levels. A cold-set gelation process was selected, allowing to evaluate the process effects in the initial denaturation and aggregation step as well as on the final properties of the cold-set gel.

6.2 MATERIALS AND METHODS

6.2.1 Materials

WPI powder (Lacprodan DI-9212) was kindly supplied by Arla Foods Ingredients (Viby, Denmark). The WPI contained 91% (in dry weight) of total protein content and trace contents of lactose (max. 0.5%) and fat (max. 0.2%). Ultrapure water obtained with a Milli-Q Ultrapure water purification system (Millipore, Bedford MA. USA) was used to prepare all solutions. Sodium chloride (ASC reagent grade) supplied by Sigma-Aldrich (Germany) was used to induce cold gelation of WPI. All other chemicals used were of analytical reagent (AR) grade.

6.2.2 Gel preparation

6.2.2.1 Whey protein solutions

WPI solutions at 7.5 % (w/v) were prepared in sodium phosphate buffer (2.5×10^{-2} mol.L^{-1}, pH 7) containing 0.02 % (w/v) of sodium azide. The dispersion was magnetically stirred at room temperature for 2 h and, if necessary, pH was adjusted to 7 with NaOH or HCl 1 mol.L^{-1} solutions. The solutions were then stored overnight at 4 °C and used on the next day for gels preparation.

6.2.2.2 Thermal treatments

Thermal treatments, OH and Cov, were performed on a double-jacketed glass cylinder containing stainless steel electrodes at each edge, as described in Chapter 4. The treatments were performed for a total of 15 min, composed by a 5 min heating period and 10 min of holding at 90 °C. The heating kinetics and thermal profile were kept similar for both types of treatment. For Cov treatments where no EF was applied, temperature was controlled circulating water in the vessel jacket from a thermo-stabilized water bath. For the OH treatments, the temperature was controlled by regulating the voltage output of a function generator (1 Hz to 25 MHz and 1 to 10 V; Agilent 33220A, Penang. Malaysia) which was then amplified in an amplifier system (Peavey CS3000, Meridian, MS, USA). In order to evaluate the influence of EF strength of and electric frequency, four OH treatments were selected (i.e. OH 20 kHz 10 V.cm^{-1}, OH 20 kHz 20 V.cm^{-1}, OH 50 Hz 10 V.cm^{-1} and OH 50 Hz 20 V.cm^{-1}). Temperature was measured with a type K

thermocouple (Omega Engineering, Inc., Stamford, CT. USA), connected to a data logger (USB-9161, National Instruments Corporation, Austin, TX. USA). During the treatments, samples were gently stirred (with a magnetic stirrer) to ensure homogeneity. At the end of the treatments, the samples were transferred to screw cap glass tubes and placed in a melting ice bath for 15 min. After reaching room temperature, a part of each solution was collected for aggregate characterization and the remaining was used in gelation experiments.

6.2.3 Cold gelation

Cold-set gelation of the thermally treated samples was induced by adding NaCl 5 mol.L^{-1} solution until a final concentration of 0.2 mol.L^{-1}. The mixture was quickly homogenized, placed in a custom-built polytetrafluoroethylene (PTFE) well plate to produce gel cylinders with 40 x 1.5 mm for rheological analysis and in 24 wells (polystyrene plate, wells flat bottom), producing gels with 5 x 5 mm for the remaining tests. The gels were let set for 24 h at room temperature before further analysis.

6.2.3 Characterization of protein aggregates and cold-set gels

6.2.3.1 Particle size analysis

Particle size measurements of the aggregates' suspensions were made by dynamic light scattering (DLS) using a Zetasizer Nano (ZEN 3600, Malvern Instruments Ltd., Malvern, U.K.) Samples of WPI aggregates were diluted at 1:10 in the same buffer used for the preparation of WPI solutions, and 1 mL of the resulting dilute solution were poured into disposable sizing cuvettes. The temperature of the cell was maintained at 25 ± 0.5 °C during the measurement. The poly-dispersity index (PDI) derived from cumulants analysis of the DLS measurements was also evaluated and describes the width or the relative variance of the particle size distribution. All measurements were carried out at least in triplicate.

6.2.3.2 Determination of accessible sulfhydryl groups

Determination of the free SH on the aggregate solutions was performed according to the methodology described in Chapter 4.

6.2.3.3 Rheological characterization of aggregate solutions and cold-set gels

Rheological measurements were performed in triplicate at 25 °C on a TA Instruments HR-1 rheometer equipped with a Peltier plate (TA Instruments, New Castle, USA). Flow curves were obtained for the aggregate suspensions using a cone-plate (60 mm, 2° angle, truncation 64 um) and performing three steps program (up-down-up) using a continuous ramp and shear rate range between 0.1 and 300 s^{-1}. The three steps program were carried out in order to eliminate the time-dependence, allowing the system to reach the steady state.

The viscoelastic properties of the cold-set gels were evaluated by oscillatory measurements. Using a plate-plate (40 mm, 1500 μm gap) the frequency sweep tests were performed between 0.1 and 10 Hz within the linear viscoelasticity domain (0.5% strain). Complex modulus (G^*) and tanδ (G''/G') were evaluated.

Mechanical properties were determined by uniaxial compression measurements using a TA HD Plus Texture Analyzer (Stable Micro Systems. UK) with an aluminium 25 mm probe. The force used to compress 80 % of the initial height was measured using a crosshead speed of 1 $mm.s^{-1}$. A trigger force of 0.05 N was used and at least 10 samples of each experimental condition were tested.

From the force-deformation data, Hencky stress (σ_H) and strain (ε_H) were calculated according to Eqs. (6.1) and (6.2), respectively (Steffe, 1996). The gel rupture point was evaluated by the maximum peak of the stress–strain curve, and the Young's modulus (E) was the slope of the first linear interval (0 - 5% deformation) of the stress–strain curve (Rosenthal, 1999; Steffe, 1996).

$$\sigma_H = F(t) \times \left[\frac{H(t)}{H_0 A_0}\right] \quad (6.1)$$

$$\varepsilon_H = -ln\left[\frac{H(t)}{H_0}\right] \quad (6.2)$$

$F(t)$ is the force at time t; A_0 and H_0 are the initial area and height of the sample, respectively; and $H(t)$ is the height at time t.

6.2.3.4 Water-holding capacity (WHC) and swelling degree

WHC of the gels was determined by weighing 5 x 5 mm cylindrical samples (≈0.5 g) before and immediately after centrifugation. The gels were placed on top of 3 layers of Whatmann #1 filter paper (Maidstone, UK), placed in centrifuge tubes and centrifuged at 25 °C and 250 g for 5 min using an EBA 20 centrifuge (Andreas Hettich GmbH & Co.KG. Tuttlingen, Germany). The WHC was determined by the

relation of the water released into the filter paper and the water in the gel before centrifugation, according to Equation 6.3.

$$WHC = 100 \times \left[1 - \left(\frac{water_{released}\ (g)}{water_{gel}\ (g)}\right)\right] \quad (6.3)$$

The swelling degree of the gels was determined on 5 x 5 mm cylindrical samples (≈0.5 g). Samples were weighted before submerging them in 5 mL of the same buffer used for the preparation of WPI solutions. After 24 h soaking at room temperature, the samples were removed from the buffer solution. The excess of liquid left on the gel surface was gently removed with filter paper and the samples were weighted. The swelling degree was expressed in percentage according to Equation 6.4.

$$Swelling\ ratio\ (\%) = \frac{W_s - W_i}{W_i} \times 100 \quad (6.4)$$

Were W_s is the mass of the swollen gel and W_i in the initial gel mass.

6.2.3.5 Protein solubility

The protein solubility of WPI gels was determined in five different solvent systems: in phosphate buffer 0.025 mol.L^{-1}, pH 7 (PB), PB and 1 % sodium dodecyl sulphate (SDS), PB and Urea 8 mol.L^{-1} (U), PB and 0.2 % 2-mercaptoethanol (2-Me) and the conjugation of all the previous. Cylindrical gel samples of 5 x 5 mm (≈0.5 g) were individually weighed, placed in glass screwcap tubes and 5 mL of each one of the solutions added. The experiments took place under agitation on an orbital shaker (KL-2 Edmund Buhler. Germany) at 60 rpm at room temperature during a period of 5 days. At days 1, 3 and 5, the samples were centrifuged at 3421 g for 5 min on an EBA 20 centrifuge (Andreas Hettich GmbH & Co.KG., Tuttlingen, Germany). After centrifugation, supernatant fractions were recovered and the soluble protein determined by absorbance at 280 nm on a UV-VIS spectrophotometer (V-560. Jasco Inc., Tokyo, Japan) using and absorbance coefficient of 0.9565 m^2.g^{-1}.

6.2.3.6 Microscopy study of the cold-set gels structure

Cold-set gels microstructure was investigated by Confocal Laser Scanning Microscopy (CLSM). Before the cold-set gels preparation, protein aggregates' solutions obtained by thermo-electric treatment were stained with rhodamine B isothiocyanate obtained from Sigma (R1755). After the staining procedure, the cold-set gel was prepared and mounted on a microscope slide, covered with a slip and hermetically sealed

to prevent evaporation. The microstructure of the samples was analysed 24 h after the preparation. The images were acquired in a Confocal Scanning Laser Microscope (Olympus BX61, Model FluoView 1000 Version 4.2.1.20), in fluorescent mode (laser excitation line 559 nm and emission filters BA 575–675, red channel), using the program FV1000-Ver4.2.1.20 (Olympus).

6.2.4 Data analysis

All data analysis, fitting, plotting and statistical analysis procedures were performed on Origin 8.1 software (OriginLab Corporation, Northampton, MA, USA). Unless otherwise stated all experiments were run at least in triplicate.

6.3 RESULTS AND DISCUSSION

6.3.1 Aggregates characterization

6.3.1.1 Particles size and SH accessibility

The first stage of protein cold-gelation consists on protein denaturation and aggregation into a stable aggregates' suspension. The aggregation extent and disulphide interactions are the key factors to define the gel properties once cold gelation is induced (Ako et al., 2010; Alting, Hamer, de Kruif, Paques, & Visschers, 2003). The effects of the thermo-electric treatments on WPI aggregation and SH groups accessibility are presented in Table 6.1.

Table 6.1: Hydrodynamic size diameter (*Z-ave*), polydispersity index (*PdI*) and free SH groups of whey protein solution and aggregates.

Sample	*Z-ave* (nm)	*PdI*	Accessible SH groups (%)
Unheated WPI	15.390 ± 2.399 ^{a}	0.592 ± 0.030 ^{a}	14.308 ± 1.336 ^{a}
Cov	152.467 ± 1.786 ^{b}	0.439 ± 0.057 ^{b}	86.774 ± 1.105 ^{b}
OH 20 kHz 10 V.cm^{-1}	137.202 ± 3.541 ^{c}	0.423 ± 0.018 ^{bc}	81.940 ± 2.182 ^{c}
OH 20 kHz 20 V.cm^{-1}	127.912 4.678 ^{d}	0.399 ± 0.058 ^{bc}	80.104 ± 1.481 ^{c}
OH 50 Hz 10 V.cm^{-1}	121.703 ± 4.248 ^{d}	0.349 ± 0.059 ^{c}	72.601 ± 3.721 ^{d}
OH 50 Hz 20 V.cm^{-1}	118.817 ± 1.867 ^{e}	0.349 ± 0.032 ^{c}	68.216 ± 2.856 ^{e}

For each column, different letters correspond to statistically significant differences ($p < 0.05$).

The thermo-electric treatments caused radical changes on the WPI solution, leading to the decrease of PdI, increase in particle size and free SH content. This demonstrates that for all the treatment conditions applied, protein aggregation was induced and SH interactions potentiated, achieving suitable conditions to promote cold gelation. Cov heating treatments resulted in aggregates with higher size and polydispersity index, while OH treatments resulted in significant ($p < 0.05$) reduction of the aggregates size and size distribution. The aggregates obtained under Cov treatment also presented higher content of accessible SH groups. SH groups are expected to be exposed during thermal denaturation, becoming available to establish disulphide bonds with other SH groups from the same or other protein molecules (Bryant & McClements, 1998). MEF-exposed samples present lowered SH accessibility, which suggests the groups were unexposed due lower structure modifications or the involvement of these groups in disulphide bonds. If disulphide crosslinking was enhanced during the aggregation process under MEF, it is possible that their stabilization was faster and thus promote aggregates of smaller dimensions and lower polydispersity. These results are in line with previous studies on the OH effect in WPI gelation, where the application of this emerging technology resulted in reduced aggregation, narrower size distributions and lower amounts of free SH groups accessibility (R N Pereira et al., 2016; Rodrigues et al., 2015). For the first time different levels of EF strength and electric frequency were evaluated in WPI aggregation. The use of OH at 20 kHz and 10 $V.cm^{-1}$ resulted in a 15 nm average size reduction compared with the Cov treatment and the increase of EF strength to 20 $V.cm^{-1}$ resulted in an additional reduction of 10 nm, however no significant differences were observed in the polydispersity index. Under the same conditions, the SH groups' accessibility was also significantly reduced when compared with the Cov treatment, but without differentiation between the two EF strengths applied. The use of treatments with an electric frequency of 50 Hz resulted in higher differentiation from the Cov treatments. The average aggregate size was reduced up to 34 nm and the SH accessibility reduced by 19 % for the EF at 20 $V.cm^{-1}$. The aggregates obtained under 50 Hz OH were also less polydisperse than the ones obtained by Cov, but not significantly different from those of OH at 20 kHz. It is clear that the OH treatments, with a significant influence of the electric frequency applied and EF strength used, resulted in differentiated aggregation and disulphide crosslinking potential.

6.3.1.2 Rheological properties of the aggregates' solutions

Once the effects of OH and its variables in the WPI aggregation and SH accessibility were verified, it is also expected that these effects can result in differentiation in terms of the mechanical properties of the

aggregates' suspensions. Figure 6.1 shows the flow curves of shear stress as a function of shear rate for the aggregates' solutions produced under different thermo-electric conditions.

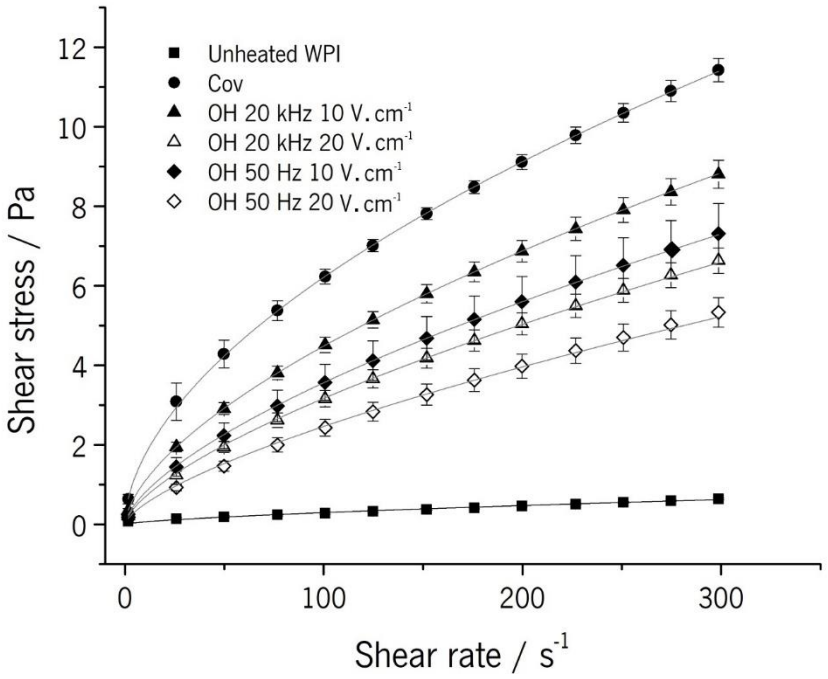

Figure 6.1: Flow curves of unheated WPI and aggregate solutions. Intermediate points were not included to facilitate visualization; lines correspond to experimental data fitting.

As expected, the changes produced at molecular level by the thermo-electric treatments and their variables, resulted in observable effects on the viscoelastic properties of the aggregates suspensions. The unheated WPI solution presented an apparent linear behaviour, while the aggregates' solutions presented a typical pseudoplastic behaviour (Ton Van Vliet et al., 2004). Within this group, it is also clear the differentiation between Cov and OH treatments, as well as between the OH treatments produced under different conditions. In order to understand the flow behaviour of the fluid samples, the power-law model was adjusted to the experimental data obtained through Equation6.5.

$$\sigma = k.\dot{\gamma}^{\,n} \qquad (6.5)$$

where σ is shear stress (Pa), $\dot{\gamma}$ is shear rate (s^{-1}), k is consistency index ($Pa{\cdot}s^{-1}$), and n is flow behaviour or power-law index. Different flow behaviours between the unheated WPI solutions and the thermo-electric produced aggregates were confirmed by the fitting parameter presented in Table 6.2.

The different behaviour of the unheated WPI solution observed in Figure 6.1 translates into a low consistency index, demonstrating the absence of a structured system and thus of interactions between

the solution constituents. The *n* value obtained is close to 1, confirming a linear behaviour, in agreement with a Newtonian fluid.

Table 6.2: Power law fitted parameters to the flow curves.

Samples	Parameters	
	***k* (Pa.s^{-1})**	***n***
Unheated WPI	0.0023 ± 0.0003	0.962 ± 0.028
Cov	0.469 ± 0.076 ^{a}	0.563 ± 0.034 ^{a}
OH 20 kHz 10 V.cm^{-1}	0.263 ± 0.025 ^{b}	0.617 ± 0.014 ^{b}
OH 20 kHz 20 V.cm^{-1}	0.134 ± 0.018 ^{cd}	0.685 ± 0.017 ^{c}
OH 50 Hz 10 V.cm^{-1}	0.170 ± 0.042 ^{d}	0.678 ± 0.035 ^{c}
OH 50 Hz 20 V.cm^{-1}	0.087 ± 0.013 ^{c}	0.709 ± 0.037 ^{c}

For each column, different letters correspond to statistically significant differences ($p < 0.05$). All correlation coefficients of model fitting to experimental data were > 0.99

For all the treated samples the *n* value obtained was lower than 1, confirming the pseudo-plastic nature of the fluids. Parameter *k* is related to the solution's viscosity and was significantly lower for the samples produced under OH, reducing up to approximately five times under OH at 50 Hz and 20 V.cm^{-1}. Both the increase of EF strength and the use of low frequencies produced significant effects on the *k* value and consequently, viscosity reduction. Moreover, the flow behaviour index also reflects the different properties induced by the OH treatments. All the OH treated samples presented an increase of the *n* value, increasing also with the EF strength and low frequency. This increase in the *n* value reflects on a flow behaviour moving towards a Newtonian flow. We have previously established that the use of OH, as well as the increase of EF strength and use of low frequency, result on aggregates' size reduction, which contributes to the lower viscosity of the suspensions. Furthermore, the use of OH during WPI aggregation led to changes in the aggregates' morphology, resulting in more elongated, fibrillar-like aggregates (R.N. Pereira et al., 2016). These differences could also contribute to the observed differences in the flow behaviour, as the elongated aggregates possibly will align with the direction of the force applied and produce less resistance, also resulting in lower viscosity of the suspensions.

6.3.2 Cold-set gels characterization

6.3.2.1 Gels microstructure

The effects of different thermo-electric pre-treatments on the gel microstructure were investigated by CLSM. Representative images of the different gels produced are presented in Figure 6.2.

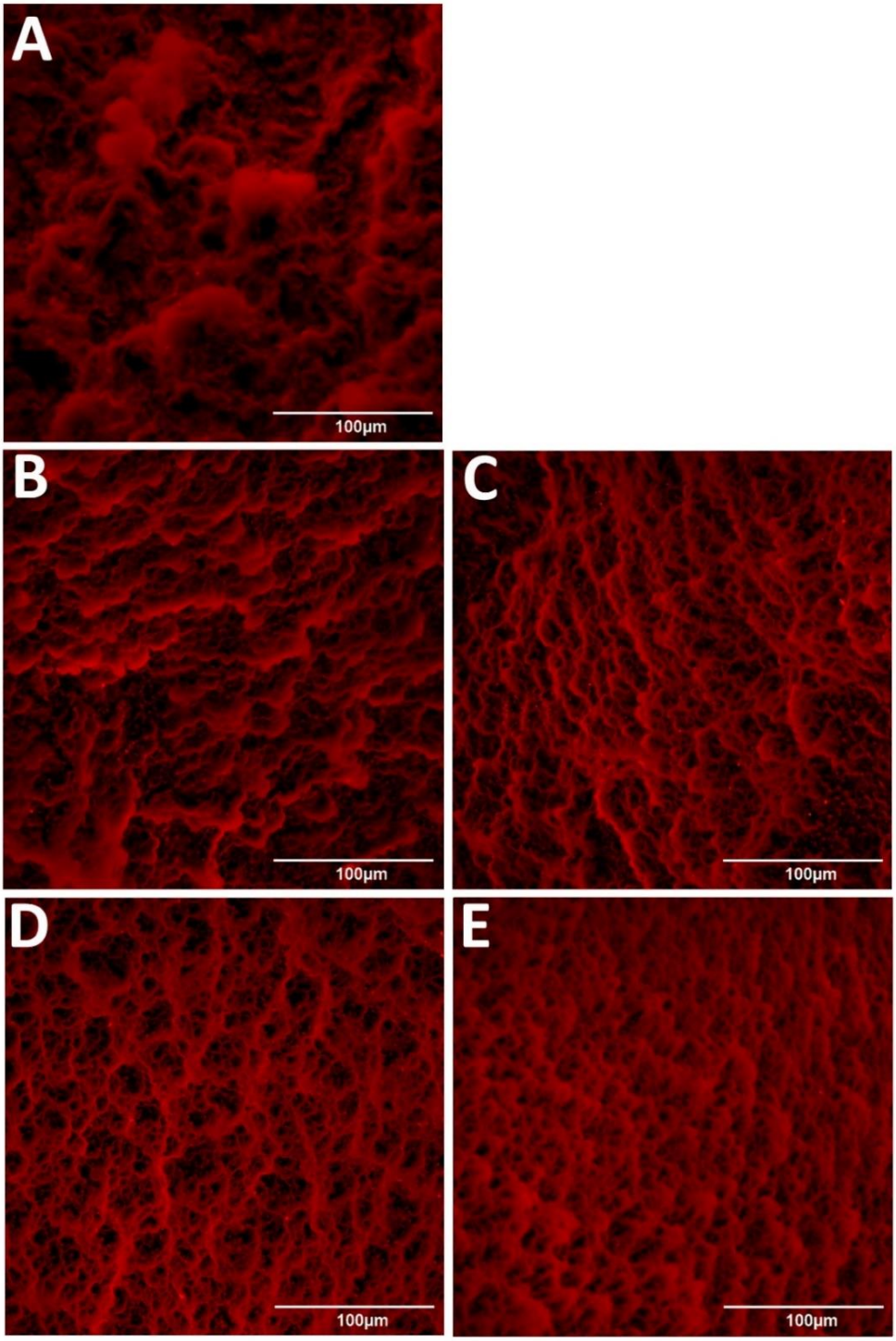

Figure 6.2: CLSM photomicrographs of WPI cold-set gels pre-treated by: (A) Cov, (B) OH 20 kHz 10 V.cm^{-1}, (C) OH 20 kHz 20 V.cm^{-1}., (D) OH 50 Hz 10 V.cm^{-1} and (E) OH 50 HZ EF 20 V.cm^{-1}.

The samples exhibit a typical gel structure composed by the protein network, here stained by rhodamine. Cov samples present an amorphous structure with compact continuous areas. In OH 20 kHz samples it is possible to observe similar compact structures but with smaller size. It is also observable the formation of patterns on the structure and a more homogeneous appearance. The OH 50 Hz does not present compact areas and displays a finer stranded pattern with uniform appearance. It is clear that the exposure to MEF during the thermal pre-treatment and aggregation results in modifications of the gelation process and gel structure. MEF effects result in gels with a finer structure, more evident when low frequencies and higher EF were applied. As previously discussed, OH treated samples presented smaller aggregates with lower amount of free SH groups. These differences on the aggregates in the gel forming solution imply different assembly of the network and potentially different physicochemical interactions established within it, resulting on the observable differences in microstructure evaluation.

6.3.2.2 Small amplitude oscillatory dynamic rheology

Viscoelastic properties of the cold-set gels formed depended on both the microstructure of the gel and the interactions between the aggregating particles. Changes on the gels viscoelastic characteristics were expected, considering the differences in the aggregation, SH accessibility and microstructure induced by different thermo-electric treatments. To confirm the cold-set gel formation and evaluate its viscoelastic behaviour, a frequency sweep of G^* modulus and tanδ in the viscoelastic linear region was performed (see Figure 6.3). The analysis of G^* shows, with similar trends for all samples, a small increase with the increase in angular frequency. Typically, stronger gels originate from chemical crosslinking and the viscoelastic moduli do not show frequency dependency, while weaker gels depend on physical interactions displaying viscoelastic moduli with a great frequency dependency. The small dependency of G^* on the frequency characterizes a soft gel, sustained by a combination of chemical crosslinking and physical interactions (Ross-Murphy, 1995). A clear differentiation between the OH and Cov samples is evident, with the higher values of G^* for Cov samples translating into a stronger structure. Figure 6.3B shows the variation of tanδ during the frequency sweep. The viscoelastic behaviour of the obtained cold-set gels was characterized by the predominance of the elastic component and thus confirming the formation of a gel. The determined tanδ values are similar for all the gels obtained, their magnitude just above 0.1 and with little frequency dependence, which are typical of a fine structure gel, (Mleko & Foegeding, 2000; Ross-Murphy, 1995; Savadkoohi & Farahnaky, 2012). The gels submitted to OH 50 Hz 20 V.cm^{-1} treatments, despite the proximity to the other samples, present higher tanδ values with tendency to increase in higher

frequencies. This denotes an increase of the viscous component or a possible damage of the structure, which is compatible with a weaker structure.

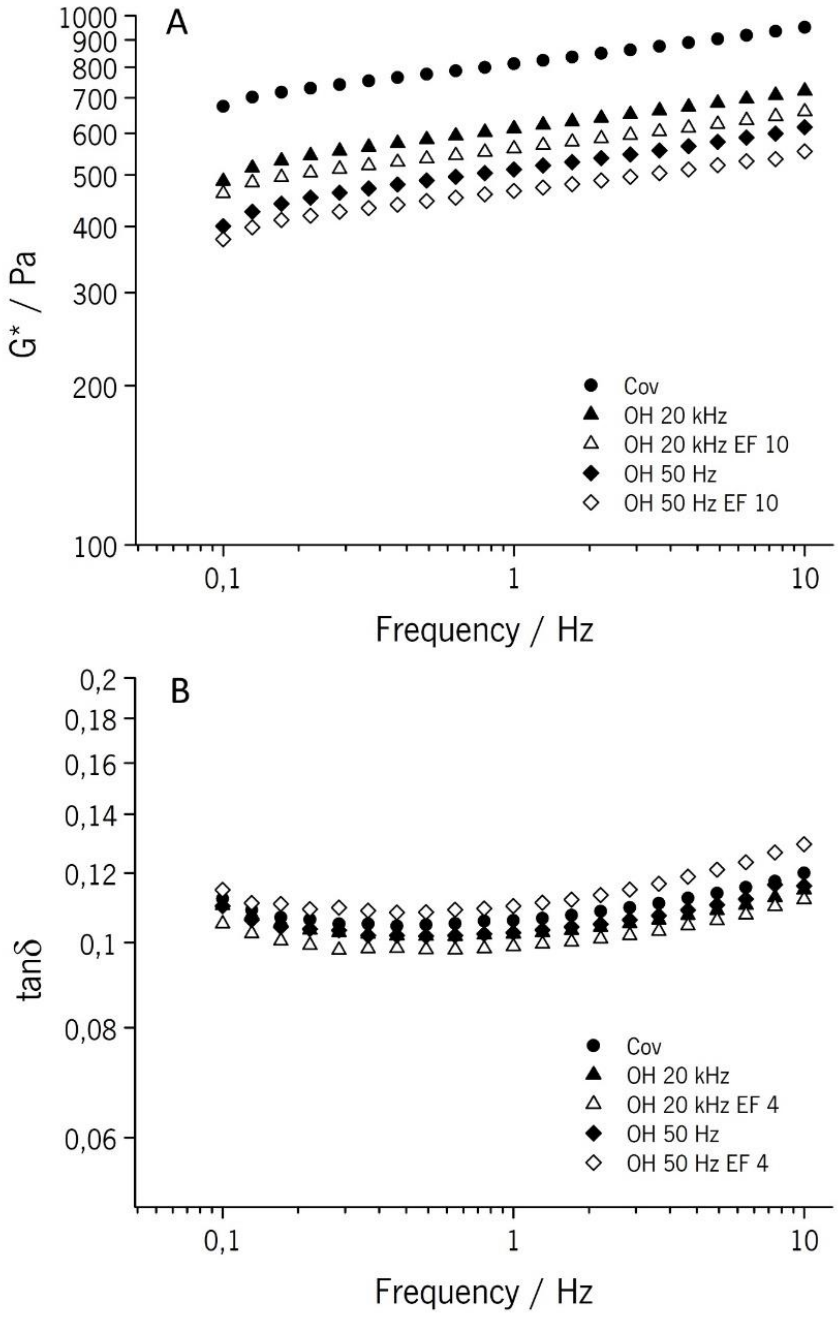

Figure 6.3: The frequency dependence of G^* (A) and tanδ (B) of the cold-set WPI gels prepared from solutions exposed to different thermo-electric conditions.

The analysis of the viscoelastic moduli at the reference frequency of 1 Hz demonstrated significant differences induced by the thermo-electric treatments performed on the gel forming solutions (Table 3). Despite of the similar general behaviour of the samples - see Figure 6.3 - G^* is higher for Cov samples,

revealing a higher structured system. For OH samples, the use of different electric frequencies resulted in the differentiation of gel strength, presenting G^* values 23 % and 37 % lower than Cov, for 20 Hz and 50 Hz respectively. The increase of the EF strength from 10 to 20 V.cm^{-1} despite of apparently contributing to the viscoelastic moduli reduction, did not reach statistical significance ($p > 0.05$).

Table 6.3: Effect of thermo-electric conditions on the cold set gels complex modulus (G^*) and tan δ measured at 1 Hz frequency.

Sample	G^* (Pa)	tanδ
Cov	809.14 ± 67.07 ^{a}	0.104 ± 0.009 ^{a}
OH 20 kHz 10 V.cm^{-1}	623.40 ± 64.01 ^{b}	0.102 ± 0.006 ^{a}
OH 20 kHz 20 V.cm^{-1}	566.79 ± 62.40 ^{bc}	0.100 ± 0.005 ^{a}
OH 50 Hz 10 V.cm^{-1}	514.29 ± 29.31 ^{cd}	0.104 ± 0.012 ^{a}
OH 50 HZ EF 20 V.cm^{-1}	464.24 ± 51.79 ^{d}	0.110 ± 0.013 ^{a}

For each column, different letters correspond to statistically significant differences ($p < 0.05$).

6.3.2.3 Mechanical properties

Figure 6.4 represents the mechanical properties of the cold-set gels obtained. Cov samples display the lowest strain at rupture and the samples subjected to OH treatment present an increasing tendency of the strain at rupture values, however the increase was only statistically significant for the OH treatment at 50 Hz (independently of the EF strength applied – see Figure 6.4A). Cov samples displayed the highest stress at rupture, significantly higher than the OH samples (see Figure 6.4B). The EF increase and use of low frequencies contributed to the reduction of the stress at rupture, only reaching statistical significance ($p < 0.05$) for the OH treatment at 50 Hz and 20 V.cm^{-1}. Overall, it is possible to conclude that Cov-treated samples presented a stronger and more rigid structure, as they break at lower strains and at higher stress, while OH-treated samples had a weaker and more elastic structure, breaking under lower stress and at higher strains. These properties were reflected on the values of Young´s modulus, representing the firmness of the network at low deformation. The significantly higher moduli observed for Cov gels translate into a more solid-like behaviour and higher capacity to store the applied force, while the OH treatment, together with the increase of EF strength and the use of lower electric frequencies contribute to a reduction of Young´s moduli. The mechanical properties of the gels were consistent with the results obtained from oscillatory rheology tests and the same general pattern was also observed for the gels mechanical properties' variations with the thermo-electric treatment applied.

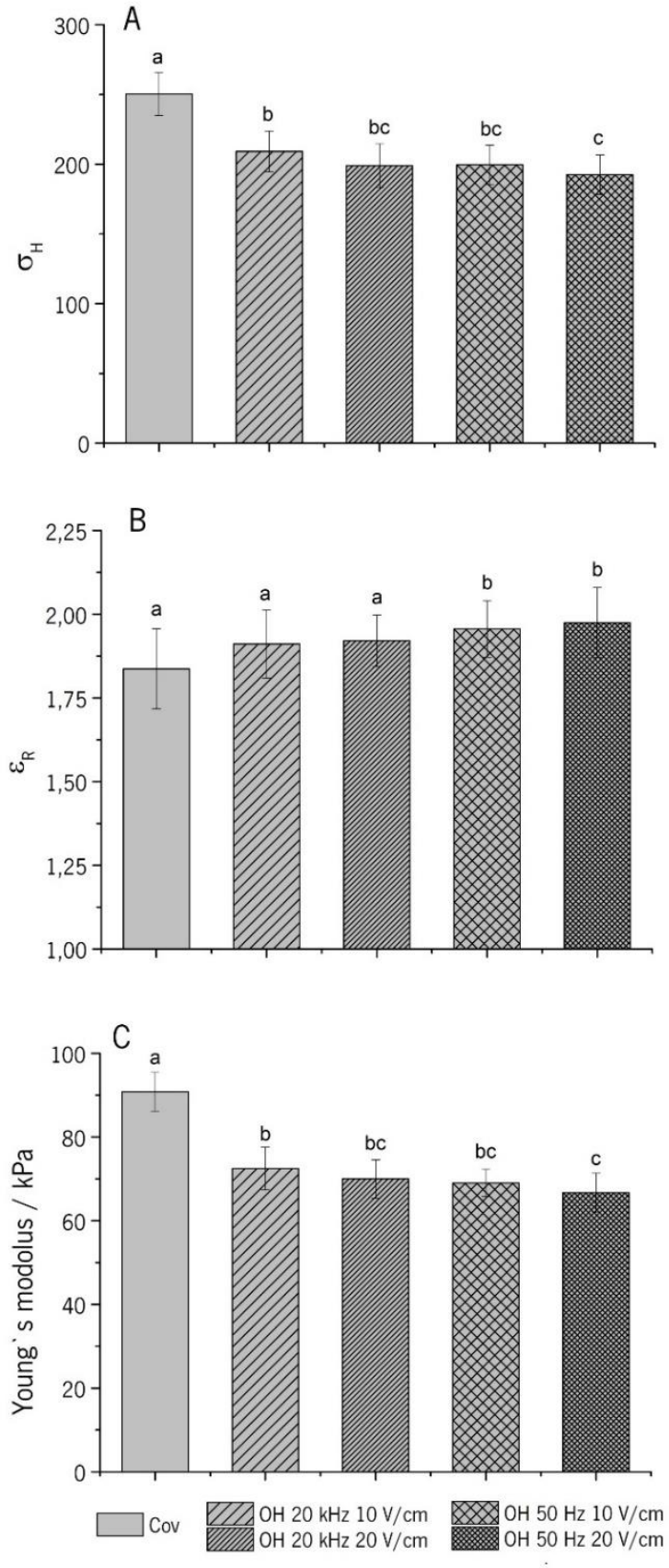

Figure 6.4: Mechanical properties of the obtained cold-set gels, (A) strain at rupture (ε_R), (B) stress at rupture (σ_R) and (C) Young's modulus. Different letters correspond to statistically significant differences ($p < 0.05$).

6.3.2.4 Network interactions

By itself, the formation of a gel network composed by smaller particles and with different SH crosslinking potential is enough to explain the differences observed in the cold-set gel rheological and mechanical properties. However, once the net-charge of the aggregate dispersions is changed and the cold-gelation process is started, the inter-aggregate interactions – e.g. hydrogen bonds, hydrophobic interactions - also play a decisive role in network formation. In order to determine the contribution of different interactions established during the network formation process and their contribution for the gel properties, gel solubility was evaluated in different solvent systems designed to disrupt specific bonds and interactions. Agents such as SDS, which disrupts hydrophobic interactions, urea at 8 $mol.L^{-1}$, which disrupts hydrogen bonds and destabilizes hydrophobic interactions, and 2-mercaptoethanol, a disulphide bond reducing agent, were used in the compositions of extraction media. PB was used as solvent to extract proteins not involved in the network formation and a conjugation of all the bond/interaction disrupting agents was used to very if the summed effects of all agents would result in the total disruption of the network. The results of the solubility experiments are presented in Figure 6.6. For the solvent containing all the agents, the gels presented quick erosion and were no longer visible after a period of a few hours. After the first 24 h, the complete solubilisation of all the gels was verified. This demonstrates that the combined action of all the disrupting agents was able to break up all the interactions involved in the network formation as expected. The gels placed in PB presented a solubility of 5 % of their total protein content after 24 h, and remained constant thereafter, throughout the 5 days of the experiment. A visual inspection of the gels through the experimental procedure revealed no apparent changes on the gel size, shape or colour. The small amount of protein dissolved was possibly the protein fraction which was not included in the network formation, thus remaining in a free state. For the solvents containing the different agents, it was observed an increase of protein solubility over time, with differentiation between samples treated with thermo-electric treatments being evaluated. The solvent containing SDS did not cause observable changes within 24 h, but at day 3 and 5 differences between samples' solubility became clear. Samples that suffered an OH pre-treatment exhibited tendentiously lower solubility in the presence of SDS, reaching significant levels for the samples exposed to 50 Hz OH treatments. This lower erosion of the OH samples in the presence of SDS may be the result of more or stronger hydrophobic interactions within the network. The use of urea results on a similar tendency, yet more pronounced and already observable after the first 24 h of treatment. OH-treated gels are less soluble, displaying significant differences at day 1 for the 50 Hz treatments and increasing with time. At day 5 the protein solubility of Cov samples reached 27 %, the OH at 20 kHz was 23 % and for the 50 Hz samples was 17 %, with no differences between the different EF

strengths used. These differences in urea action reflect in the amount of hydrogen bonds stabilising the network, showing the predominance of these interaction on the OH treated samples. The use of 2-Me revealed an opposite tendency, with the OH treated samples displaying higher solubility and thus lower disulphide crosslinking. This behaviour is defined since day 1 but only statistically significant for the 50 Hz treatments. Throughout the experimental time the protein solubility increases, ranging from 21 % of the Cov samples to 34 % of the OH at 50 Hz. Like in the previous example, differences were significant ($p < 0.05$) for Cov and OH treatments and among OH samples treated at different frequencies. At the end of the experiment, visual inspection of the gels revealed changes in their appearance (see Figure 6.5). The gels immersed in PB for 5 days remained practically unchanged, as gels exposed to SDS and urea presented considerable swelling and became amorphous, while retaining the integrity. The gels exposed to 2-Me lost structural integrity and precipitated under the form of insoluble aggregates. The different solubility in the solvents tested show different physicochemical interactions in the gels produced following the several thermo-electric treatments used.

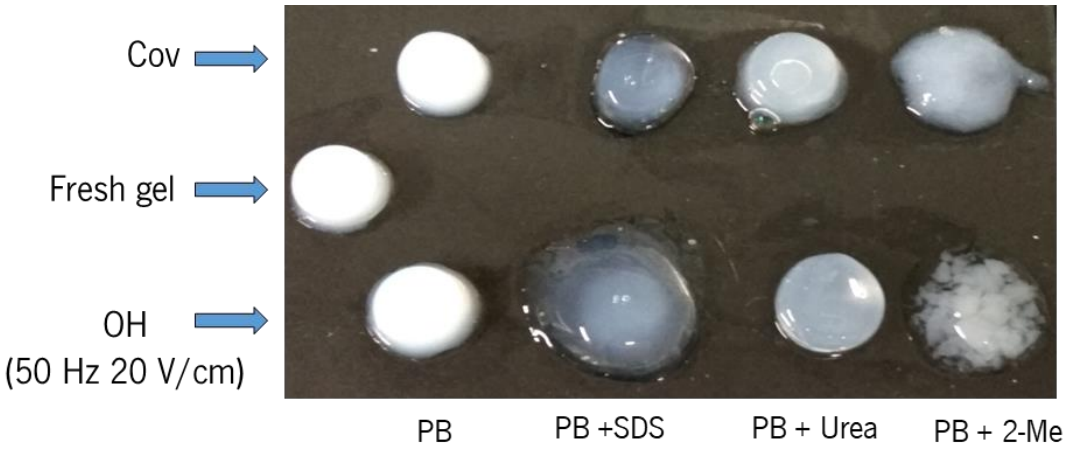

Figure 6.5: Example of the visual aspect of the gels after 5 days of the solubility tests in different agents and an example of a freshly prepared gel not submitted to the test.

Relatively to the Cov gels, OH-treated samples were more susceptible to disulphide disruption. The lower amount of disulphide crosslinking proposed for the OH-treated samples justifies their higher solubilisation on the solvent containing 2-Me. However, it is interesting to note the higher stability in hydrophobic and hydrogen bond disruption solvents. It has been demonstrated that the application of MEF results in different protein conformations and induces higher hydrophobic groups exposition during protein denaturation (see Chapter 4 and 5). These facts associated with lower disulphide crosslinking can result in a network with more predominance of hydrophobic interactions stabilized by hydrogen bonds.

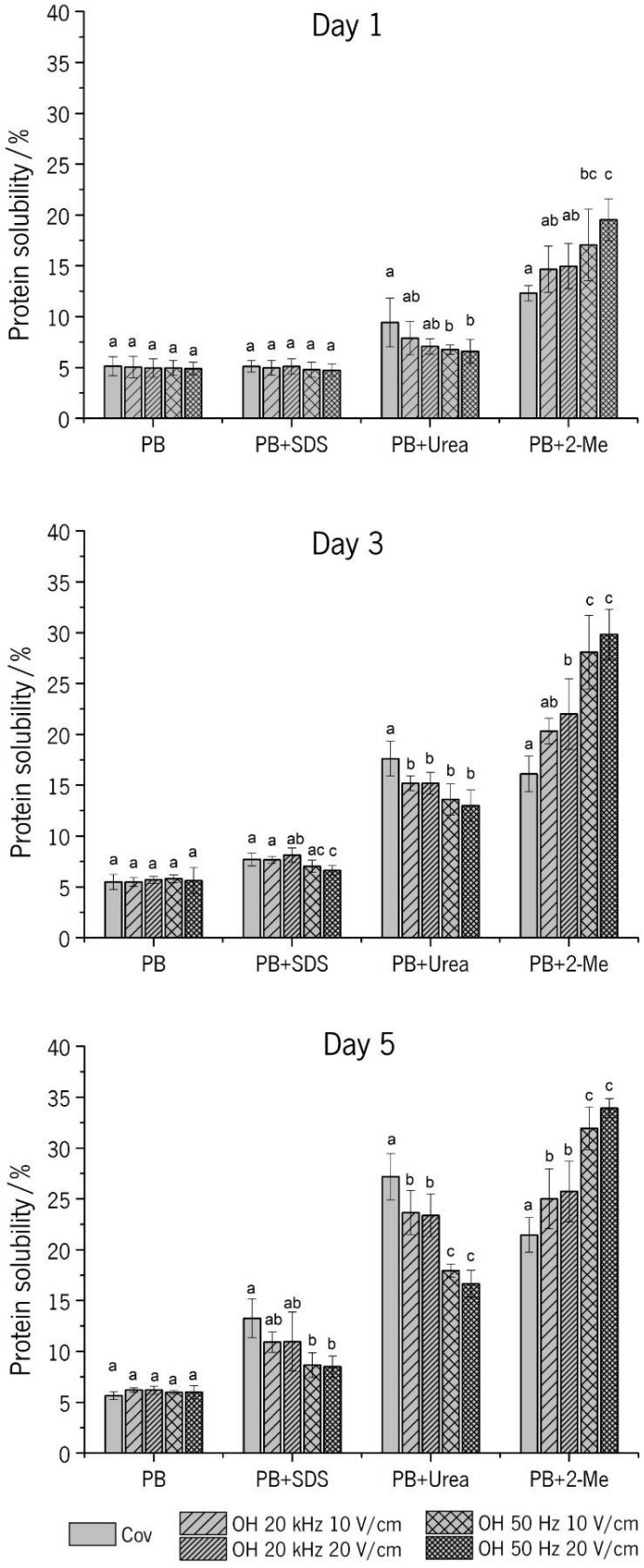

Figure 6.6: Protein solubilisation in different solvent systems through a period of 5 days. For each solvent system at each day, different letters correspond to statistically significant differences ($p < 0.05$).

Figure 6.7 shows the results obtained for the swelling degree and WRC of the WPI cold-set gels. Once more, the OH-treated samples presented a distinguished behaviour from the Cov samples, with higher values of swelling degree and higher WRC. The EF increase and use of low frequencies tend to increase these parameters; however, no statistically significant ($p > 0.05$) differences were found among the OH samples. The increase of swelling and WRC of the OH-treated gels could be explained by the fact that OH gels had a finer structure and were less firm (less hard), so the water–protein interactions are favoured. Furthermore, the lower amount of chemical crosslinking, and more physical interactions, result on a weaker, more flexible structure, capable to absorb and retain more water.

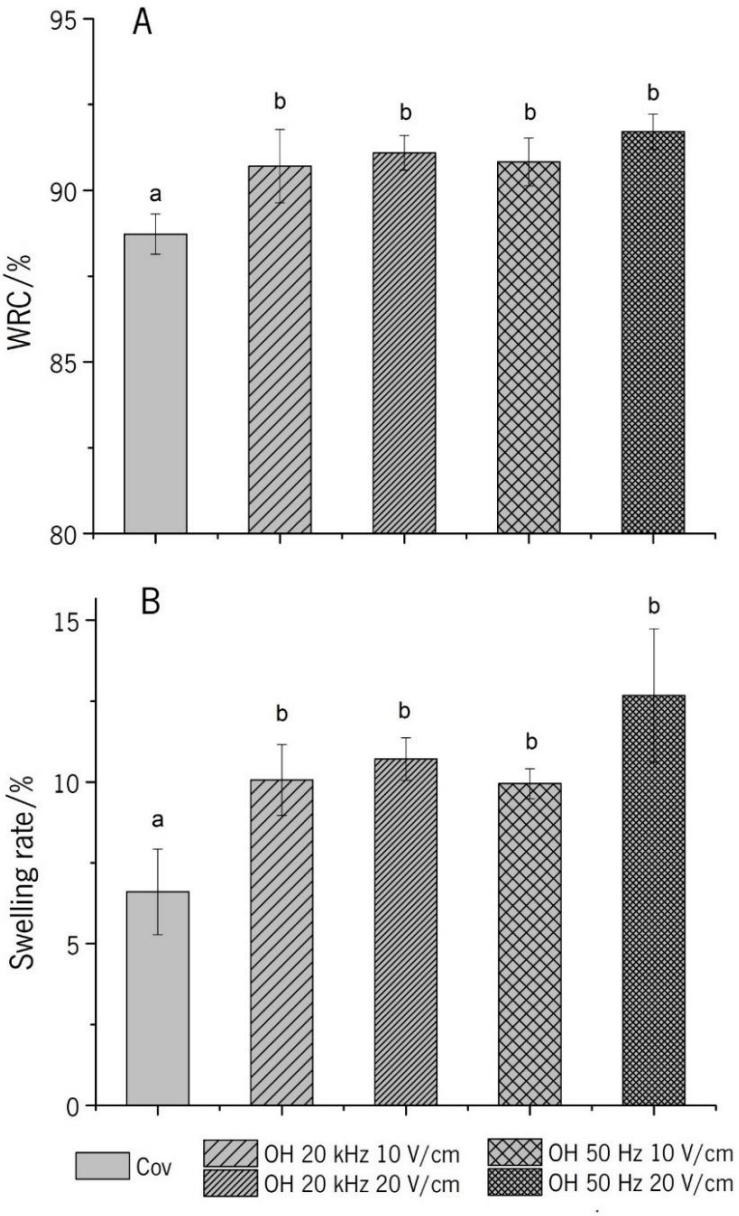

Figure 6.7: Swelling degree (A) and WRC (B) of the obtained cold-set gels. Different letters correspond to statistically significant differences ($p < 0.05$).

6.3.4 OH and electric effects on WPI gelation

In the previous chapters we have confirmed the ability of MEF to induce changes at molecular level during whey protein denaturation, potentially affecting protein functionality. In this study, we used the previously established knowledge of OH effects and EF variables on whey protein structure and further evaluated them on WPI functionality. The obtained data allowed establishing a mechanism for the WPI cold gelation process under Cov and OH heating methods (see Figure 6.8). OH treatments performed during the initial protein denaturation and aggregation stage resulted in smaller aggregates with lower fractions of accessible SH. The higher thermal uniformity typically obtained under OH and the additional EF effects may influence the protein interactions and aggregation process, favouring a fast disulphide crosslinking and resulting on a quick stabilization of the aggregates. These smaller aggregates, with lower amount of free SH content also resulted in a system with a lower viscosity, when compared with Cov-treated samples. These differences were also reflected in the further gelation of the aggregates' solutions, resulting in cold-set gels with a finer network, i.e. a weaker, softer and more elastic structure, with higher WRC and swelling behaviour. Cold-set protein gels' properties are dependent on the pre-heated aggregates characteristics (Ton van Vliet et al., 2004). Aggregates size and disulphide/free SH content are reported as the main aspects to consider in the network formation and final properties of the gels (Alting, Hamer, de Kruif, et al., 2003; Ju & Kilara, 1998; Nicolai et al., 2011). The lower amount of free SH groups in the aggregates led to lower levels of disulphide crosslinking in the resultant gels and the promotion of physical interactions. This explains the formation of weaker and more flexible gels, with a higher WRC and swelling degree. Also, the less rigid networks have a higher capacity to swell and less propensity to expel water (Alting, Hamer, de Kruif, et al., 2003).

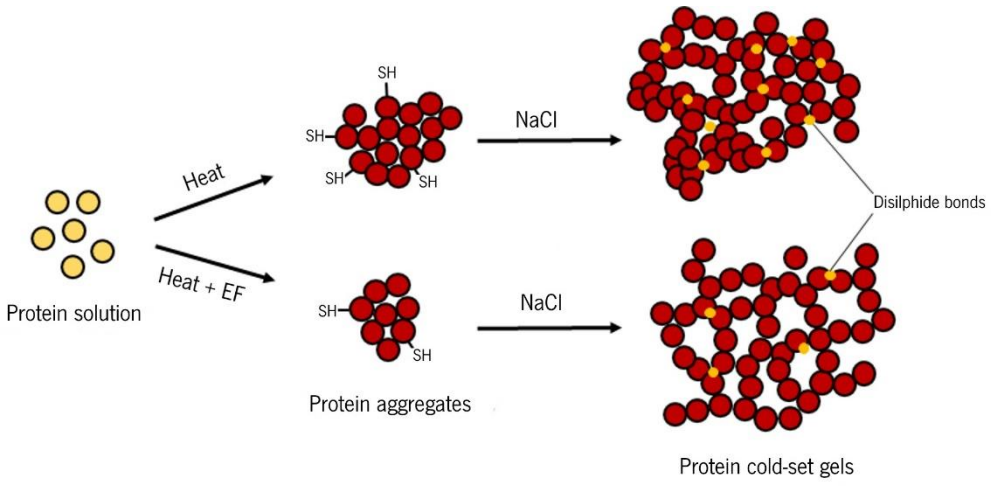

Figure 6.8: Cold gelation mechanism for WPI gels produced by Cov and OH methods.

Overall, it was demonstrated that the effects promoted by the presence of EF in protein structure result on a cascade of events, culminating in changes in the gel functional properties. The electrical field strength and frequency have demonstrated to be relevant in defining structural variations and several aspects of functionality. However, as the complexity of the structures increased (i.e. from aggregates to a continuous network), their effects were diluted by other factors involved. Ultimately, despite the increase of EF strength and especially the use of low frequencies, resulted in variations of microstructure, viscoelastic properties, mechanical properties and physicochemical interactions of the gels, they were not reflected in WRC and swelling and only the treatment type was significant. Once demonstrated the basic mechanism of OH and its variables on WPI gelation, further studies are needed to better explore these effects and fully disclosure their potential to tune protein networks.

6.4 CONCLUSIONS

The use of OH have previously demonstrated the potential of changing the gel forming properties of whey proteins, however, the action of MEF during OH was unclear and its specific effects in the protein structure or aggregation mechanisms remained speculative. In this study, we were able to elucidate some of these effects and specific action during the WPI gelation process. The use of OH and different electrical variables during WPI pre-treatment resulted in differences in protein aggregation, also reflected on the cold gelation of the WPI aggregates and final gel properties. Furthermore, the electrical variables used contributed to the differentiation of OH-treated samples, being the MEF-related effects potentiated by the increase of EF strength and particularly by the use of low frequencies. For the first time it was unveiled that MEF effects at molecular level result in a cascade of events ultimately originating differentiated functional properties such as gel forming ones. These findings represent a step forward in the understanding of OH and MEF technological applications. They also contribute to establish EF-based technologies as potential tools to change and control protein gel properties (from nano- to micro-scale) and potential applications.

6.5 REFERENCES

Ako, K., Nicolai, T., & Durand, D. (2010). Salt-Induced Gelation of Globular Protein Aggregates: Structure and Kinetics. *Biomacromolecules*, *11*(4), 864–871. https://doi.org/10.1021/bm9011437

Alting, A. C., Hamer, R. J., de Kruif, C. G., Paques, M., & Visschers, R. W. (2003). Number of thiol

groups rather than the size of the aggregates determines the hardness of cold set whey protein gels. *Food Hydrocolloids*, *17*(4), 469–479. https://doi.org/10.1016/S0268-005X(03)00023-7

Alting, A. C., Hamer, R. J., De Kruif, C. G., & Visschers, R. W. (2003). Cold-set globular protein gels: Interactions, structure and rheology as a function of protein concentration. *Journal of Agricultural and Food Chemistry*, *51*(10), 3150–3156. https://doi.org/10.1021/jf0209342

Amin, S., Barnett, G. V., Pathak, J. A., Roberts, C. J., & Sarangapani, P. S. (2014). Protein aggregation, particle formation, characterization & rheology. *Current Opinion in Colloid & Interface Science*, *19*(5), 438–449. https://doi.org/10.1016/j.cocis.2014.10.002

Bryant, C. M., & McClements, D. J. (1998). Molecular basis of protein functionality with special consideration of cold-set gels derived from heat-denatured whey. *Trends in Food Science & Technology*, *9*(4), 143–151. https://doi.org/10.1016/S0924-2244(98)00031-4

Chi, E. Y., Krishnan, S., Randolph, T. W., & Carpenter, J. F. (2003). Physical stability of proteins in aqueous solution: Mechanism and driving forces in nonnative protein aggregation. *Pharmaceutical Research*, *20*(9), 1325–1336. https://doi.org/10.1023/A:1025771421906

De Vries, H., Mikolajczak, M., Salmon, J. M., Abecassis, J., Chaunier, L., Guessasma, S., … Trystram, G. (2018). Small-scale food process engineering — Challenges and perspectives. *Innovative Food Science and Emerging Technologies*, *46*(March), 122–130. https://doi.org/10.1016/j.ifset.2017.09.009

Guo, M. (Ed.). (2019). *Whey Protein Production, Chemistry, Functionality, and Applications*. Chichester, UK: John Wiley & Sons, Ltd. https://doi.org/10.1002/9781119256052

Ju, Z. Y., & Kilara, A. (1998). Gelation of pH-Aggregated Whey Protein Isolate Solution Induced by Heat, Protease, Calcium Salt, and Acidulant. *Journal of Agricultural and Food Chemistry*, *46*(5), 1830–1835. https://doi.org/10.1021/jf9710185

Mleko, S., & Foegeding, E. A. (2000). pH Induced Aggregation and Weak Gel Formation of Whey Protein Polymers. *Journal of Food Science*, *65*(1), 139–143. https://doi.org/10.1111/j.1365-2621.2000.tb15969.x

Nicolai, T., Britten, M., & Schmitt, C. (2011). β-Lactoglobulin and WPI aggregates: Formation, structure and applications. *Food Hydrocolloids*, *25*(8), 1945–1962. https://doi.org/10.1016/j.foodhyd.2011.02.006

Pereira, R. N., Rodrigues, R. M., Ramos, O. L., Malcata, F. X., Teixeira, J. A., & Vicente, A. A. (2016). Production of Whey Protein-Based Aggregates Under Ohmic Heating. *Food and Bioprocess Technology*, *9*(4), 576–587. https://doi.org/10.1007/s11947-015-1651-4

Priyadarshini, A., Rajauria, G., O'Donnell, C. P., & Tiwari, B. K. (2018). Emerging food processing technologies and factors impacting their industrial adoption. *Critical Reviews in Food Science and Nutrition*, *0*(0), 1–20. https://doi.org/10.1080/10408398.2018.1483890

Ramos, O. L., Pereira, R. N., Rodrigues, R., Teixeira, J. A., Vicente, A. A., & Xavier Malcata, F. (2014). Physical effects upon whey protein aggregation for nano-coating production. *Food Research International*, *66*. https://doi.org/10.1016/j.foodres.2014.09.036

Rodrigues, R. M., Martins, A. J., Ramos, O. L., Malcata, F. X., Teixeira, J. A., Vicente, A. A., & Pereira, R. N. (2015). Influence of moderate electric fields on gelation of whey protein isolate. *Food Hydrocolloids*, *43*, 329–339. https://doi.org/10.1016/j.foodhyd.2014.06.002

Rosenthal, A. J. (1999). *Food Texture: Measurement and Perception*. Aspen Publishers Inc.,U.S.

Ross-Murphy, S. B. (1995). Structure–property relationships in food biopolymer gels and solutions. *Journal of Rheology*, *39*(6), 1451–1463. https://doi.org/10.1122/1.550610

Savadkoohi, S., & Farahnaky, A. (2012). Dynamic rheological and thermal study of the heat-induced gelation of tomato-seed proteins. *Journal of Food Engineering*, *113*(3), 479–485. https://doi.org/10.1016/j.jfoodeng.2012.06.010

Steffe, J. F. (1996). *Rheological Methods in Food Process Engineering*. Freeman Press.

van Vliet, T. (2000). Structure and rheology of gels formed by aggregated protein particles. In *Hydrocolloids* (pp. 367–377). Elsevier. https://doi.org/10.1016/B978-044450178-3/50047-0

Vliet, T. Van, Lakemond, C. M. M., & Visschers, R. W. (2004). Rheology and structure of milk protein gels, *9*, 298–304. https://doi.org/10.1016/j.cocis.2004.09.002

CHAPTER 7.

MEF EFFECTS IN PROTEIN-BASED SCAFFOLDS FOR TISSUE ENGINEERING

7.1-INTRODUCTION

There is a growing interest in the use of proteins as building blocks in biomedical applications, such as control delivery systems and scaffolds for tissue engineering (Drury & Mooney, 2003; Gebauer & Skerra, 2009; Gomes, Leonor, Mano, Reis, & Kaplan, 2012; Li et al., 2015). Particularly in scaffold production, several fabrication techniques – *e.g.* freeze-drying, solvent casting, foaming, electrospinning or 3D printing – have been used to attain the desired functional properties (Eltom, Zhong, & Muhammad, 2019; Weigel, Schinkel, & Lendlein, 2006). Protein functionalization is a necessary step associated to these fabrication techniques, usually achieved by chemical modification, enzymatic hydrolysis or crosslinking through the use of strong reducing agents. The use of these strategies may bring negative implications since some of these agents present toxicity or low biocompatibility issues (Charulatha & Rajaram, 2003; Drury & Mooney, 2003; Weigel et al., 2006). As response to these limitations new strategies must be developed; the knowledge and methodologies from adjacent biotechnology areas could bring interesting perspectives into the biomedical field.

The previously discussed protein functionalization and supramolecular formation strategies, may add important contributions to scaffolds' production methods. In fact, despite of the literature available on physical methods to promote protein functionalization, and processes such as cold-gelation of proteins in food related applications, the process is yet to be fully exploited in other areas. Ribeiro and co-authors (Ribeiro et al., 2016; Ribeiro, Gomes, & Cavaco-Paulo, 2012) have successfully adopted this approach to develop scaffolds for tissue engineering, using a combination of globular proteins, such as bovine serum albumin (BSA) or human serum albumin (HSA) and alpha-casein, a smaller and amorphous protein. In this methodology the protein solutions were thermally treated and the gelation was induced by addition of Ca^{2+} ions, resulting in the formation of tuneable scaffolds for cell culture and proliferation. The developed process relied on a mild thermal processing and the use of ditiotreitol (DTT) as a reducing agent in order to further destabilize the proteins, followed by Ca^{2+} addition to induce crosslinking. In fact, DTT is commonly used in the gel preparation processes and has been applied for scaffold development in other works (Yan, Saiani, Gough, & Miller, 2006). However, DTT by itself or in synergy with media constituents may compromise cell viability and needs to be eluted from the scaffolds prior to their use (Thibodeau, Kocsis-Bédard, Courteau, Niyonsenga, & Paquette, 2001; L. Tartier, Y.L. McCarey, J.E. Biaglow, 2000; Solovieva, Solovyev, Kudryavtsev, Trizna, & Akatov, 2008). The use of emerging technologies and a rational optimization of the gel forming conditions, based on protein structural changes and functionality, are interesting alternatives to develop tuneable scaffolds for tissue engineering.

The aim of this study is to optimize the production of protein-based scaffolds for tissue engineering, based on the methodology and formulations previously established by Ribeiro and co-authors. It is our goal to optimize the thermal treatments' conditions in order to promote an adequate level of conformational changes that allow inducing protein aggregation and obtain stable scaffolds without the use of reducing agents for network formation. Along with this optimization, the use of OH was assessed and its MEF-related effects on the produced scaffolds properties were evaluated.

7.2 MATERIALS AND METHODS

7.2.1 Materials

BSA and casein sodium salt from bovine milk were purchased from Sigma-Aldrich (Steinheim, Germany) and used without further purification. All other reagents were of analytical grade and purchased from Sigma-Aldrich (Steinheim, Germany).

7.2.2 Preparation of BSA/casein scaffolds

The scaffolds were obtained by salt-induced cold gelation in the presence of calcium chloride ($CaCl_2$) at pH 7.07. Shortly, protein solutions of BSA in water and casein in Tris 5 x 10^{-2} mol.L^{-1}, pH 7.4 were prepared separately and mixed to the final concentration of 4.19 % (w/v) of BSA and 0.69 % (w/v) of casein. The solutions were thermo-electrically treated to promote protein denaturation and aggregation, cooled down to room temperature for 1 h and finally $CaCl_2$ (0.1 mol.L^{-1}) was added. The mixtures were stirred to homogenize the samples, casted on 48-well plates, left to gel overnight, frozen at -20 °C and freeze dried to remove the solvent completely. Resulting scaffolds with a diameter of 5 mm and a height of 9 mm were kept at room temperature until further use.

7.2.3 Thermo-electric treatments and experimental design

Thermo-electric treatments, by OH or heat exchange, were conducted as described in Chapter 4. In order to optimize the scaffold production conditions, a Box-Behnken design with 3 factors in 3 levels was used. The factors selected were temperature, treatment time and EF applied, on intervals of 70 to 85 °C, 5 to

30 minutes and 0 to 40 $V.cm^{-1}$ respectively. 70 °C is the denaturation temperature of BSA and 85 °C was found to be the limit temperature before thermal gelation of the protein solutions occurred. MEF variables were restricted to the variation of EF at a fixed frequency of 20 kHz. In previous chapters it was observed that the use of low frequencies resulted in more appreciable effects regarding protein functionalization, however it may cause secondary phenomena such as electrochemical reactions and erosion of the electrodes material to the surrounding medium. Despite these phenomena were residual or non-observable during the previously reported experiments, it was decided to avoid any procedure that might bring negative implications during the cell culture experiments.

Data from *in vitro* degradation, swelling and porosity of the obtained scaffolds were used as response or dependent variables. The desirability function analysis (DFA) derived from the model was applied to estimate a desirability value, i.e. a measure of how close the fitted value is to a desired value within pre-established limits (Vera Candioti, De Zan, Cámara, & Goicoechea, 2014).

7.2.4 Characterization of the gel forming solution

To improve the understanding of the conditions needed to produce the scaffolds, a characterization of the gel forming solutions was performed after the thermo-electric treatments. Particle size analysis, determination of accessible sulfhydryl groups, protein´s intrinsic, and ANS fluorescence determinations were performed as described in Chapters 4 and 5.

7.2.5 Scaffolds characterization

7.2.5.1 Functional properties and stability

In vitro degradation

The obtained scaffolds were incubated in PBS at 37 °C for a period of 15 days. Solutions were changed every 24 h and at designated time points, samples were recovered, washed with distilled water, dried in a desiccator, and weighed. The extent of degradation was estimated according the Equation 7.1.

$$Weight\ loss\ (\%) = \left(\frac{(m_i - m_f)}{m_i}\right) \times 100 \qquad (7.1)$$

where m_i is the initial dry mass of the sample and m_f is the final dry mass.

Swelling ratio

Dry scaffolds were submerged in PBS buffer 37 °C and left for 24 h. The samples were recovered, the excess of buffer gently removed with a filter paper and the wet weight of the scaffolds was determined. The swelling ration was calculated according to Equation 7.2.

$$Swelling\ ratio = \frac{Ws-Wd}{Wd} \quad (7.2)$$

where *Ws* is the mass of the swollen material, and *Wd* is the initial dry mass.

Porosity

The porosity of the scaffolds was determined by a similar procedure to the swelling degree but using distilled water. The porosity values were obtained according to Equation 7.3.

$$Porosity\ (\%) = \left(\frac{Ws-Wd}{dw}\right) \times \frac{100}{V} \quad (7.3)$$

where *Ws* and *Wd* are the mass of the swollen and lyophilized scaffold, respectively, *dw* is the density of water, and *V* is the volume of the scaffold in the swollen state.

Microstructural morphology

The sample´s microstructure was characterized using a desktop scanning electron microscope (SEM) (Phenom-World BV, The Netherlands) and all images were acquired using the ProSuite software. Before the SEM observation, the samples were fractured and placed on Aluminium pin stubs the (including surface and cross section of each sample) with electrically conductive carbon adhesive tape (PELCO Tabs™). After ensuring a correct adhesion to the pin, the samples were gently blown with compressed air to remove detached material; no coating was used on the imaging process. The Aluminium pin stub was then placed inside a Phenom Charge Reduction Sample Holder. The analysis was conducted at 5 kV with intensity image.

Contact angle

Contact angle measurements were performed in a Data Physics OCA20 device. The tests were conducted at room temperature and ultrapure water was used as test liquid. The contact angles were measured by depositing ultrapure water drops (3 μL) on the sample surface and analysed with SCA20 software. At least five measurements in each sample were performed in different scaffold surface locations and the average contact angle was taken as the result for each sample.

Mechanical properties

Mechanical properties were determined by uniaxial compression measurements using a TA HD Plus Texture Analyzer (Stable Micro Systems. UK) with an aluminium 25 mm probe. Prior the mechanical tests, the scaffolds were hydrated in PBS for 24 h, the excess of liquid gently removed with a filter paper and placed on the texture analyser platform. The force used to compress 80 % of the initial height was measured using a crosshead speed of 1 $mm.s^{-1}$. A trigger force of 0.05 N was used and at least 10 samples of each experimental condition were tested.

7.2.6 Cell culture

Normal human skin fibroblasts immortalized by overexpression of telomerase (BJ-5ta cell line) were maintained according to ATCC recommendations (four parts of Dulbecco's modified Eagle's medium (DMEM) contain ing 4 mmol/l-glutamine, 4.5 $g.L^{-1}$ sodium bicarbonate and 1 part of Medium 199, supplemented with 10% (v/v) of fetal bovine serum, 1% (v/v) of penicillin/streptomycin solution and 10 $g.ml^{-1}$ hygromycin B). Cells culture was incubated at 37 °C in a humidified atmosphere with 5 % CO_2, and the culture medium was replaced every 2 days.

Cytotoxicity evaluation

BJ-5ta cells were used as model of general cytotoxicity. Degradation and leachable products from the scaffolds (conditioned by 24 h contact with the scaffolds) were used to evaluate cytotoxicity. The scaffolds were disinfected by immersion three times in PBS containing 1 % (v/v) penicillin/streptomycin for 20

min, and by immersion in sterile PBS for 30 min to remove any remaining penicillin/streptomycin present on the scaffold microstructure. The disinfected scaffolds were incubated in 2 mL of medium at 37 °C for 24 h, and the medium was recovered and used as conditioned media. Cells seeded (10×10^3 cells/100 μL/well) on 96-well tissue culture polystyrene plates the day before experiments, were exposed to the conditioned medium and further incubated at 37 °C in a humidified atmosphere with 5% CO_2. Cells exposed to culture medium incubated without the presence of the scaffolds were used as control of the effect of the scaffolds' leachables. Metabolic viability was assessed at the end of 24 and 48 h of contact, using the MTT (3-(4,5-dimethylthiazol-2-yl)-2,5-diphenyltetrazoliumbromide) assay (Liu & Schubert, 2002).

Cell culture in the scaffolds

The influence of scaffold's properties on cell proliferation was evaluated by the MTS method. The MTS cell proliferation assay is a colorimetric sensitive quantification of viable cells in proliferation and cytotoxicity assay. The method is based on the reduction of MTS tetrazolium compound by viable cells to generate a coloured formazan product that is soluble in cell culture media. This conversion is thought to be carried out by NAD(P)H-dependent dehydrogenase enzymes in metabolically active cells (Malich, Markovic, & Winder, 1997) The scaffolds were disinfected and equilibrated for 24 h at 37 °C in medium without FBS prior to cell seeding. The scaffolds were carefully placed in 24-well plates and 200 μL of cell suspension (5×10^5 cells.mL^{-1}) were poured onto the top of each scaffold and allowed to infiltrate. After 2 h incubation, fresh medium (1 mL) was added to each scaffold and the plate was incubated for either 120 or 192 h with half of the culture media being renewed every 2 days. At the end of the defined time points, the cells/scaffold constructs were collected to a new 24-well plate and 1 mL of fresh medium with MTS was added to each well. The cells/scaffolds were incubated for 4 h at 37 °C in a humidified atmosphere with 5 % CO_2, and the absorbance was measured at 490 nm. Scaffolds without cells were used as control for the influence of the constructs' components on the MTS protocol.

Cell adhesion was further assessed by SEM for a detailed visualization of cell-material interactions. For SEM analysis, the cells/scaffolds constructs were soaked in a fixation solution (1 mL of 2.5 % glutaraldehyde (Merck) in PBS) for 1 h at room temperature, rinsed with distilled water and dehydrated by immersion for 30 min in a series of successive ethanol-water solutions (55 %, 70 %, 80 %, 90 %, 95 %

and 100 % v/v of ethanol). The samples were then dried at room temperature and coated with a thin gold layer using a sputter coater prior to SEM analysis.

7.2.7 Data analyses

All data analyses, fitting, plotting and statistical analyses procedures were performed on Origin 8.1 software (OriginLab Corporation. Northampton. MA. USA). Unless otherwise stated all experiments were run at least in triplicate.

7.3 RESULTS AND DISCUSSION

7.3.1 Optimization of the scaffolds' production conditions

Swelling, porosity and degradation are decisive factors to define the viability of a material to be used as scaffold (O'Brien, 2011), therefore these factors were selected as response variables to the experimental design. Table 1 presents the experimental design points, independent variables and response variables.

Table 7.1: Independent variables and responses used on the Box-Behnken experimental design.

	Independent variables			Response variables		
Assay	*T* (°C)	*t* (min)	*EF* (V.cm^{-1})	Swelling degree	Porosity (%)	Degradation (%)
1	70	5	20	0	0	100
2	85	5	20	12.07	84.97	62.33
3	70	30	20	0	0	100
4	85	30	20	8.39	85.86	19.35
5	70	17.5	0	0	0	100
6	85	17.5	0	8.68	84.72	20.41
7	70	17.5	40	0	0	100
8	85	17.5	40	10.06	95.17	23.38
9	77.5	5	0	11.79	100.30	100
10	77.5	30	0	7.34	83.43	69.42
11	77.5	5	40	7.66	100.16	100
12	77.5	30	40	9.77	100.72	100
13	77.5	17.5	20	10.18	102.10	100
14	77.5	17.5	20	10.08	98.71	100
15	77.5	17.5	20	10.23	101.16	100

The design points carried at 70 °C did not originated self-supporting gels and thus it was not possible to produce a stable scaffold. These samples when in contact with aqueous medium immediately dissolved and therefore it was attributed values of zero to the porosity and swelling factors and 100 % to the degradation. The design points corresponding to 77.5 °C produced self-supporting gels and stable scaffolds, however they presented high degradation rates and did not resist the 15 days of stability test. Only the samples treated at 85 °C endured the maximum test period.

Figure 7.1 shows desirability levels and limits based on the mathematical model constructed in the design analysis.

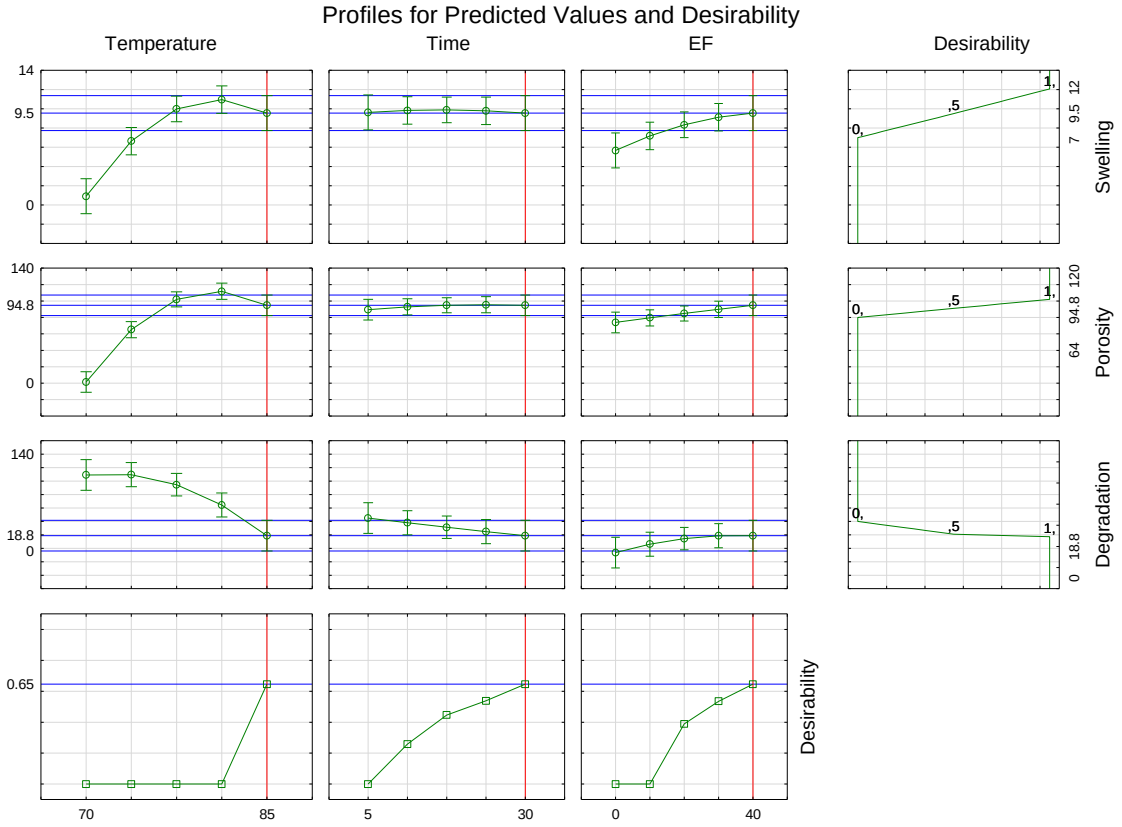

Figure 7.1: DFA analysis for the values of scaffold´s swelling, porosity and degradation, under the effects of temperature, time and EF strength used during the aggregation process.

This methodology is useful to find operating conditions that ensure agreement with established criteria for the involved responses. In this way it provides the best value of the desirable joint response (Mang et al., 2015; Vera Candioti et al., 2014). The desirability limits were established within the response variables range in order to minimize degradation and maximize porosity and swelling. The optimal point (OP) was determined as treatment at 85 °C for 30 minutes and at an EF of 40 $V.cm^{-1}$. The temperature was the

most decisive factor influencing the optimization, and only the temperature of 85 °C allowed the formation of stable scaffolds. Treatment time only contributed to the degradation of the scaffolds, reducing this response variable with the increasing treatment time. The variation of the EF did not determine the formation of stable scaffolds at 85 °C, but it affected the three response variables. The presence of an EF during the aggregation process increases the scaffold degradation rate and was positively correlated with the increase of the scaffolds swelling and porosity. The optimization of the treatment temperature, time and treatment type (heat exchange and OH with different voltages applied) allowed obtaining stable protein scaffolds with adequate porosity and swelling degree. Further studies were carried out in scaffolds produced from solutions treated at 85 °C for 30 min in order to validate their applicability. Given the ability of the EF to tune the scaffolds' properties and the novelty of OH use in this application, EF variations were considered in the validation tests. In this sense, tree variations of the optimal conditions were considered, at temperature and treatment time aforementioned and using EF of 0.1 $V.cm^{-1}$ (a residual value), 20 $V.cm^{-1}$ and 40 $V.cm^{-1}$ designated OP1, OP2 and OP3 respectively.

The characterisation of the native protein solution, aggregates solution after thermo-electric treatments and scaffolds properties (i.e. swelling, porosity and degradation) were subjected to a Principal Component Analysis (Figure 7.2). This allowed validating the optimal conditions and correlating the scaffolds' properties with structural and functional changes induced by the different thermo-electric treatments. On the PCA projection, the untreated protein solution was isolated form all the thermo-electrically treated samples. For this solution, degradation was considered to be 100 %, while swelling and porosity were considered to be zero. Besides, the sample was characterized by high levels of free SH groups, intrinsic and extrinsic fluorescence and low particles size. These factors were negatively correlated with swelling and porosity and positively correlated with degradation. Treatment conditions that did not originate self-supporting networks (i.e. 1, 3, 5 and 7) could not be tested for degradation, swelling and porosity, thus these variables were also considered 100 %, zero and zero respectively. Despite this similar assumption to the unheated protein solution, this group of treatments were distinguished by the reduction of the free SH groups, intrinsic and extrinsic fluorescence and size increase when compared with the unheated solution. The changes are consistent with the occurrence of low levels of protein denaturation and aggregation. The remaining samples, correspond to the ones that formed self-supporting networks, were positioned on the left side of the projection plot. Their positioning was influenced by the reduced degradation, positive swelling and porosity but also, particle size increase and fluorescence reduction. These changes are consistent with significant structural changes induced by the thermo-electric treatments at higher temperatures. The optimal points and the point 4 of the experimental design (with

equivalent treatment conditions) were positioned at the left and upper part of the distribution, corresponding to the scaffolds produced by larger aggregates and with lower degradation. The remaining scaffolds placed on the negative *yy* and *xx* quadrant of the projection were less stable but presented higher swelling and porosity. This analysis demonstrates that an adequate modulation of the functional properties of a protein system, caused by structural modifications, attained the formation of stable scaffolds with desired properties. The major advance and innovation for this process is the use of just physical methods and natural components, avoiding the use of DTT as reducing agent and thus decreasing the potential toxicity and adhesion problems resultant from its presence.

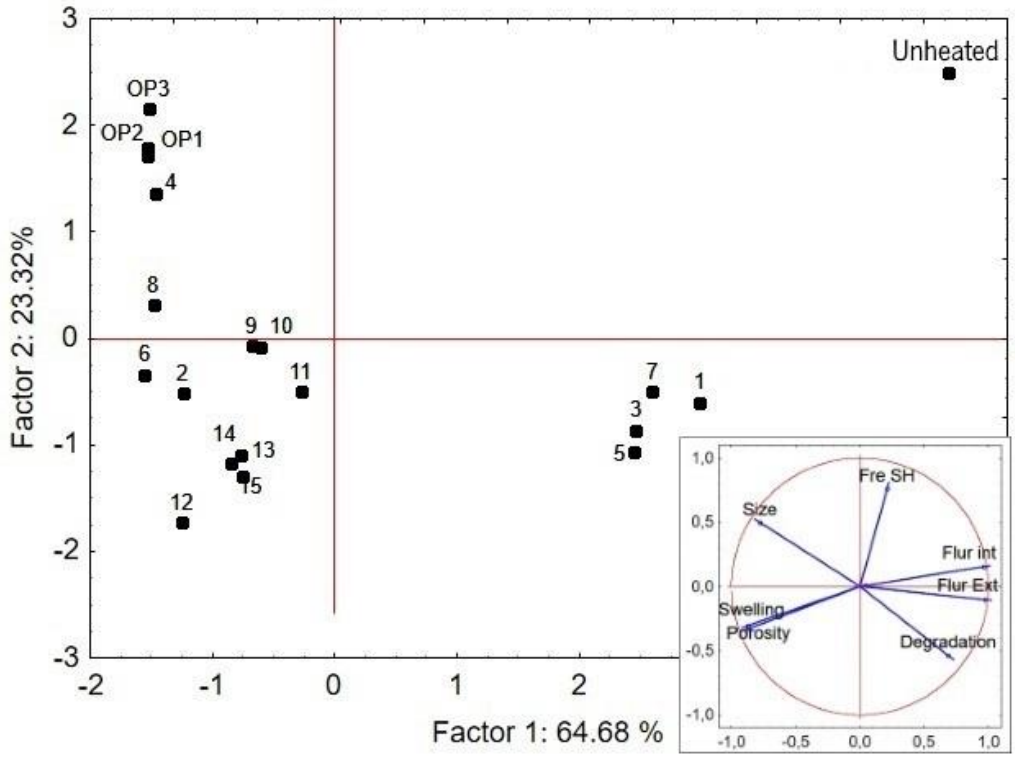

Figure 7.2: Principal component analysis of the experimental design points (1-15), the produced scaffolds at the optimal conditions under 0.1 V.cm^{-1} (OP1), 20 V.cm^{-1} (OP2) and 40 V.cm^{-1} (OP3), and unheated protein solution.

7.3.2 Scaffolds characterization

The obtained scaffolds, regardless of the condition used in their production, presented a similar appearance with white colour, high homogeneity and spongy appearance, as shown in Figure 7.3. After the establishment of the optimal conditions to promote protein aggregation and network formation, the scaffolds were further characterized to evaluate the influence of EF intensity on scaffolds' functional properties.

Figure 7.3: Representative image of a BSA/casein scaffold produced by cold-gelation induced by Ca^{2+}.

7.3.2.1 Microstructure

Porosity and architecture are relevant factors on the development of scaffolds. These structures must present a high surface area and pores with adequate size to lodge the cells. Pore interconnectivity is also important to allow cellular propagation and the diffusion of nutrients and oxygen to the interior of the structure (O'Brien, 2011; Weigel et al., 2006). The scaffold micro-structure will also influence the surface properties, swelling, mechanical properties and degradation rate. In Figure 7.4 it is possible to observe the microstructure and pore geometry of the produced scaffolds.

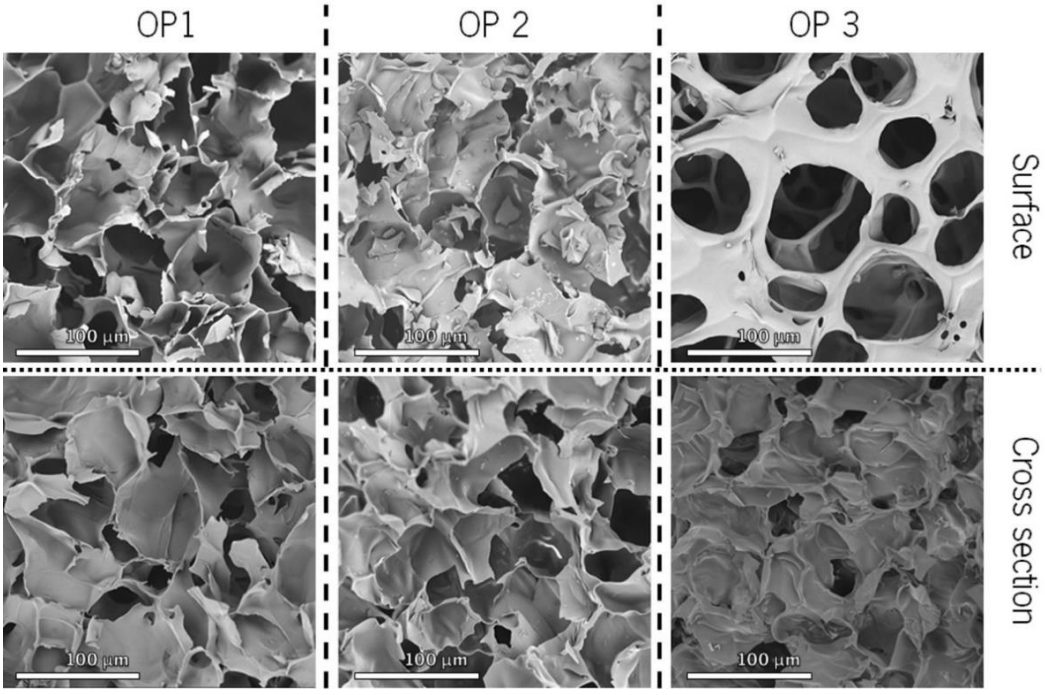

Figure 7.4: SEM micrographs of the scaffolds' surface (top) and cross section (bottom) for OP1, OP2 and OP3.

The samples present a high porous structure with uniform pore distribution at the surface and on the cross section. Samples OP1 and OP2 present irregular pore shapes with apparent fracture debris on the surface. In sample OP3 it is apparent a more regular pore geometry on the surface, interconnectivity and thinner walls on the cross sections. These changes on the scaffolds' geometry may be the result of the different EF intensities applied during pre-treatments of the samples and thus bring implications on the scaffolds' performance regarding cell adhesion and proliferation.

7.3.2.2 Contact angle, swelling ration and porosity

The gel forming solutions, temperature, time of treatment, and gelation procedure was similar for all the OP tested conditions. Therefore, the differences observed in the scaffolds' properties must be related with the use of different voltage gradients during the thermo-electric treatments (*i.e.* 0.1, 20 and 40 $V.cm^{-1}$). To further elucidate the effect of EF the contact angle, the swelling ratio and the porosity of the scaffolds were determined (see Table 7.2). These properties are related with the contact, uptake and space occupied by the aqueous media in the scaffolds' matrix and therefore critical for scaffolds' performance. The contact angle is associated with the surface properties of the scaffolds, affecting wettability, the capacity of the scaffold to rehydrate and cell adhesion (Kim et al., 2007). The increase of the EF intensity resulted on an increase of contact angle. It is interesting to note that the sample OP3, with significant higher contact angle, also presented a different surface pore geometry. The higher uniformity and apparent integrity on the surface of the scaffold can explain the higher contact angle determined, as the effective surface area in contact with the water drop was higher. It was also determined a positive correlation between EF increase and surface hydrophobicity of the aggregates' solutions, which implies a higher exposure of hydrophobic groups caused by the EF action. This may impact the network interactions established and surface properties, helping to explain the differences in morphology and contact angle observed.

Once the scaffolds were submerged in PBS or water and stabilized for 24 h, the swelling ratio and porosity were determined. There was a significant ($p < 0.05$) increase on the samples swelling degree with the increase of EF strength. It was expected an opposite correlation between the surface properties (contact angle) and the swelling of the scaffolds, as higher contact angle reflects a higher hydrophobic character of the surface. However, as discussed previously, the surface´s microstructure differences observed, rather than physicochemical affinity, may be responsible for the differences on the contact angle. In

addition, the existing differences on the surface properties of the lyophilized scaffolds could fade once the scaffolds were rehydrated. In any case, the increase of swelling ratio brings positive implications by facilitating the infiltration of the cells into the scaffolds, increasing the surface area, improving the absorption of fluids, transfer of nutrients and metabolites within the matrix (Peter et al., 2010). The porosity reflects the fluid uptake in relation with the volume of the scaffolds. A porous architecture implies a high surface area, contributing to the in and out-flow of nutrients and metabolites but also allowing higher cell-matrix interactions and cell loading. The variation of the EF causes a change on the scaffolds' porosity, with positive correlation on the EF increase and porosity. The microstructure analysis revealed, especially for sample OP3, a more regular pore distribution with an apparent higher interconnectivity, which would contribute for higher fluid uptake, higher swelling and porosity.

Table 7.2: Contact angle, swelling ratio and porosity of the obtained scaffolds.

Samples	Contact angle	Swelling ratio	Porosity (%)
OP1	92.37 ± 6.80 ^{a}	8.87 ± 0.22 ^{a}	84.65 ± 3.38 ^{a}
OP2	95.17 ± 5.94 ^{a}	9.53 ± 0.18 ^{b}	88.29 ± 1.35 ^{ab}
OP3	106.39 ± 7.38 ^{b}	10.03 ± 0.07 ^{c}	90.89 ± 3.64 ^{b}

For each column, different letters correspond to statistically different values ($p < 0.05$)

7.3.2.3 Mechanical properties

After rehydration, the scaffolds were submitted to mechanical tests by compressing them to 80 % of the initial length. This compression did not cause rupture of the scaffolds structure and they returned to the original shape, once the load was removed. This revealed the high mechanical resistance and flexibility of the structures obtained. Furthermore, the quantification of the force used to compress the scaffolds was used to evaluate their hardness (see Figure 7.5). The compression tests revealed a relatively high resistance of the scaffolds, with the compression requiring forces between 20 and 25 N. Moreover, all the samples (OP1, OP2, and OP3) presented significant differences ($p < 0.05$), being the hardness inversely correlated with the EF used in the pre-treatments. This reduction can be related with higher swelling and porosity of these samples, as they uptake more fluid and a higher fraction of the samples is composed by aqueous media. The scaffolds' structural properties may also contribute to their structural resistance as they are dependent of the characteristic of the "building block" used in the network formation (Alting, Hamer, De Kruif, & Visschers, 2003). The previous analysis of the aggregates'

suspension used to produce the scaffolds have demonstrated size reduction and increase of free SH groups with the EF increase. The fact that the network constituted by smaller aggregates can explain the lower hardness, but with the higher amount of free SH groups it was expected a higher disulphide crosslinking in the scaffolds and stronger structures. This was not verified and the swelling and hardness data actually suggest a weaker and more elastic network.

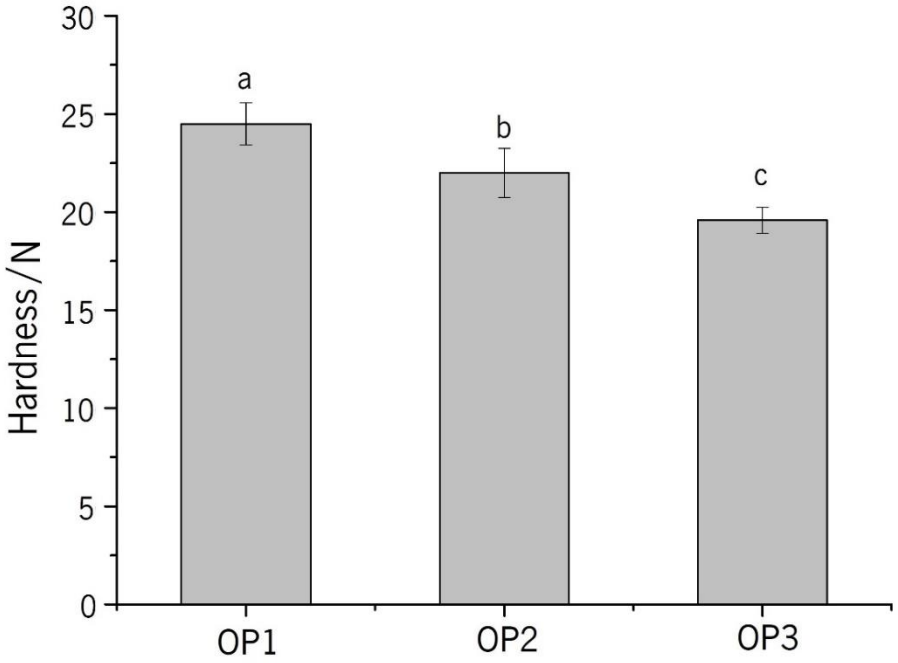

Figure 7.5: Hardness of the obtained scaffolds in the OP conditions and different EF values. Different letters correspond to statistically different values ($p < 0.05$).

7.3.2.4 *In vitro* degradation rate

The degradation rate of a scaffold for tissue engineering is a decisive factor for its application. The material ideally must provide a stable support for cellular proliferation but should degrade progressively to allow the tissue to fully form and replace the scaffold (Gomes et al., 2012). The *in vitro* degradation of the scaffolds produced was determined in PBS at 37 °C for a period of 15 days. Figure 7.6 shows the degradation profiles along the experimental time, with an initial degradation at day 1 of around 12 % and above 20 % in day 15. The degradation profiles were similar for all the samples, with a slight increase in degradation rate with the increase of the EF used during the pre-treatment. The degradation rate is dependent on the physicochemical interactions involved in the network formation process and on

properties like porosity and swelling degree. The higher porosity and swelling capacity of the samples OP2 and OP3 may contribute to higher elution of proteins forming the structure and to the increase of the degradation rates.

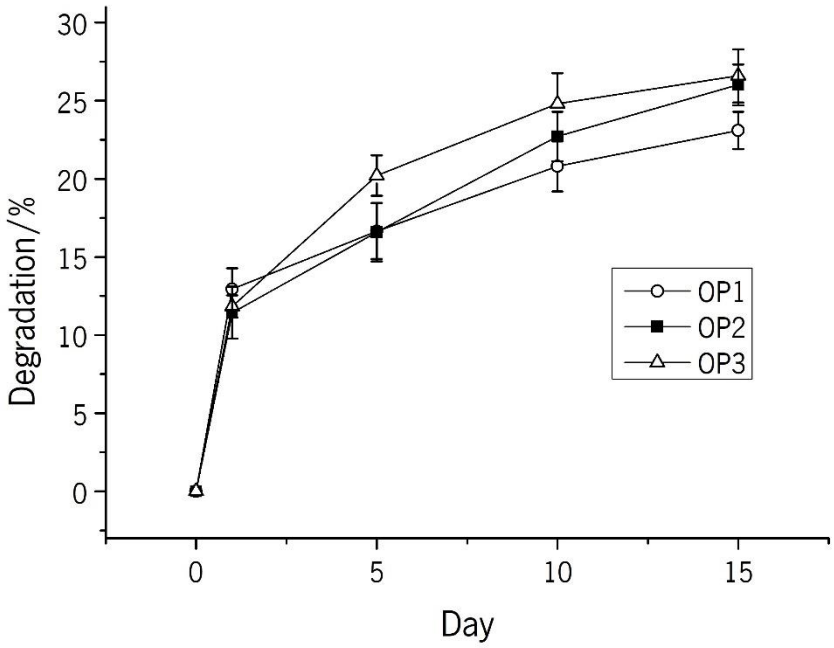

Figure 7.6: *In vitro* degradation rate of the obtained scaffolds.

The degradation of the scaffolds must also be related with the physicochemical interactions established within the network. During the aggregates suspension's characterization, we were able to observe differences on the overall aggregates' properties in response to different values of EF used during their production. This may contribute to the formation of protein networks with different interactions and stabilities, as described in the previous chapter. Overall, the degradation profile was in agreement with other works and was adequate to be used as a support for cellular growth.

7.3.3. Cell viability and proliferation

Biocompatibility of the scaffolds' material and of its degradation by-products are essential to ensure an adequate performance and should not induce inflammatory response nor cytotoxicity. In order to evaluate the cytotoxicity induced by eluded constituents and degradation by-products from the scaffolds, BJ-5ta fibroblasts were exposed to culture medium pre-conditioned by contact with the scaffolds for 24 h. The

results in cell viability after 24 h and 48 h by indirect contact are presented in Figure 7.7. Regardless of the exposure time, there was no decrease on the cellular metabolic activity for the contact with any of the conditioned solutions, which indicates that none of the scaffolds' components presents cytotoxicity for the cells, thus supporting their use for tissue engineering applications. These results also represent an improvement facing the previous formulation of BSA/casein scaffolds, where cell viability was between 70 and 95 %, thus showing a moderate cytotoxicity (Ribeiro et al., 2016, 2012). The improvement in cell viability was very probably related to the elimination of DTT from the formulation. In fact, the optimization of the protein thermal treatment conditions induced an adequate denaturation and aggregation, allowing to eliminate the use of reducing agents and improving the scaffolds properties. Since this was one of the main goals of this work, it is possible to state that the objective was fulfilled. It is also important to highlight that the use of OH and the inherent MEF effects does not result in cytotoxicity or negative implications on the cell culture.

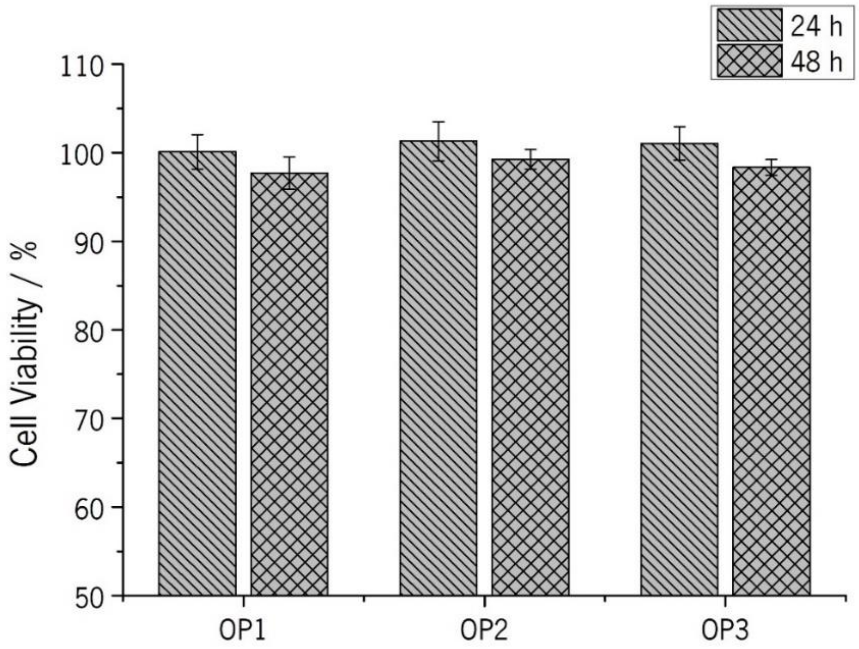

Figure 7.7: BJ-5ta cell viability measured by MTT assay at 24 and 48 h of culture with conditioned medium pre-conditioned by contact with scaffolds for 24 h. The data represents mean ± SD of three independent experiments, compared with negative controls for 24 h and 48 h.

Further, the evaluation of the scaffolds' ability to support cellular adhesion and proliferation was performed by seeding BJ-5ta cells on the scaffolds and allow them to grow for 5 to 8 days. Figure 7.8 shows the proliferation of the fibroblast cells after the designated culture times. All the scaffolds presented

an increase in the number of cells, proving their ability to sustain the proliferation of cells. After 5 days in culture, the OP1 almost tripled the initial cell inoculum with $2.6 \times 10^5 \pm 6.5 \times 10^4$ cells, but OP2 and OP3 presented much higher proliferation rates with $6.4 \times 10^5 \pm 1.2 \times 10^5$ and $7.0 \times 10^5 \pm 1.3 \times 10^5$ cells, respectively. The cell quantification at day 8 also revealed an increase in the number of cells, with OP1 standing out with the higher increase during this period. A clear tendency is observed from OP1 to OP3, with the scaffolds produced by exposure to successively higher EF presenting higher cell proliferation and higher initial growth rates. The observed behaviour of the cell proliferation can be related with a similar trend caused by the higher EF to increase the contact angle, swelling, porosity and degradation rate of the scaffolds, as well as to reduce the hardness of the structure. The increase in contact angles is related to higher hydrophobicity and/or surface charge of the proteins, modified by the EF. These changes in surface properties may facilitate the adhesion of the cells to the matrix, once electrostatic and hydrophobic contributions play a decisive role in such phenomenon (Burke et al., 2017; Kim et al., 2007). Higher swelling and porosity also facilitate the proliferation and dispersion of the cells, while also allowing a better in- and out-flow of nutrients, metabolites and gas exchanges. The higher degradation rates and lower hardness of the structure also allow the cells to proliferate and replace the scaffold´s matrix with cellular material.

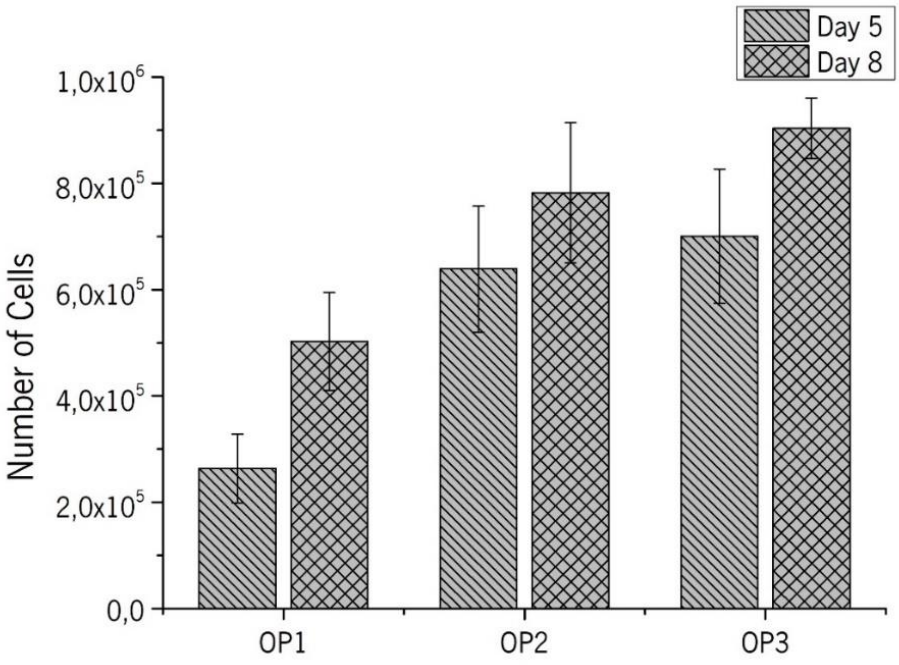

Figure 7.8: Cell adhesion and growth on the scaffolds 5 and 8 days after seeding.

The proliferation and adhesion of the cells to the scaffolds matrix was also confirmed by SEM on dehydrated scaffolds (see Figure 7.9). In the micrographs it is possible to observe cells perfectly adhered and included on the scaffold´s surface (marked by the arrows). These results suggest that BSA/casein scaffolds produced by OH pre-treatment under the influence of different MEF intensities are biocompatible as they favour cell spreading and promote cell adhesion and proliferation.

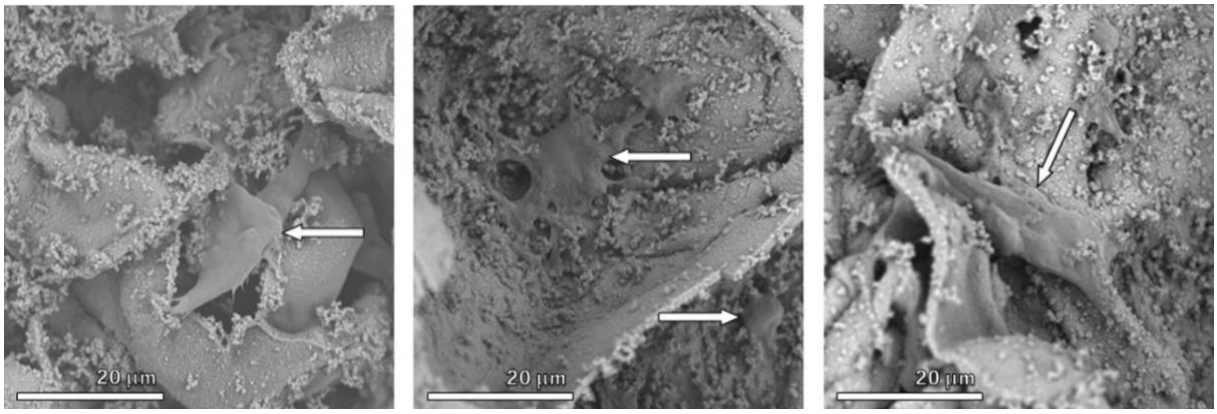

Figure 7.9: Representative SEM micrographs of cells adhesion to the scaffolds 8 days after seeding; arrows indicate cells positioning.

7.4 CONCLUSIONS

The potential of using proteins as building blocks to produce scaffolds for tissue engineering was explored and the optimization of the processing conditions allowed obtaining scaffolds without the use of reducing agents in their production. Scaffold´s properties such as stability, swelling and porosity were correlated with the high levels of structural modifications, aggregation and interactions established by the proteins forming the network. The variation of the EF strength during the denaturation and aggregation process resulted in scaffolds with distinctive functional properties. These scaffolds presented no cytotoxicity to BJ-5ta fibroblast cells, representing and improvement facing formulations that used DTT during the production method. The obtained scaffolds were adequate to support cellular growth, favouring cell adhesion and proliferation by the higher contact angle, porosity, swelling and degradation rates promoted by the use of higher EF during their production. OH demonstrated to be a promising technique to promote protein functionalization and to tune the scaffolds' functional properties with advantages regarding cellular adhesion and proliferation.

7.5 REFERENCES

Alting, A. C., Hamer, R. J., De Kruif, C. G., & Visschers, R. W. (2003). Cold-set globular protein gels: Interactions, structure and rheology as a function of protein concentration. *Journal of Agricultural and Food Chemistry*, *51*(10), 3150–3156. https://doi.org/10.1021/jf0209342

Burke, M., Armstrong, J. P. K., Goodwin, A., Deller, R. C., Carter, B. M., Harniman, R. L., ... Perriman, A. W. (2017). Regulation of Scaffold Cell Adhesion Using Artificial Membrane Binding Proteins. *Macromolecular Bioscience*, *17*(7), 1600523. https://doi.org/10.1002/mabi.201600523

Charulatha, V., & Rajaram, A. (2003). Influence of different crosslinking treatments on the physical properties of collagen membranes. *Biomaterials*, *24*(5), 759–767. https://doi.org/10.1016/S0142-9612(02)00412-X

Drury, J. L., & Mooney, D. J. (2003). Hydrogels for tissue engineering: scaffold design variables and applications. *Biomaterials*, *24*(24), 4337–4351. https://doi.org/10.1016/S0142-9612(03)00340-5

Eltom, A., Zhong, G., & Muhammad, A. (2019). Scaffold Techniques and Designs in Tissue Engineering Functions and Purposes: A Review. *Advances in Materials Science and Engineering*, *2019*. https://doi.org/10.1155/2019/3429527

Gebauer, M., & Skerra, A. (2009). Engineered protein scaffolds as next-generation antibody therapeutics. *Current Opinion in Chemical Biology*, *13*(3), 245–255. https://doi.org/10.1016/j.cbpa.2009.04.627

Gomes, S., Leonor, I. B., Mano, J. F., Reis, R. L., & Kaplan, D. L. (2012). Natural and genetically engineered proteins for tissue engineering. *Progress in Polymer Science*, *37*(1), 1–17. https://doi.org/10.1016/j.progpolymsci.2011.07.003

Kim, S. H., Ha, H. J., Ko, Y. K., Yoon, S. J., Rhee, J. M., Kim, M. S., ... Khang, G. (2007). Correlation of proliferation, morphology and biological responses of fibroblasts on LDPE with different surface wettability. *Journal of Biomaterials Science, Polymer Edition*, *18*(5), 609–622. https://doi.org/10.1163/156856207780852514

L. Tartier, Y.L. McCarey, J.E. Biaglow, I. E. K. and K. D. H. (2000). Apoptosis induced by dithiothreitol in HL-60 cells shows early activation of caspase 3 and is independent of mitochondria. In *Cell*

Death Differ (pp. 1002–1010).

Li, P.-S., -Liang Lee, I., Yu, W.-L., Sun, J.-S., Jane, W.-N., & Shen, H.-H. (2015). A Novel Albumin-Based Tissue Scaffold for Autogenic Tissue Engineering Applications. *Scientific Reports*, *4*(1), 5600. https://doi.org/10.1038/srep05600

Liu, Y., & Schubert, D. (2002). Cytotoxic Amyloid Peptides Inhibit Cellular 3-(4,5-Dimethylthiazol-2-yl)-2,5-Diphenyltetrazolium Bromide (MTT) Reduction by Enhancing MTT Formazan Exocytosis. *Journal of Neurochemistry*, *69*(6), 2285–2293. https://doi.org/10.1046/j.1471-4159.1997.69062285.x

Malich, G., Markovic, B., & Winder, C. (1997). The sensitivity and specificity of the MTS tetrazolium assay for detecting the in vitro cytotoxicity of 20 chemicals using human cell lines. *Toxicology*, *124*(3), 179–192. https://doi.org/10.1016/S0300-483X(97)00151-0

Mang, D. Y., Abdou, A. B., Njintang, N. Y., Djiogue, E. J. M., Loura, B. B., & Mbofung, M. C. (2015). Application of desirability-function and RSM to optimize antioxidant properties of mucuna milk. *Journal of Food Measurement and Characterization*, *9*(4), 495–507. https://doi.org/10.1007/s11694-015-9258-z

O'Brien, F. J. (2011). Biomaterials & scaffolds for tissue engineering. *Materials Today*, *14*(3), 88–95. https://doi.org/10.1016/S1369-7021(11)70058-X

Peter, M., Binulal, N. S., Nair, S. V., Selvamurugan, N., Tamura, H., & Jayakumar, R. (2010). Novel biodegradable chitosan–gelatin/nano-bioactive glass ceramic composite scaffolds for alveolar bone tissue engineering. *Chemical Engineering Journal*, *158*(2), 353–361. https://doi.org/10.1016/j.cej.2010.02.003

Ribeiro, A., Gomes, A. C., & Cavaco-Paulo, A. M. (2012). Developing scaffolds for tissue engineering using the Ca 2+ -induced cold gelation by an experimental design approach. *Journal of Biomedical Materials Research Part B: Applied Biomaterials*, *100B*(8), 2269–2278. https://doi.org/10.1002/jbm.b.32797

Ribeiro, A., Volkov, V., Oliveira, M. B., Padrão, J., Mano, J. F., Gomes, A. C., & Cavaco-Paulo, A. (2016). BSA/HSA ratio modulates the properties of Ca2+-induced cold gelation scaffolds. *International Journal of Biological Macromolecules*, *89*, 535–544. https://doi.org/10.1016/j.ijbiomac.2016.05.012

Solovieva, M. E., Solovyev, V. V., Kudryavtsev, A. A., Trizna, Y. A., & Akatov, V. S. (2008). Vitamin B12b enhances the cytotoxicity of dithiothreitol. *Free Radical Biology and Medicine*, *44*(10), 1846–1856. https://doi.org/10.1016/j.freeradbiomed.2008.02.002

Thibodeau, P. A., Kocsis-Bédard, S., Courteau, J., Niyonsenga, T., & Paquette, B. (2001). Thiols can either enhance or suppress DNA damage induction by catecholestrogens. *Free Radical Biology and Medicine*, *30*(1), 62–73. https://doi.org/10.1016/S0891-5849(00)00446-9

Vera Candioti, L., De Zan, M. M., Cámara, M. S., & Goicoechea, H. C. (2014). Experimental design and multiple response optimization. Using the desirability function in analytical methods development. *Talanta*, *124*, 123–138. https://doi.org/10.1016/j.talanta.2014.01.034

Weigel, T., Schinkel, G., & Lendlein, A. (2006). Design and preparation of polymeric scaffolds for tissue engineering. *Expert Review of Medical Devices*, *3*(6), 835–851. https://doi.org/10.1586/17434440.3.6.835

Yan, H., Saiani, A., Gough, J. E., & Miller, A. F. (2006). Thermoreversible Protein Hydrogel as Cell Scaffold. *Biomacromolecules*, *7*(10), 2776–2782. https://doi.org/10.1021/bm0605560

CHAPTER 8.

FINAL REMARKS

8.1 GENERAL CONCLUSIONS

The work presented in this thesis is the result of a systematic study that aimed at evaluating the effects of MEF technology on whey proteins, assessing and characterizing at the molecular level the influence that MEF exert on the structure of whey proteins, their potential to establish interactions with identical or other molecules and on the formation of supramolecular structures. It was intended to exploit the potential of MEF on the development of protein networks of pure and enriched fractions of whey proteins, aiming at the production of food-grade structures for application in the food, pharmaceutical and biomedical areas. The main contributions of the present work are summarized below:

- The interpretation of complementary information obtained by *in situ* multi-spectroscopy techniques allowed unravelling some of the very complex structural dynamics of β-lg thermally induced unfolding.
- The existence of reversible conformational changes occurring at low temperatures (35-60 °C) were confirmed and differentiated from the quenching phenomenon.
- For the first time, MEF influence was verified at molecular level in thermal processing treatments. MEF exposed β-lg presented changes in its secondary structure, Trp exposure, surface hydrophobicity, free thiol reactivity and possibly intramolecular disulphide crosslinking. For the conditions used (i.e. electric field strength, frequency and time of exposure) the disturbances imposed are not sufficient to disrupt the protein fold and MEF effects are therefore synergic with the thermal effects.
- MEF specific action and extent were pH dependent – i.e. solutions of β-lg at pH 7 revealed to be more responsive to MEF.
- The presence of MEF during β-lg's thermal unfolding resulted in changes in the estimated T_m values and in different structural features. Thermal transition and structural changes were largely influenced by the electrical frequency and by the EF strength applied. The use of low frequencies (50 Hz) presented greater effects in β-lg's thermal transitions; and the increase of the EF strength was positively correlated with a higher degree of structural changes.
- The presence of MEF was also reflected in the protein's affinity to hydrophobic compounds, namely ANS affinity increase and retinol binding conservation.
- The use of OH and different MEF variables during WPI pre-treatment resulted in different pathways of protein aggregation. MEF action resulted in smaller aggregates, with lower amount of free thiol groups and less viscous solutions.

- Changes in protein denaturation and aggregation also reflected on the gelation of the WPI and final gel properties; changes in the electrical variables applied contributed for the differentiation of the OH treated samples, being the MEF related effects potentiated by the increase of EF strength and particularly for the use of low frequencies (i.e. 50 Hz).
- OH was successfully used in the production of innovative protein-based scaffolds for tissue engineering; control of MEF variables demonstrated to be an adequate technique to promote protein functionalization and to tune the scaffold´s functional properties.
- The formation of stable scaffolds was found to be dependent from the time-temperature binomial, but the variation of the EF was able to influence functional properties such as the contact angle, swelling, porosity, hardness and degradation rate.
- The changes imposed by the presence of MEF during the scaffold´s production method did not reveal negative effects in the materials cytotoxicity and resulted in drastic improvements in cellular proliferation.

Overall the use of OH for thermal processing and the presence of MEF result in changes in proteins' structure and conformation. These changes at molecular level result in a cascade of events, ultimately originating differentiated functional properties of the structures formed. The control of MEF variables allows tuning denaturation and protein aggregation, acting as a methodology to control protein functionality. The use of OH allowed the development of protein-structured systems with distinctive properties and should allow multiple applications, gathering the requirements to be used in the biotechnology, pharmaceutical, biomedical and food industries.

8.2 GUIDELINES FOR FUTURE WORKS

This thesis has provided very important insights about the effect of MEF in whey protein structure, aggregation and gelation, acting as a proof of concept for the use of MEF as a functionalization tool in processing and biotechnology areas. However, this was a first approach to the topic and further work is needed to fully elucidate and exploit its technological potential. Therefore, some guidelines for future works are as follows:

- Further explore MEF variables in a broader range of conditions, i.e. broader voltage and electrical frequency values.

- Application of MEF treatments to other protein fractions and isolates (e.g. other animal proteins and vegetable proteins).
- Evaluate the capacity of the MEF-produced protein systems in interacting, transport and release bioactive compounds.
- Evaluate the MEF-produced protein systems in terms of their behaviour in a simulated gastrointestinal tract and of the cytotoxicity of their intact and hydrolysed forms.
- Further explore MEF potential to tune and control other biotechnological processes involving protein structural stability, interactions and supramolecular structures formation.

8.3 FUTURE PERSPECTIVES

OH and MEF technology finds today a vast number of applications in several fields such as food technology, chemical engineering and biotechnology. OH as a thermal processing technology can replace traditional heating, bringing competitive advantages regarding operation times, heating effectiveness, end-product quality (both in organoleptic and nutritional aspects), energetic efficiency, maintenance costs and environmental impact. There is now a growing body of evidence that shows that OH is not limited to thermal treatments, such as pasteurization or sterilization , and MEF´s non-thermal effects play a decisive role in microorganisms and enzymes inactivation or in proteins' functionalization. The possibility of a fine-tuned control of processing parameters such as heating rate, EF and electric frequency, places MEF as a promising tool to enhance and develop new functionalities or to induce relevant changes on important macromolecules such as proteins (including enzymes) and polysaccharides. The easiness to create and adapt OH and MEF principles to certain niche applications in bioprocessing – e.g. aiming at functionalization/transformation and extraction – of value-added molecules will start to expand rapidly.

SUPPLEMENTARY MATERIAL

β-LACTOGLOBULIN CHARACTERIZATION

The β-lg purified from commercial whey protein isolate was characterized to ensure purity and conformation. Techniques as by HPLC, SDS-PAGE, CD and fluorescence, were used to evaluate and compare the purified protein with commercial β-lg from Sigma-Aldrich (lyophilized powder ≥ 90% PAGE).

Figure S1 shows the SDS-PAGE performed with both proteins. In this particular assay, no boiling step or reducing agents were used in order to avoid structural changes or cleavage of chemical aggregates. A predominance of the monomeric form of the protein was verified for both samples (≈18 kDa bands) with a residual presence of dimers (≈36 kDa bands). These results confirm the presence of the desired protein in similar conditions to the commercial version.

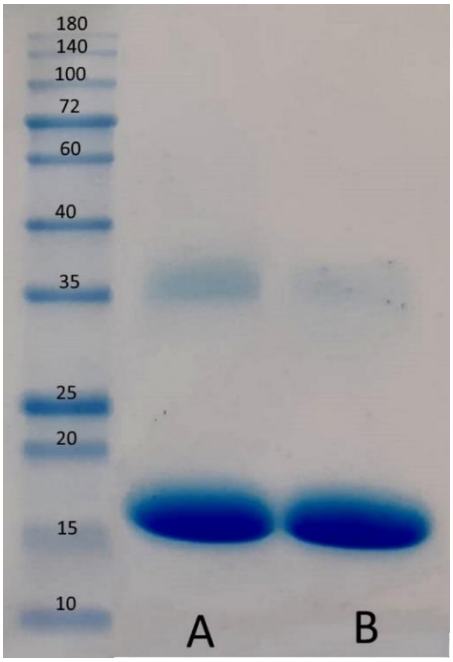

Figure S1: SDS-PAGE of commercial (A) and purified (B) β-lg. Molecular marker is presented on the left.

Further on, the samples were examined by HLPC for quantification and to confirm purity. Figure S2 presents the chromatograms of commercial and purified β-lg. It is possible to observe the two peaks in each chromatogram, overlapping almost perfectly. The two peaks correspond to the variants B (first peak) and A (second peak) of the protein. The quantification of the purified sample determined total protein content of 87.9 % in the sample, of which 99 % corresponded to β-lg. The remaining fraction of the samples was attributed to moisture and residual salts content.

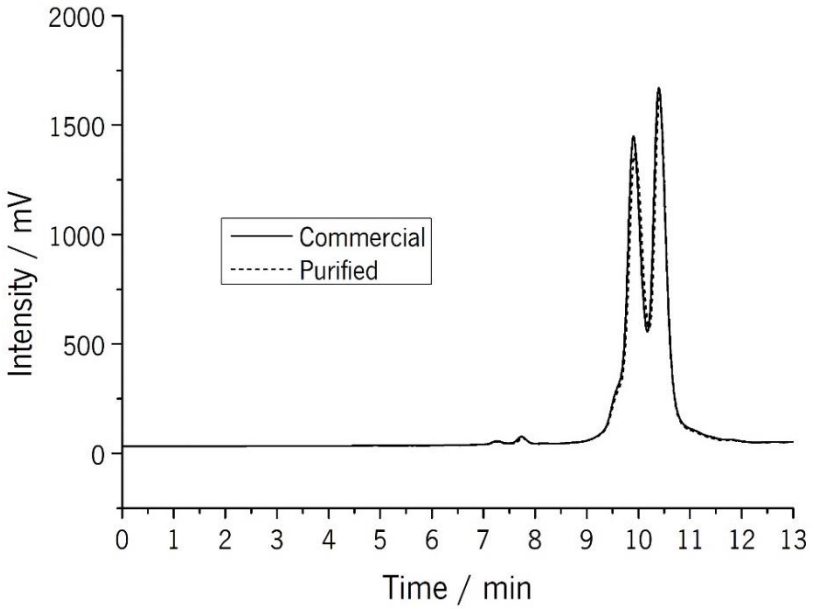

Figure S2: Chromatogram of commercial and purified β-lg.

In order to study structural aspects of a protein, structural and conformation integrity must be confirmed. Figure S3 presents the far-UV CD spectra of commercial and purified proteins. The samples presented a similar spectrum, also in agreement with the characteristic spectra reported in literature, confirming the integrity of the secondary structure of the obtained protein.

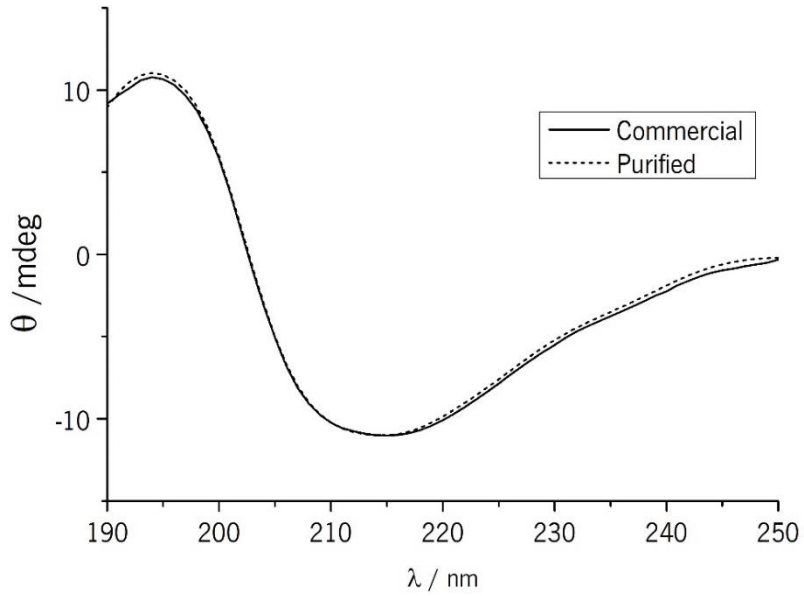

Figure S3: Far-UV CD spectra of commercial and purified β-lg.

The specific conformation, associated with the protein´s tertiary structure plays a decisive role in the function and stability. The conformation of β-lg was checked by evaluation of the near-UV CD spectra and the intrinsic fluorescence associated with Trp. The near-UV CD spectra presented in Figure S4 are concordant in both proteins, where most important features are the Trp peak between 290 to 305 nm and tyrosine peak between 275 and 282. The purified β-lg displays slightly more intensity on the Trp peak, suggesting an increased a higher contribution of the tryptophan residues on the purified sample. Fluorescence spectroscopy is a sensitive technique to study protein conformation and the use of an excitation wavelength of 295 nm allows to specifically probe the Trp positioning within the structure. In Figure S5 the fluorescence spectra of the commercial and purified proteins are presented, where a great similarity was observed between the samples. The peak at the maximum fluorescence intensity, located at 330 nm, demonstration that Trp was positioned on a hydrophobic region as expected. Only a marginal difference on the peak intensity was detected, demonstrating a higher contribution of Trp on the purified protein, which is in agreement with the near-UV CD spectrum. In both cases only a small difference in intensity and no shift was observed, suggesting that Trp was placed in similar microenvironments but with slightly different accessibilities.

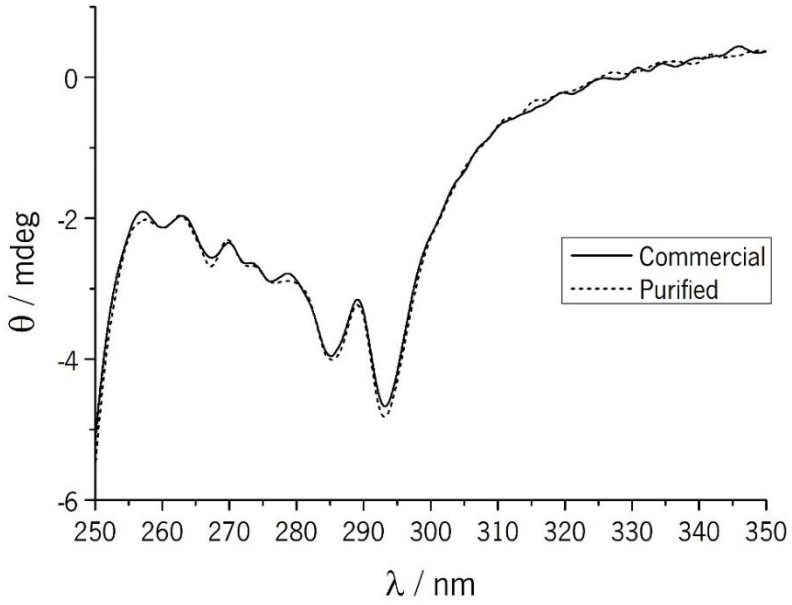

Figure S4: Near-UV CD spectra of commercial and purified β-lg.

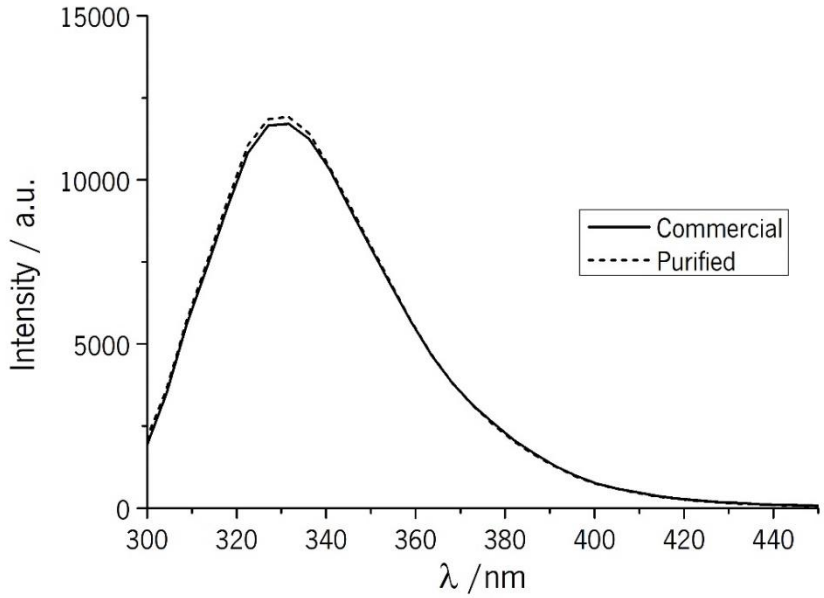

Figure S5: Intrinsic fluorescence spectra of commercial and purified β-lg.

Overall, the high matching level of the near-UV and far-UV CD spectra and intrinsic fluorescence lead to the conclusion that both samples corresponded to the same protein and in a similar conformation.

SUPPLEMENTARY MATERIAL FORM CHAPTER 4

Table S1: Average and standard deviation of the ellipticity at 208 nm, maximum intensity for both Trp and ANS fluorescence and percentage of free SH, for the treatments at pH 3

Sample		CD (θ 208 nm)	Maximum Trp fluorescence (a.u.)	Maximum ANS fluorescence (a.u.)	Free thiol groups (%)
Unheated		-8.83 ± 0.38 ^{a}	15801.50 ± 1.67 ^{ab}	4849.54 ± 6.75 ^{a}	7.44 ± 1.16 ^{a}
50 °C	Conventional	-9.54 ± 0.14 ^{ab}	16041.99 ± 5.83 ^{a}	5070.18 ± 88.39 ^{ab}	8.11 ± 1.78 ^{ab}
	Ohmic	-9.59 ± 0.15 ^{ab}	15972.36 ± 91.80 ^{a}	5068.89 ± 138.13 ^{ab}	7.67 ± 1.59 ^{a}
60 °C	Conventional	-9.41 ± 0.14 ^{ab}	16217.97 ± 16.29 ^{a}	5093.23 ± 30.27 ^{ab}	7.36 ± 1.20 ^{ac}
	Ohmic	-9.53 ± 0.19 ^{ab}	16052.44 ± 94.41 ^{a}	5116.95 ± 127.04 ^{ab}	6.83 ± 0.92 ^{ac}
70 °C	Conventional	-9.52 ± 0.10 ^{ab}	16170.31 ± 199.34 ^{a}	4882.84 ± 157.22 ^{a}	6.37 ± 0.77 ^{abc}
	Ohmic	-9.43 ± 0.27 ^{ab}	16181.86 ± 286.24 ^{a}	4830.03 ± 377.96 ^{a}	6.47 ± 0.94 ^{abc}
80 °C	Conventional	-9.51 ± 0.29 ^{ab}	16203.92 ± 184.81 ^{a}	5371.61 ± 33.98 ^{b}	7.56 ± 0.90 ^{a}
	Ohmic	-9.82 ± 0.24 ^{b}	16087.82 ± 227.93 ^{a}	5449.61 ± 134.70 ^{b}	5.89 ± 0.77 ^{c}
90 °C	Conventional	-10.56 ± 0.20 ^{c}	15502.89 ± 112.91 ^{bc}	9158.72 ± 124.43 ^{c}	16.86 ± 1.45 ^{d}
	Ohmic	-10.83 ± 0.18 ^{c}	15164.52 ± 112.82 ^{c}	10053.02 ± 228.77 ^{d}	20.99 ± 1.02 ^{e}

For each column, different letters correspond to statistically significant differences ($p < 0.05$).

In Chapter 4, only the results of the treatments at 90 °C were presented (with exception for the free SH quantification). As can be observed on Table S1 the majority of the treatments below this temperature did not produce significant differences between the treatment type or between the treatments and the control samples.

Table S2: Average and standard deviation of the ellipticity at 208 nm, maximum intensity for both Trp and ANS fluorescence and percentage of free SH, for the treatments at pH 4.3.

Sample		CD (θ 208 nm)	Maximum Trp fluorescence (a.u.)	Maximum ANS fluorescence (a.u.)	Free thiol groups (%)
Unheated		-8.34 ± 0.13 ^{a}	14393.66 ± 37.58 ^{a}	2462.07 ± 14.21 ^{a}	10.38 ± 2.09 ^{a}
50 °C	Conventional	-8.45 ± 0.11 ^{a}	14524.22 ± 77.58 ^{a}	2451.96 ± 11.62 ^{a}	12.97 ± 0.24 ^{b}
	Ohmic	-8.39 ± 0.22 ^{a}	14405.18 ± 22.61 ^{a}	2473.11 ± 15.45 ^{a}	12.07 ± 0.15 ^{c}
60 °C	Conventional	-8.46 ± 0.53 ^{a}	14593.42 ± 54.54 ^{a}	2571.32 ± 25.62 ^{b}	13.81 ± 0.69 ^{d}
	Ohmic	-8.64 ± 0.15 ^{a}	14369.86 ± 76.45 ^{a}	2596.45 ± 37.30 ^{b}	12.70 ± 0.31 ^{bc}
70 °C	Conventional	-8.58 ± 0.32 ^{a}	14517.38 ± 137.48 ^{a}	2700.36 ± 11.21 ^{c}	14.72 ± 0.16 ^{e}
	Ohmic	-8.37 ± 0.28 ^{a}	14291.61 ± 174.39 ^{a}	2585.15 ± 54.92 ^{b}	13.39 ± 0.17 ^{bd}

For each column, different letters correspond to statistically significant differences ($p < 0.05$).

Table S3: Average and standard deviation of the ellipticity at 208 nm, maximum intensity for both Trp and ANS fluorescence and percentage of free SH, for the treatments at pH 5.7

Sample		CD (θ 208 nm)	Maximum Trp fluorescence (a.u.)	Maximum ANS fluorescence (a.u.)	Free thiol groups (%)
Unheated		-7.93 ± 0.05 ^{a}	12591.29 ± 34.90 ^{a}	871.55 ± 1.77 ^{a}	9.37 ± 0.41 ^{a}
50 °C	Conventional	-8.46 ± 0.13 ^{ab}	12681.67 ± 67.96 ^{a}	888.39 ± 2.24 ^{ab}	9.58 ± 1.20 ^{a}
	Ohmic	-8.73 ± 0.11 ^{b}	12588.33 ± 57.40 ^{a}	896.20 ± 4.72 ^{b}	10.29 ± 0.39 ^{a}
60 °C	Conventional	-8.23 ± 0.12 ^{ab}	12588.29 ± 43.95 ^{a}	879.36 ± 7.49 ^{a}	10.79 ± 0.86 ^{ab}
	Ohmic	-8.43 ± 0.47 ^{ab}	12601.53 ± 107.91 ^{a}	923.71 ± 11.17 ^{c}	10.74 ± 0.77 ^{ab}
70 °C	Conventional	-8.31 ± 0.18 ^{ab}	12687.07 ± 35.05 ^{a}	952.42 ± 9.99 ^{d}	11.62 ± 0.87 ^{bc}
	Ohmic	-8.33 ± 0.10 ^{ab}	12540.67 ± 104.98 ^{a}	997.92 ± 8.29 ^{e}	12.40 ± 0.18 ^{c}

For treatments at pH 5.7, in each column, different letters correspond to statistically significant differences ($p < 0.05$).

The treatments performed at pH 4.3 and 5.7 do not present any change in secondary structure or Trp fluorescence, for thermal treatments below 70 °C. Only ANS fluorescence and free SH show some differentiation between treated samples and the controls. At pH of 4.3 ANS fluorescence shows a significant increase ($p < 0.05$) with the 60 and 70 °C treatments, being this increase higher for the conventionally treated samples. All treated samples present significant increases of free SH and ANS fluorescence, when compared to the control; conventionally treated samples have higher exposure of SH when compared to the OH ones. Despites no structural changes and low

changes on β-lg´s conformation the conventional treatments show an overall higher impact on protein conformation, as opposed to the results for all other pH values tested.

The set of treatments at pH 5.7 is the one showing lower differentiation. A slight increase in ellipticity is observed with the thermal treatments but without differentiation among them. Trp fluorescence presents no significant changes ($p > 0.05$), suggesting very little or no change at all in the structural features of β-lg. Again, ANS florescence and SH exposure are the parameters presenting more variability within the treatments. ANS florescence suffers a progressive increase with the temperature and a tendency to be higher with the OH treatment. As for the SH exposure, a slight increase with the temperature is also noticed but without differentiation between treatment type.

Table S4: Average and standard deviation of the ellipticity at 208 nm, maximum intensity for both Trp and ANS fluorescence and percentage of free SH, for the treatments at pH 7

Sample		CD (θ 208 nm)	Maximum Trp fluorescence (a.u.)	Maximum ANS fluorescence (a.u.)	Free thiol groups (%)
Unheated		-8.88 ± 0.16 ^{a}	11832.04 ± 14.74 ^{a}	1178.42 ± 6.50 ^{a}	7.21 ± 0.13 ^{a}
50 °C	Conventional	-9.07 ± 0.32 ^{ab}	11768.99 ± 33.45 ^{a}	1164.07 ± 88.93 ^{a}	7.56 ± 0.16 ^{a}
	Ohmic	-9.32 ± 0.15 ^{ab}	11780.41 ± 18.60 ^{a}	1200.71 ± 138.24 ^{a}	7.13 ± 0.08 ^{a}
60 °C	Conventional	-9.23 ± 0.20 ^{ab}	11769.64 ± 59.82 ^{a}	1323.86 ± 30.43 ^{a}	9.79 ± 0.08 ^{b}
	Ohmic	-9.68 ± 0.26 ^{b}	11773.53 ± 36.01 ^{a}	1337.86 ± 127.72 ^{a}	8.90 ± 0.07 ^{c}
70 °C	Conventional	-10.48 ± 0.21 ^{c}	12292.34 ± 152.44 ^{b}	2557.73 ± 157.26 ^{b}	25.16 ± 0.21 ^{d}
	Ohmic	-10.93 ± 0.26 ^{c}	12452.15 ± 28.78 ^{b}	2947.44 ± 377.80 ^{c}	23.88 ± 0.07 ^{e}
80 °C	Conventional	-12.27 ± 0.34 ^{d}	13290.14 ± 31.29 ^{c}	4818.51 ± 33.67 ^{d}	46.39 ± 0.11 ^{f}
	Ohmic	-13,15 ± 0.15 ^{e}	13515.21 ± 90.51 ^{d}	5158.81 ± 134.15 ^{e}	43.16 ± 0.13 ^{g}
90 °C	Conventional	-13.42 ± 0.14 ^{e}	13725.68 ± 75.14 ^{e}	5763.76 ± 124.47 ^{f}	56.99 ± 0.37 ^{h}
	Ohmic	-13.94 ± 0.13 ^{f}	13947.16 ± 19.38 ^{f}	6113.32 ± 228.34 ^{g}	50.51 ± 0.18 ^{i}

For each column, different letters correspond to statistically significant differences ($p < 0.05$).

For the treatments at pH 7, none of the treatments below 70 °C produced any statistically significant changes on the parameters determined, with exception for the free SH groups, which